STAT

Page Denied

Declassified in Part - Sanitized Copy Approved for Release @ 50-Yr 2014/01/31 : CIA-RDP81-01043R002900240002-8

STAT

INVESTIGATION PERTAINING TO ELIMINATION OF AMBIGUITIES DUE TO HIGH PULSE REPETITION RATES

copy 17

FINAL REPORT

December 1, 1953 - May 1, 1956

Signal Corps Contract
No. DA-36-039 SC-56696

Department of the Army Project
No. 3-99-05-022

Signal Corps Project
No. 122B

STAT

U.S. Army
Signal Corps Engineering Laboratories
Fort Monmouth, New Jersey

Research

ITUTE OF TECHNOLOGY

STAT

STAT

Page Denied

Next 1 Page(s) In Document Denied

Declassified in Part - Sanitized Copy Approved for Release @ 50-Yr 2014/01/31 : CIA-RDP81-01043R002900240002-8

INVESTIGATION PERTAINING TO ELIMINATION OF AMBIGUITIES DUE TO HIGH PULSE REPETITION RATES

FINAL REPORT

December 1, 1953 - May 1, 1956

Signal Corps Contract
No. DA-36-039 SC-56696

Department of the Army Project
No. 3-99-05-022

Signal Corps Project
No. 122B

U.S. Army
Signal Corps Engineering Laboratories
Fort Monmouth, New Jersey

[redacted]

STAT

Declassified in Part - Sanitized Copy Approved for Release @ 50-Yr 2014/01/31 : CIA-RDP81-01043R002900240002-8

INVESTIGATION PERTAINING TO ELIMINATION OF AMBIGUITIES DUE TO HIGH PULSE REPETITION RATES

FINAL REPORT

December 1, 1953 - May 1, 1956

OBJECT

The object of this development is to obtain a design for a piece of equipment which, when either integrated into new radars, or applied to existing ones, shall enhance the performance of the radar by increasing the number of target "hits" per scan beyond the limit normally set by maximum unambiguous range.

Signal Corps Contract No. DA-36-039 SC-56696
Signal Corps Technical Requirements
No. SCL-2803, 30 July 1953
Amendment No. 1, 6 December 1954

Department of the Army Project No. 3-99-05-022

Signal Corps Project No. 122-B

[redacted]

STAT

Declassified in Part - Sanitized Copy Approved for Release @ 50-Yr 2014/01/31 : CIA-RDP81-01043R002900240002-8

STAT

Declassified in Part - Sanitized Copy Approved for Release @ 50-Yr 2014/01/31 : CIA-RDP81-01043R002900240002-8

List of Figures

Declassified in Part - Sanitized Copy Approved for Release @ 50-Yr 2014/01/31 : CIA-RDP81-01043R002900240002-8

GLOSSARY OF SYMBOLS

Symbol	Meaning	Page of First Appearance
A	amplitude of input signal	217
B	effective brightness	130
B_i	effective brightness due to i type luminescent-centers	130
B_{io}	initial value of B_i	130
B_{imax}	saturation effective brightness due to i type luminescent-centers	136
c	speed of light	222
C_x	target capacitance per unit area	172
CRT	abbreviation for "cathode ray tube"	30
f	frequency	120
f_M	maximum unambiguous repetition rate	221
f_s	repetition rate	223
F_{AS}	ambiguity suppression figure-of-merit	11
F_{NS}	noise suppression figure-of-merit	10
FRI	abbreviation for "false range indicating"	9
h	Planck's constant	120
HTA	abbreviation for "higher time around"	9
I_{bR}	electron beam current during read operation	175
I_{bW}	electron beam current during write operation	172
I_s	signal current	173
I_{sR}	signal current during read operation	174
J_{bR}	relative beam current during read operation	174
J_{bW}	relative beam current during write operation	172

Symbol	Meaning	Page of First Appearance
J_{sR}	relative signal current during read operation Additional subscripts have the meanings: B for the baseline FRI for a FRI echo TRI for a TRI echo	174 180 181 182
K	constant of proportionality	217
n	number of intervals in a PIM modulation cycle	30
N_C	number of transition-electrons in the conduction-band per unit area of the CRT screen	123
N_{ei}	number of excited i type luminescent-centers per unit area of the CRT screen	121
N_{eio}	initial value of N_{ei}	126
N_i	number of i type luminescent-centers per unit area of the CRT screen	121
N_T	number of transition-electrons in the high-energy-electron traps per unit area of the CRT screen	124
N_{XS}	number of electrons in excess of the number of holes in the phosphor per unit area of the CRT screen	125
p_{ci}	probability time density that conduction-band electrons will drop to excited i type luminescent-centers	123
p_{di}	probability time density of decay of i type luminescent-centers	121
p_{ei}	probability time density of excitation of i type luminescent-centers	131
p_{et}	probability time density that electrons will escape from high-energy-electron-traps	123
$p_{fi}(f)$	frequency density of radiation from the decay of i type luminescent-centers	127

Symbol	Meaning	Page of First Appearance
p_{tt}	probability time density that conduction-band electrons will become trapped in high-energy-electron-traps	123
PIM	abbreviation for "pulse interval modulation"	15
PRF	abbreviation for "pulse repetition frequency"	9
Q.P.R.	abbreviation for "Quarterly Progress Report"	16
r	barrier grid transmission ratio	172
R_M	maximum range of the radar	222
R_o	output load impedance	173
$s_v(f)$	spectral sensitivity distribution of Vidicon tube	129
S_N^V	voltage signal-to-noise ratio	195
t	time	125
T_a	averaging time interval	218
$T_{i,j}$	time interval between i and j	208
T_M	time length of the PIM modulation cycle	210
T_w	averaging time interval during writing	216
T_r	averaging time interval during reading	216
TRI	abbreviation for "true range indicating	10
v	speed	208
v_d	speed deviation	221
V_N	amplitude of random noise	10
v_R	scan speed during read operation	174
V_{se}	average secondary electron energy in electron volts	172

Symbol	Meaning	Page of First Appearance
V_{tb}	target-to-barrier grid charging voltage	170
	Additional subscripts have the meanings:	
	oW at start of write operation	172
	nW after n write sweeps	
	oR at start of read operation	173
	B for the baseline	180
	FRI for a FRI echo	181
	TRI for a TRI echo	182
	1R after one read sweep	175
V_{TB}	actual target-to-barrier grid voltage	170
v_W	scan speed during write operation	172
V_{EQ}	equilibrium target-to-barrier grid voltage	170
V_{FRI}	amplitude of a FRI echo	11
V_{in}	input signal	218
V_{out}	output signal	217
V_{out}^{amp}	amplitude of output signal	217
V_{TRI}	amplitude of a TRI echo	10
x_d	head position deviation	224
x_g	head air-gap width	218
x_i	distance between heads	208
x_r	read-head air-gap width	216
x_w	write-head air-gap width	216
α_i	decay constant of i type luminescent-centers	125
δ	target secondary emission ratio	174
η_i	excitation constant of i type luminescent-centers	133
λ	wavelength	221
π_i	luminous power output per unit area of the CRT screen	128

II PURPOSE

The purpose of this contract is to continue the study and development of techniques which will permit the use of high pulse repetition rates in long range radars and MTI radar without the range ambiguities which normally are present as the result of returns from "second-time-around", "third-time-around" and "higher-time-around" echoes.

III. ABSTRACT

The performance of a radar, with respect to the detection of weak target echoes and MTI operation, is improved by increasing the pulse repetition frequency (PRF). A practical upper limit to the PRF is reached when higher-time-around echoes cause ambiguous range indications. Advantage can be taken of a high PRF if the false-range-indicating (FRI) echoes can be discriminated from the true-range-indicating (TRI) echoes. The operation is further enhanced if the discriminated FRI echoes are suppressed sufficiently so that they do not clutter up the radar display. Methods for accomplishing both the discrimination and the suppression of the FRI echoes which also utilize the high PRF to improve the signal-to-noise ratio (S_N) have been devised in the course of this research project.

Modulation of the time interval between successive transmitter pulses produces a distinctly and readily usable discrimination between TRI echoes and FRI echoes. No suppression of the FRI echoes or random noise is accomplished by the pulse interval modulation (PIM) alone. Several ambiguity filters, which suppress the FRI echoes and random noise, have been evolved for use in the PIM System, based on optical-electronic, electrostatic-storage, and magnetic-storage devices. The Optical-Electronic Ambiguity Filter has been both theoretically and experimentally investigated, and

first order figures-of-merit have been determined. Preliminary theoretical and experimental investigation of the Storage-Tube Ambiguity Filter indicate potential superiority over the Optical-Electronic Ambiguity Filter in both effectiveness and practicality, even though the experimental figures-of-merit obtained so far for the Optical-Electronic Ambiguity Filter exceed those for the Storage-Tube Ambiguity Filter. The Magnetic-Storage Ambiguity Filter is first introduced in this report. The first order determination of some of the important system parameters and figures-of-merit indicates substantial promise for this system, but no experimental work has been done. A special point to note is that all these ambiguity filters utilize their non-linear characteristics to give ambiguity and random noise suppression much greater than can be obtained by an ideal linear integrator. The ambiguity suppression figure-of-merit (F_{AS}) and the noise suppression figure-of-merit (F_{NS}) of an ideal linear integrator are n and $\sqrt{n}$, respectively, where n is the number of pulses integrated.

Operation of the transmitter at several different pulse repetition frequencies simultaneously (Mixed PRF) produces a high net PRF and imparts the distinctive information to the signal necessary for discrimination between TRI echoes and FRI echoes. Periodic filters (comb filters) perform the actual discrimination between TRI echoes and FRI echoes and also suppress

the FRI echoes and random noise. The Comb-Type Ambiguity Filter, for use in the Mixed PRF System, has been given preliminary theoretical investigation but no experimental work has been done.

Two special items considered during the last quarter of the project, in conjunction with the Optical-Electronic Ambiguity Filter, were the transient response of CRT phosphors and the subrange combining system. General equations for the transient brightness build-up and decay in a phosphor were formulated. Assumptions applicable to the special conditions of usage in the Optical-Electronic Ambiguity Filter were used to simplify the form of the equations and a preliminary experimental verification of results derived from these equations was made. The first three subrange displays of the echo information presented by the Optical-Electronic Ambiguity Filter were successfully combined into a single continuous range display. The extension of this system to more subranges is possible by the addition of duplicate system components.

Declassified in Part - Sanitized Copy Approved for Release @ 50-Yr 2014/01/31 : CIA-RDP81-01043R002900240002-8

IV PUBLICATIONS, LECTURES, REPORTS AND CONFERENCES

A. Publications: No publications resulted from the project during the eighth quarter.

B. Lectures:

Title	Lecturer	Place	Date
"Transient Behavior of Phosphors"	H. M. Musal	Illinois Institute of Technology	24 February 1956

C. Reports:

Ref. No.	Title	Author	Date
21	Monthly Performance Summary	G.I. Cohn	November, 1955
22	Monthly Performance Summary	G.I. Cohn	December, 1955
6095-35	Optical-Electronic Ambiguity Filter Subrange Combining System	H. M. Musal	March, 1956
6095-36	Storage-Tube Ambiguity Filter	H.M. Musal	April, 1956
6095-44	Magnetic-Storage Ambiguity Filter	H.M. Musal	April, 1956
6095-45	Transient Response of Phosphors	H.M. Musal	February, 1956
6095-46	Experimental Equipment for PIM System and Ambiguity Filters	R.F. Purnell	April 1956

D. Conferences:

No conferences were held in connection with the project during the eighth quarter.

Declassified in Part - Sanitized Copy Approved for Release @ 50-Yr 2014/01/31 : CIA-RDP81-01043R002900240002-8

V FACTUAL DATA

INTRODUCTION

Statement of Problem

The performance of a radar system is directly dependent on the signal to noise ratio. Signal integration is one method of improving the signal to noise ratio. The higher the pulse repetition rate (PRF), the greater the amount of integration possible, and consequently, the larger the signal to noise ratio. Signal to noise ratio improvement with high PRF's is possible when the noise is completely random, and also when the noise is an undesired signal such as echoes from stationary or slowly moving targets, i.e., clutter. For example, in MTI radars an increase in PRF improves pulse to pulse cancellation of echoes from stationary and slowly moving targets thereby increasing the ratio of desired signal (response to moving targets) to undesired signal (clutter).

If the distance to a target is such that the echo due to a given transmitter pulse does not return to the radar prior to the transmission of one or more subsequent pulses, the echoes are called higher-time-around (HTA) echoes. The detected HTA echoes can produce as many different false range indicating (FRI) echoes on the radar indicator as there are transmitter pulses radiated between the one causing the echo and the return of an echo from a target at maximum range. As the PRF is raised to improve the signal to noise ratio, the number of HTA detectable echoes is

Declassified in Part - Sanitized Copy Approved for Release @ 50-Yr 2014/01/31 : CIA-RDP81-01043R002900240002-8

increased from none to many. Since there is an additional range indication for each detectable HTA echo, the range display is ambiguous unless some means is introduced for identifying which of the many range indications is the true one.

The presence of the multiple range indications for each target quickly clutters up the indicator display, especially when more than a few targets are present, even with the true range indicating (TRI) echoes differentiated from the FRI echoes. Consequently, it is highly desirable to devise means not only of distinguishing the TRI echoes, but also of eliminating the FRI echoes from the display.

In order to compare the relative performance capabilities of different systems, it is necessary to determine the figures of merit of each system. The noise suppression figure of merit of a system is taken as :

$$F_{NS} = \frac{\left.\dfrac{V_{TRI}}{V_{Nrms}}\right|_{out}}{\left.\dfrac{V_{TRI}}{V_{Nrms}}\right|_{in}}$$

where V_{TRI} is the amplitude of a TRI echo, and V_{Nrms} is the rms amplitude of the random noise. For a larger figure of merit the radar is more sensitive, i.e., smaller and more distant targets are detectable.

Increasing the PRF increases the radar figure of merit at the expense of introducing FRI echoes. Once the FRI echoes have been discriminated, they play the same undesirable role as ordinary noise. The effectiveness or figure

of merit of a FRI echo filter or ambiguity suppressor is basically defined as

$$F_{AS} = \frac{\left.\dfrac{V_{TRI}}{V_{FRI}}\right|_{out}}{\left.\dfrac{V_{TRI}}{V_{FRI}}\right|_{in}}$$

Since at the input of the ambiguity filter the amplitude of the FRI echoes from a given target is the same as the amplitude of the TRI echoes, the formula for the ambiguity suppression figure of merit reduces to:

$$F_{AS} = \left.\frac{V_{TRI}}{V_{FRI}}\right|_{out}$$

In order for the increased PRF to have no objectionable effects, it is necessary to reduce the amplitude of the FRI echoes below the random noise level. Thus, the ambiguity suppression figure of merit should be made greater than the signal to random noise ratio at the output of the filter.

In a research program of the type undertaken here, it is of paramount importance to determine these figures of merit both theoretically and experimentally as functions of all radar parameters which have a significant influence on them. From this information the optimum performance for a specified system can be determined and the best system of any suggested group can be singled out.

Methods of Ambiguity Elimination

In order to eliminate ambiguities due to high pulse

Declassified in Part - Sanitized Copy Approved for Release @ 50-Yr 2014/01/31 : CIA-RDP81-01043R002900240002-8

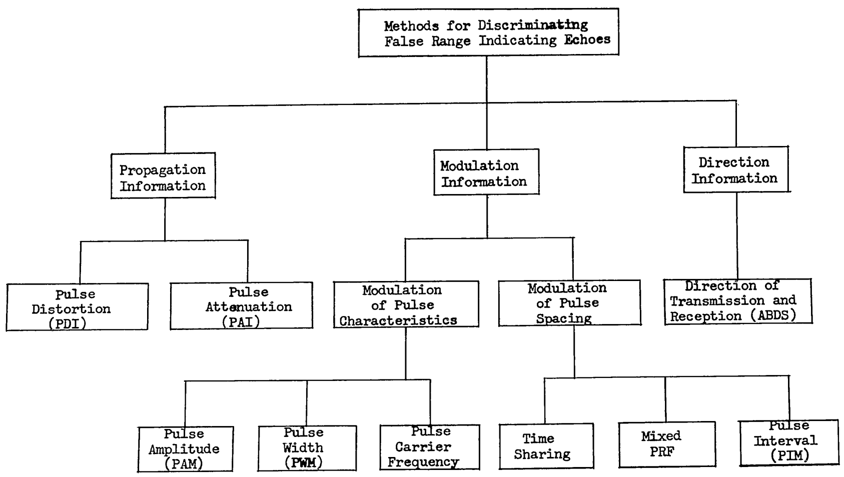

Methods for Discriminating False Range Indicating Echoes

Figure 1

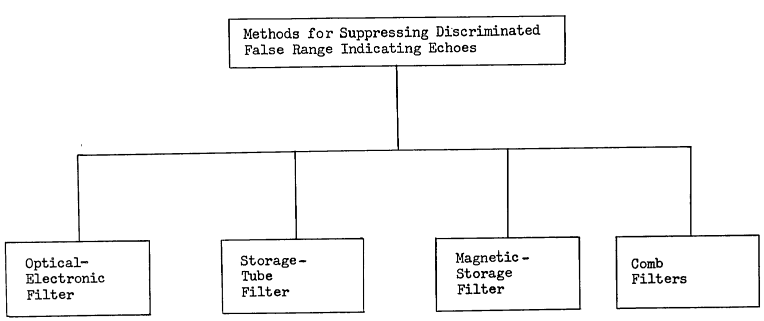

Methods for Suppressing Discriminated False Range Indicating Echoes

Figure 2

Declassified in Part - Sanitized Copy Approved for Release @ 50-Yr 2014/01/31 : CIA-RDP81-01043R002900240002-8

repetition rates the FRI echoes must first be discriminated from the TRI echoes. The possible methods for accomplishing this, which have been devised and investigated at the Electronics Research Laboratory of Illinois Institute of Technology, are shown in the block diagram of Figure 1

After the FRI echoes have been discriminated they must be suppressed. Several possible methods which may be applied are shown in the block diagram of Figure 2 These techniques not only suppress the FRI echoes but also increase the signal-to-random noise ratio.

METHODS FOR DISCRIMINATING FALSE RANGE INDICATING ECHOES

Introduction

In order to discriminate TRI echoes from FRI echoes information is necessary to determine which transmitter pulse caused the echo. This information may be provided by the natural characteristics of pulse propagation or by modulation of the transmitter output.

The natural means of discrimination are Pulse Attenuation Information, Pulse Distortion Information, and Antenna Beam Displacement Sorting. No extensive investigation of these means of discrimination was done since the first two are impractical and ABDS awaits the development of a suitable rapid scan antenna.

Methods of modulating the transmitter output investigated are Pulse Amplitude Modulation, Pulse Width Modulation, Pulse Carrier Frequency Modulation, Pulse Code Modulation, Pulse Interval Modulation, Time Sharing, and Mixed Pulse Repetition Frequency. Of these methods PAM and PWM are impractical because of the variations in target characteristics; PCFM appears much less practical than other methods because of complex equipment requirements; PCM breaks down when several targets are present; and Time Sharing is limited in operation. Of the two remaining systems, PIM and Mixed PRF, both of which appear practical, the PIM system was devised first and consequently has been investigated more completely. The Mixed PRF system has been investigated theoretically and appears to have merit.

Pulse Attenuation Information

Under certain conditions the attenuations which a pulse undergoes during propagation can be used to determine the approximate distance traveled by the pulse, and hence provide a basis for resolving ambiguous range readings. Since the energy in a pulse falls off with the fourth power of the distance, there is considerable range information conveyed by the strength of the echo relative to the transmitted pulse. Ambiguity elimination based on this information would have worth-while possibilities if the reflection coefficients of the targets and the attenuation due to weather conditions were known. Since the reflection coefficients of the targets and the attenuation due to weather conditions generally are unknown, this method is considered to be impractical.[1]

Pulse Distortion Information

A pulse propagating in a media becomes distorted as it travels. One cause of such distortion is due to the dispersive nature of the media, that is, the different frequencies composing the pulse propagate with different velocities. Another cause of distortion is the heterogeniety of the media which causes the pulse to split up and travel over a number of paths, each having slightly

[1]Signal Corps Contract DA36-039 SC-15555 First Q.P.R. June 1952-September 1952, pp 50-53.

different length. When the pulse energy recombines at the receiver the components are no longer in the same time relationship. In the atmosphere the second effect (that due to heterogeniety) appears to be predominant. Tests carried out by O. E. De Lange[1] using 3 millimicrosecond pulses at 4000 megacles over a 22 mile path showed multipath transmission with path differences as great as seven feet. This was sufficient to provide complete separation of the received pulses. Distortion in the individual pulse shapes was undiscernable compared to that which occurred due to combination of the pulses which had traveled different paths.

A target having extension in the radial direction from the radar antenna will broaden the received echo by an amount approximately proportional to this extension. Because of this fact and the fact that the geometry of the target and the exact atmospheric conditions are not likely to be readily available, the distortion due to propagation does not provide a practical basis for ambiguity elimination.[2]

Antenna Beam Displacement Sorting

The directional information contained in the transmitted pulse can be utilized to provide a method for

[1]O. E. De Lange, "Propagation Studies at Microwave Frequencies by Means of Very Short Pulses", B.S.T.J. 31, 11-103 (January 1952).

[2]Signal Corps Contract DA36-039 SC-15555 First Q.P.R. June 1952-September 1952, p 54.

preventing the occurrence of false range indications. During the interval between the sending of a transmitter pulse and the reception of an echo due to that pulse the radar antenna rotates through an angle proportional to the transit time of the pulse and hence to the range of the target returning the echo. This information may be utilized to prevent range ambiguities by employing separate antenna beams, which rotate about the same axis, for reception and transmission. The receiver antenna beam lags behind the transmitter antenna beam by just the amount required so that by the time the echo returns the receiver antenna beam will have rotated into the position occupied by the transmitter antenna beam when the pulse was fired.

Absence of false range indications is achieved by rotating the antenna beams with an angular velocity such that completely different angular sectors are illuminated by successive transmitter pulses, without having any un-illuminated angular sectors.

The principal disadvantages to this system are the duplication of receiver equipment necessary in order to observe more than one sub-range simultaneously and the special antenna scanner required.[1]

Pulse Amplitude Modulation

In this method, range ambiguities are eliminated by

[1]Signal Corps Contract DA36-039 SC-15555 First Q.P.R. June 1952-September 1952, pp 55-58. Second Q.P.R. September 1952-December 1952, pp 52-62.

utilizing pulse amplitude information inserted in successive pulses at the transmitter. Each transmitter pulse amplitude is increased over that of the previous one by the same amount until n pulses of different heights are obtained, after which the modulation cycle is repeated. The envelope of the transmitter pulse amplitude is a saw-tooth wave. The amplitudes of successive echoes from a given target have a similar saw-tooth envelope which lags in phase behind that of the transmitter envelope by an amount which is proportional to the target range. Measurement of this phase lag gives an approximate indication of the range and can hence be used to eliminate false range readings.

This is accomplished by feeding the amplitude modulated video output of the receiver through a variable gain amplifier which has its gain controlled by a wave form having the inverse variation to that of the transmitter modulation wave form. The gain controlling wave form is shifted in phase so as to match the phase delay of the desired echo envelope. Then, in the output of this amplifier, echoes from targets located at the chosen range will have constant pulse amplitudes whereas echoes from targets at other ranges will have amplitude variations. The output of the variable gain amplifier is passed through a blanking circuit which removes the echoes with variable amplitudes and passes the constant amplitude unambiguous signals. The blank-

Declassified in Part - Sanitized Copy Approved for Release @ 50-Yr 2014/01/31 : CIA-RDP81-01043R002900240002-8

ing pulse is generated by a circuit which compares each echo with the echo from the same target due to the previous transmitter pulse and whenever the amplitude difference exceeds a specified amount, a blanking pulse is generated. The extent of the range displayed unambiguously is influenced by the setting of the amplitude comparitor.

This method has two paramount disadvantages. One is the fact that the transmitter peak power capabilities are largely wasted by the amplitude modulation unless the per cent modulation is small. Another is that the method cannot integrate signals below the noise level because information must be extracted for sorting before integration of the TRI echoes is possible.[1]

Pulse Width Modulation

In this method range ambiguities are eliminated by utilizing pulse width information inserted in successive pulses at the transmitter. The transmitter pulse width is modulated so that n successive pulses have different widths, after which the cycle is repeated. The radar's major range is subdivided into as many sub-ranges as there are different pulse widths in a modulation cycle, and the information in each sub-range is separately displayed. Extra apparatus would be required to present all sub-ranges on one display.

The difference in width between an echo and the

[1]Signal Corps Contract DA36-039 SC-15555 First Q.P.R. June 1952-September 1952, pp 46-49.

transmitter pulse sent out just prior to reception of the echo is utilized to sort the echo signal into the channel which displays the sub-range in which the actual target exists. A method of accomplishing this is as follows. Each received echo triggers a pulse generator which produces a pulse of the same width as the last transmitter pulse generated. The width of this pulse is compared with that of the echo just received and a voltage proportional to the difference in widths is generated. This voltage is applied to the switching circuit or tube which connects the signal to the proper channel.

The principal drawback to this method is that it cannot integrate received signals below the noise level because information from individual pulses must be utilized in order to sort the echoes into the proper sub-ranges. Another disadvantage is that the variation in pulse width purposely inserted must be prohibitively large in order to prevent variations in pulse width due to the radial extension of the target from giving false range indications.[1]

Pulse Carrier Frequency Modulation

With this system, successive pulses are transmitted on different frequencies so that ambiguous pulses can be separated on a frequency basis. Theoretically this method is highly suitable for ambiguity elimination when MTI

[1]Signal Corps Contract DA36-039 SC-15555 First Q.P.R. June 1952-September 1952, pp 34-38.

operation is not required, but it appears to be inherently incompatible with coherent MTI systems. The PCFM system is very inefficient in its use of the radio spectrum since it requires several times the bandwidth of a conventional radar system. It requires essentially a complete separate receiver for each frequency unless the application is such as to require the display of only one sub-range at a time. The problem of automatic frequency control is very severe with PCFM unless a master oscillator power amplifier arrangement can be used for the transmitter. This awaits the commercial availability of suitable output tubes.[1]

Pulse Code Modulation

In this method, a group of pulses is transmitted in place of each single pulse in an ordinary radar. Successive pulse groups differ by the relative spacing between the pulses or number of pulses in a group. After n different pulse groups the modulation cycle is repeated. The information conveyed by the coding of the echoes in each group can be utilized to sort them into the appropriate channels.

The principal drawback to this method is that overlapping of code groups resulting from closely spaced targets will destroy the pulse group coding. Another

[1]Signal Corps Contract DA36-039 SC-15555 First Q.P.R. June 1952-September 1952, pp 11-33. Second Q.P.R. September 1952-December 1952, pp 17-27.

drawback is the difficulty of transmitting these high power pulses in such quick succession. This method also suffers from the inability to integrate signals below the noise level.[1]

Time Sharing Radar

This system employs a radar having two different repetition rates available. The operating time is divided between these two repetition rates manually or automatically.

Discrimination between TRI echoes and FRI echoes is based on the fact that the range position of a FRI echo on the display depends upon the time interval between successive transmitter pulses. By switching the transmitter repetition rate the FRI echoes are caused to change range position on the display while the TRI echoes remain fixed in range position. This allows the operator to discriminate between the TRI echoes and the FRI echoes.

The discussion above applies most directly to an A- scope presentation of a fixed azimuthal direction, however, the system is usable even when a PPI display is used. The main virtue of this system is its simplicity and ease of incorporation into existing radars, and thus is especially applicable to existing radars having higher time around echoes. The disadvan-

[1]Signal Corps Contract DA36-039 SC-15555 Final Report June 1952-August 1953, p 26.

tage of this system is that even though the FRI echoes are discriminated they are not easily suppressed. This requires the operator to select the TRI echoes from the display.[1]

Mixed PRF Radar

The Mixed PRF Radar is an extension of the Time Sharing Radar. In this system several different pulse repetition frequencies are used simultaneously instead of sequentially as in the Time Sharing Radar.

The transmitter is triggered by a signal formed from the sum of the outputs of n PRF generators of unequal PRF's. The transmitter output pulses are therefore nonuniformly spaced. The highest single PRF of the individual PRF generators is chosen to be the highest unambiguous PRF allowable for the radar. Thus the average overall PRF can approach n times the unambiguous pulse repetition rate and consequently ambiguous or many time around echoes are present. Means for separating the TRI echoes from the FRI echoes must be applied.

Since the echo spectrum of echoes from each PRF is a different comb spectrum, separation of the FRI echoes from the TRI echoes is possible by the use of comb filters. The echo responses are applied to n sharply-tuned comb filters in parallel, each of which will pass only echoes from a particular PRF. Since each PRF is be-

[1]Signal Corps Contract DA36-039 SC-56696 First Q.P.R. December 1953-March 1954 pp 13-17. Second Q.P.R. March 1954-June 1954 pp 16-20.

low the maximum unambiguous PRF, each channel, representing the output of one comb filter, presents the complete radar range in one indicator sweep.

To obtain the full signal to noise integration improvement, the n channels must be combined into one display. Conceptually simplest is a system which features a cathode ray tube with n electron guns all scanning the same line on the face of the tube and each intensity modulated by the output of one of the n channels. Another scheme involves n storage tubes. Each storage tube stores the signal output from one channel and then a simultaneous read (and erase) of all storage tubes would add the stored information from all channels. This summed signal would then be the signal for the final scope display.[1]

In the Mixed PRF system employing comb filters the discrimination and elimination of the FRI echoes is accomplished simultaneously in the comb filters. The characteristics of comb filters for this application are discussed in the section on ambiguity filters.

Pulse Interval Modulation

In this system, the transmitter operates like a conventional radar except that the pulse repetition

[1]Signal Corps Contract DA36-039 SC-56696 Fifth Q.P.R. February 1955-April 1955, pp 55-72. Sixth Q.P.R. May 1955-July 1955, pp 9-45.

period is non-uniform. Since modulation of the pulse repetition period can be accomplished in the triggering circuits preceding the keyer, this type of modulation is readily accomplished. In general, the amount of variation required in the repetition period is small enough to permit the ordinary resonant charging systems to be used in the pulse generating network without difficulty.

When the echoes are received they are applied to the vertical deflection or intensity modulation system of an oscilloscope, the linear horizontal sweep of which is triggered by each transmitted pulse of the radar. Let T_j be the round trip echo time for a particular target. If T_j is less than the duration of the sweep, the echo will appear in the same position on every sweep since T_j is constant. On the other hand, if T_j is somewhat longer than the sweep duration, it will appear on the next sweep (as an ambiguous echo) in a position corresponding to $T_j - T_{i,i+1}$ where $T_{i,i+1}$ is the interval between the two adjacent transmitted pulses. Since T_j is constant but $T_{i,i+1}$ is not constant, the position of the ambiguous echo on the trace will vary from one sweep to the next. Thus the FRI echoes appear spread out whereas the TRI echoes all coincide. More distant targets can be viewed as proper responses by introducing a fixed delay T_D into the sweep trigger system. Then the position of the echo will correspond to $T_j - T_D$ which is fixed since T_D is constant. Of course, in this case, if $T_j < T_D$, the

target will appear ambiguous since it will be presented on the preceding sub-range display which is synchronized with an earlier transmitted pulse. Thus only one sub-range at a time is displayed as unambiguous but any sub-range may be chosen to be so displayed. Several displays could be operated simultaneously, each set for a different sub-range, thus displaying the total range.[1]

The advantages of the PIM system are integration of true range indicating echoes in the presence of noise, applicability to existing radars, and simplicity of equipment involved. The disadvantage of having the radar's major range resolved into several sub-ranges is relatively minor, since in some cases only one (the nearest) sub-range is of interest or if desired the separate sub-range displays can be re-combined into a single major range display. Because of these promising advantages, simulation equipment was designed and constructed for experimentation and demonstration.

The pulse interval modulation system provides a means for discriminating the FRI echoes. In order to suppress the discriminated FRI echoes, an ambiguity

[1] Signal Corps Contract DA36-039 SC-15555 First Q.P.R. June 1952-September 1952, pp 39-45. Second Q.P.R. September 1952-December 1952, pp 28-51. Third Q.P.R. December 1952-March 1953, pp 10-58. Final Report June 1952-August 1953, pp 29-62, 70-143. Signal Corps Contract DA36-039 SC-56696 First Q.P.R. December 1953-March 1954, pp 18-85. Second Q.P.R. March 1954-June 1954, pp 21-45. Third Q.P.R. June 1954-August 1954, pp 68-78. Interim Report December 1953-January 1955, pp 32-57.

suppression filter must be used. An optical-electronic filter, an electrostatic storage tube filter, and a magnetic storage filter have been devised for this function. These are described in the section on ambiguity filters.

METHODS FOR SUPPRESSING DISCRIMINATED FALSE RANGE INDICATING ECHOES

Introduction

Several methods for suppressing false range indicating (FRI) echoes have been devised, as shown in Figure 2 in the section entitled INTRODUCTION of this report. It was pointed out there that it is highly desirable to suppress the discriminated FRI echoes so that they will not clutter up the indicator display. The ambiguity filters devised to suppress the FRI echoes are used either with the PIM system or the Mixed PRF system.

The Optical-Electronic, Storage-Tube, and Magnetic-Storage Ambiguity Filters are particularly applicable to the PIM discrimination method. The Optical-Electronic Ambiguity Filter has been investigated both theoretically and experimentally. Despite practical difficulties encountered in its operation, experimental ambiguity suppression figures-of-merit as high as 80, and noise suppression figures-of-merit as high as 100, were obtained. A comprehensive theoretical analysis of the Storage-Tube Ambiguity Filter has not been completed but the experimental investigation indicates that the filter is meritorious practically as well as theoretically. Experimental ambiguity suppression figures-of-merit as high as 50, and noise suppression figures-of-merit as high as 15, have been obtained under very restrictive operating conditions. The Magnetic-Storage Ambiguity Filter is introduced for the first time in this report. No experimental work has been done, however, this filter appears to have an excellent potentiality if the problem of high frequency magnetic recording can be solved. This is essentially a problem of obtaining the high relative speed between the heads and the magnetic-storage media necessary for adequate resolution.

The Comb-Filter Ambiguity Filter, used in the Mixed PRF system, actually performs both the discrimination and the suppression functions of the system. No experimental work on either the Mixed PRF system or the Comb-Filter Ambiguity Filter has been done.

Optical-Electronic Ambiguity Filter

The A- scope display (on a CRT) of echo information received by a PIM radar consists of TRI echoes, under which the baseline is broken on every sweep, and FRI echoes, under which the baseline is broken only once every n sweeps. Considering only the baseline, then, TRI echoes are characterized by dark breaks in an otherwise bright line. The baseline under the FRI echoes is slightly less bright than the baseline where no echoes appear. The large difference in brightness between the baseline and the TRI echo positions, in comparison to the small difference in brightness between the baseline and the FRI echo positions is the basis for the ambiguity suppression in the Optical-

Electronic Ambiguity Filter.

The A- scope display of the TRI and FRI echoes from the PIM radar receiver (on the Primary CRT) is focused on the photosensitive target of a Vidicon camera tube in the Scanner (TV pick-up camera). The Vidicon electron beam reads the information from the photosensitive target by scanning along the baseline of the A- scope picture on the target. The output current of the Vidicon tube depends upon the amount of light which has impinged on the target between successive scans of the Vidicon electron beam. The baseline where no echoes appear yields a large steady output current. The output current drops to near zero when the break under a TRI echo is scanned, and drops only slightly when the baseline under a FRI echo is scanned. The changes in output current constitute the output signal of the filter. The output signal due to a TRI echo is larger than that due to a FRI echo, and thus suppression has been accomplished.

Theoretical analysis of the behavior of the Primary CRT phosphor, the behavior of the Vidicon tube, and the effects of pertinent system parameters have been made. Experimental verifications of these analyses have also been made.

The maximum theoretical ambiguity suppression figure-of-merit increases without limit as n increases. The maximum experimental value obtained was 80 with an n of 12. The maximum theoretical noise suppression figure-of-merit obtained from the restricted theoretical analysis was 135, and an experimental value of approximately 100 was obtained with the equipment used under the optimum operating conditions.[1]

Storage-Tube Ambiguity Filter

In the Storage-Tube Ambiguity Filter an electrostatic barrier grid storage-tube is used to store and integrate the echo information. The information is written on the target by either deflection-modulation of the electron beam (exactly as information is written on the phosphor of the Primary CRT in the Optical-Electronic Ambiguity Filter) or by negative-intensity-modulation of the electron beam. The multiple writing sweeps produce a charge pattern on the target of the storage-tube similar to the brightness pattern on the phosphor of the Primary CRT in the Optical-Electronic Ambiguity Filter. During the reading operation in the storage-tube the charge pattern is removed by scanning the baseline of the charge picture and the output signal that is obtained is similar to the output signal from the Vidicon of the Optical-Electronic Ambiguity

[1]Signal Corps Contract No. DA-36-039 SC-56696 Third Q.P.R. June 1954-August 1954, pp 13-67. Interim Report December 1954-January 1955, pp 58-109. Fifth Q.P.R. February 1955-April 1955, pp 73-106. Sixth Q.P.R. May 1955-July 1955, pp 126-186. Seventh Q.P.R. August 1955-October 1955, pp 8-97.

Filter. A more detailed review of the operation of the Storage-Tube Ambiguity Filter is presented in the section entitled STORAGE-TUBE AMBIGUITY FILTER of this report.

Some preliminary theoretical analyses of the operation of the Storage-Tube Ambiguity Filter have been made. A theoretical derivation of the ambiguity suppression figure-of-merit for noiseless operation is presented in this report. The theoretical determination of the noise suppression figure-of-merit remains to be made. Some experimental determinations of both these figures-of-merit have been made.

The maximum theoretical ambiguity suppression figure-of-merit for noiseless operation is infinitely large, even for finite values of n, if the optimum operating parameters are used. The maximum experimental value obtained was 50 under non-optimum operating conditions with an n of 15. The maximum experimental noise suppression figure-of-merit obtained was approximately 15 under the same operating conditions.[1]

Magnetic-Storage Ambiguity Filter

The Magnetic-Storage Ambiguity Filter is first introduced in this report. A moving magnetic-storage

[1]Signal Corps Contract No. DA-36-039 SC-56696 Second Q.P.R. March 1954-June 1954, pp 124-142. Third Q.P.R. June 1954-August 1954, pp 103-128. Interim Report December 1953-January 1955, pp 110-155. Fifth Q.P.R. February 1955-April 1955, pp 15-54. Section entitled STORAGE-TUBE AMBIGUITY FILTER, of this report.

Declassified in Part - Sanitized Copy Approved for Release @ 50-Yr 2014/01/31 : CIA-RDP81-01043R002900240002-8

media (tape, drum, etc.) is used to store the echo information from the PIM radar receiver. By the use of multiple recording and reading heads the echo information returned during n successive pulse intervals is compared and selective TRI echo integration and FRI echo and random noise suppression are performed. The magnetic-storage device also provides the PIM triggering pulses for the radar transmitter. Details of this system are presented in the section entitled MAGNETIC-STORAGE AMBIGUITY FILTER of this report.

Some preliminary theoretical analyses of the operation of the Magnetic-Storage Ambiguity Filter have been made. A simplified derivation of the minimum magnetic-storage media speed necessary to record and read out the echo signal is presented in this report. Using the results of this derivation, equations for the speed stability necessary for efficient TRI echo integration and the write-head and read-head spacings and spacing accuracy necessary for efficient TRI echo integration have been derived. No experimental investigation of the filter has been made.

The maximum theoretical ambiguity suppression figure-of-merit for noiseless linear operation of all the system elements is n. The maximum theoretical noise suppression figure-of-merit, under the same

conditions, is $\sqrt{n}$.[1]

Comb-Type Ambiguity Filter

The Comb-Type Ambiguity Filter is used with the Mixed PRF radar system to provide discrimination and suppression of FRI echoes and random noise. The echo return from a target illuminated by a Mixed PRF radar system to provide discrimination and suppression of FRI echoes and random noise. The echo returns from a target illuminated by a Mixed PRF radar transmitter is a composite of n periodic echo pulse trains with repetition rates equal to the individual PRF's that make up the composite triggering PRF for the transmitter. The total composite echo return is fed into n periodic filters (comb-filters) in parallel, the periodicities of the filters being equal to the individual PRF's in the composite triggering PRF. The outputs of the comb-filters are the echoes due to the single individual PRF to which the comb-filter is tuned. Although the sum of the n different individual PRF's may be sufficiently large so as to cause higher-time-around echoes (and consequently range ambiguities), the individual PRF's are selected to be below the maximum unambiguous PRF, and thus the output of each comb-filter

[1] Section entitled MAGNETIC-STORAGE AMBIGUITY FILTER, of this report.

presents the entire radar range with no range ambiguities. The outputs of the n comb-filters are added together to take full advantage of the high composite PRF in integrating the TRI echoes and suppressing the random noise without the range ambiguities that would ordinarily be present in the absence of the ambiguity filter.

The comb-filters that were theoretically investigated were of the delay line type, using linear amplifiers constant time delay devices, and linear adders in both feedback and non-feedback circuits. Methods of approximating any desired comb-filter pass band shape were devised. The transient response of comb-filters was given some preliminary theoretical investigation. The ambiguity suppression figures-of-merit and the noise suppression figures-of-merit for some simple feedback type comb-filters were derived for idealized operating conditions. No experimental work on any of the delay line type comb-filters was done.

The theoretical ambiguity suppression figure-of-merit and the theoretical noise suppression figure-of-merit for a Comb-Type Ambiguity Filter using a simple feedback type comb-filter increase as the feedback loop gain increases. For a loop gain of 0.95, a maximum ambiguity suppression figure-of-merit of 20 and a maximum noise suppression figure-of-merit of 9

are theoretically possible.[1]

[1] Signal Corps Contract No. DA-36-039 SC-56696 Fifth Q.P.R. February 1955-April 1955, pp 55-72 and pp 119-170. Sixth Q.P.R. May 1955-July 1955 pp 9-45 and pp 187-229.

DESCRIPTION OF EXPERIMENTAL EQUIPMENT

INTRODUCTION

Equipment has been assembled and built to simulate a PIM radar system for experimental and demonstrational purposes. This consists of a PIM Radar Simulator, Optical-Electronic Ambiguity Filter, and Storage-Tube Ambiguity Filter.

Figures 3 and 4 show front and rear views of the complete group of equipment. The rack on the left in Figure 3 is the PIM Radar Simulator, consisting of the PIM Modulator, Noise Generator and Signal and Noise Mixer, Counter, Artificial Echo Unit, Voltage Regulator, and Power Supply. The other two racks compose the Optical-Electronic Ambiguity Filter. The center rack contains the Staircase Voltage Generator, Horizontal and Vertical Deflection Amplifiers, Tektronix Pulse and Waveform Generators, Voltage Regulator, and Power Supply. The rack on the right contains the TIC Vertical Deflection Amplifier, 5 Channel Oscilloscope with the Dage TV Camera mounted in front, High Voltage Power Supply, Voltage Regulator, and Dual D.C. Power Supply. At the left of the racks is the Storage-Tube Ambiguity Filter consisting of the Storage Tube Unit with the Potential Shifter on the front and the Tektronix Read Amplifier. The Tektronix Model 535 Oscilloscope on the portable dolly is used as the Secondary Indicator in both the Optical-Electronic and

Declassified in Part - Sanitized Copy Approved for Release @ 50-Yr 2014/01/31 : CIA-RDP81-01043R002900240002-8

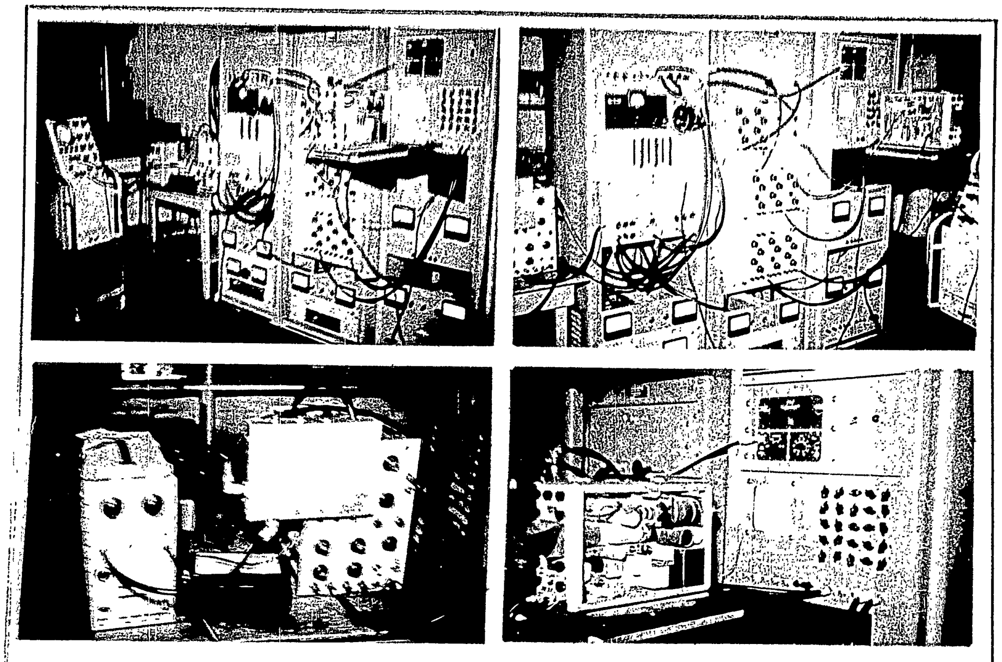

FT' xperimental Equipment

Figure 3

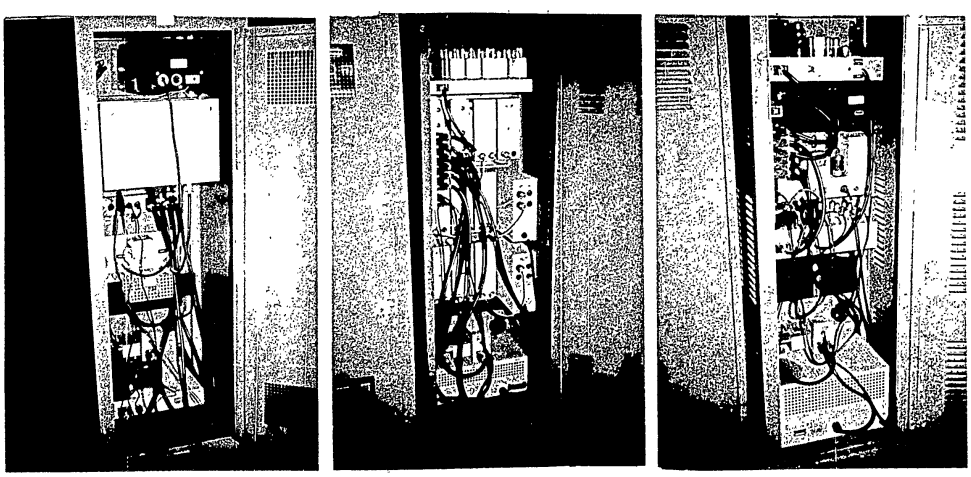

Rear Views of FT' quipment Racks

Figure 4

Storage-Tube Ambiguity Filters, in addition to its use in conventional circuity work.

PIM RADAR SIMULATOR

A block diagram of the PIM Radar Simulator, which produces simulated transmitter pulses and target echoes and a counter output pulse once each modulation cycle, to trigger the Gate Generator in the Storage-Tube Ambiguity Filter, is shown in Figure 5. The PIM Radar Simulator is composed of a PIM Modulator, Counter, Artificial Echo Unit, Random Noise Generator, and Noise and Echo Mixer.

The PIM Modulator produces the transmitter pulse output which is a train of pulse interval time modulated pulses. The modulation of the time interval is a synchronous sawtooth function. To provide synchronization of the sawtooth function with the pulse train a preset counter is used to count the output pulses. The counter returns a pulse to the PIM Modulator to initiate the sawtooth modulating function for every n pulses from the PIM Modulator.

The Artificial Echo Unit produces two echo simulating pulses for every transmitter pulse, each of which is displaced from the transmitter pulse by a fixed but controlled period of time. These two pulses simulate returns from two different targets. To provide a response that more closely approximates that of an actual radar the output of the Artificial Echo Unit is mixed in the Signal and Noise Mixer with the output of a Random Noise Generator. The output of the Signal and Noise Mixer is the Simulated Target Response.

Declassified in Part - Sanitized Copy Approved for Release @ 50-Yr 2014/01/31 : CIA-RDP81-01043R002900240002-8

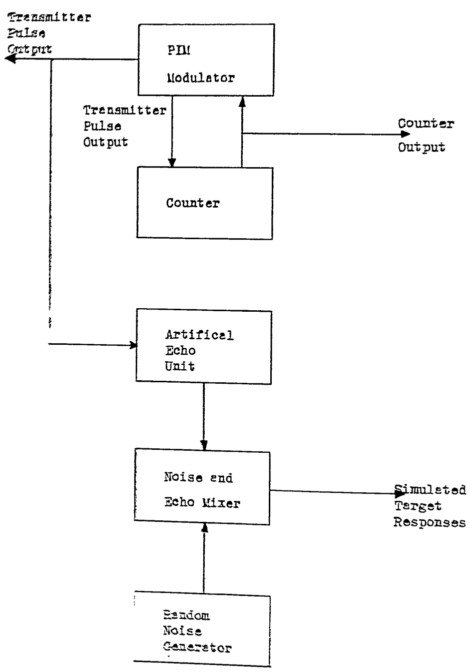

PIM Radar Simulator

Figure 5

PIM Modulator

The output of the PIM Modulator is a train of interval modulated pulses. The average pulse interval can be varied from 25 to 500 microsecond. The major period in which modulation of the pulse intervals takes place is chosen to be 2000 microseconds.

Figure 6 is a block diagram of the PIM Modulator and Figure 7 is the schematic diagram. The Pulse Generator V3 is a free running multivibrator, which generates the transmitter pulses. The frequency of the Pulse Generator is controlled by the time constant of the grid circuit of V3A and the potential applied to this grid. The average frequency is controlled by the adjustment of R105 which is in the grid circuit of V3A. The Pulse Generator is modulated by the sawtooth of voltage across the 25K resistance in the cathode circuit of V2B, which is the modulator. The sawtooth modulating voltage is generated in V1, the Sawtooth Generator. The Sawtooth Generator is triggered by the output pulse of the counter. The time constant of the plate circuit is controlled by the Linearity Control to provide a linear sawtooth voltage on the plate of the Sawtooth Generator of 2000 microsecond duration. This sawtooth of voltage is amplified in V2A and fed to the grid of the Modulator Cathode follower V2B.

The modulated train of pulses from the Pulse Generator is fed to two Pulse Amplifiers, V4 and V5, for

Declassified in Part - Sanitized Copy Approved for Release @ 50-Yr 2014/01/31 : CIA-RDP81-01043R002900240002-8

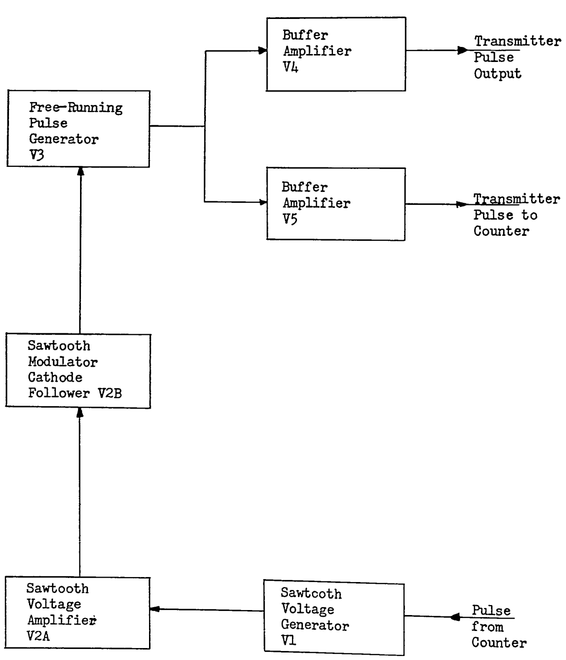

PIM Modulator

Figure 6

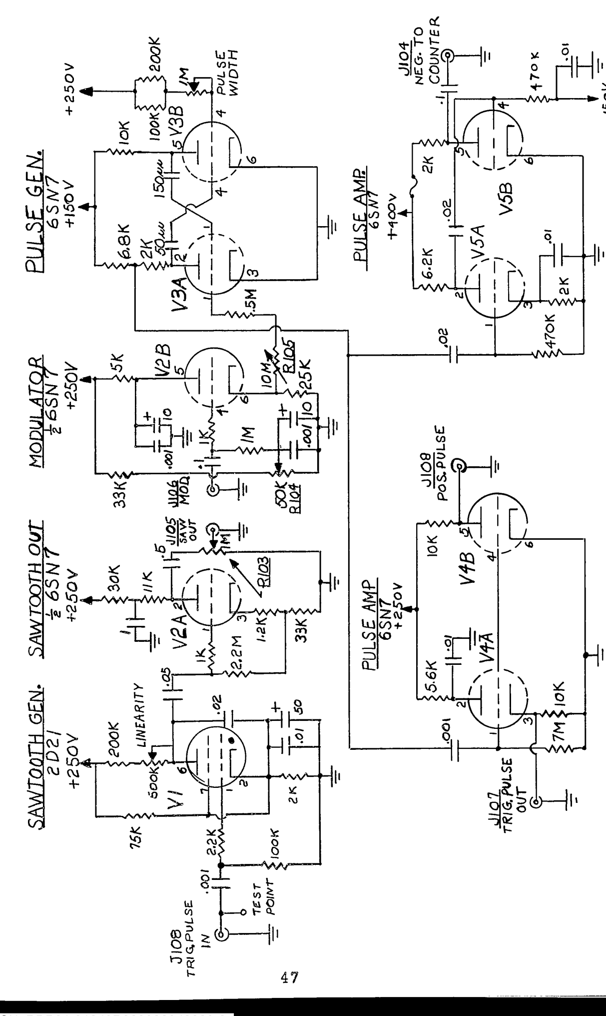

PIM Modulator

Figure 7

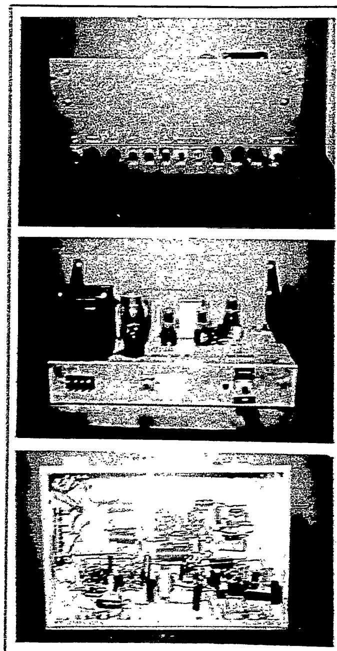

Panel View

Rear View

Bottom View

PIM Modulator

Figure 8

distribution to the output jacks.[1]

Figure 8 shows the Panel, Rear, and Bottom views of the PIM Modulator.

Counter

This is a Model 5423R Berkeley Counter and acts as a dividing Circuit. By pre-selecting a number n on the keyboard of the Counter, there will appear one pulse at the output of the Counter for every n pulses at the input. The output pulse of the Counter is fed back to the Modulator to re-cycle the modulation period.

Artificial Echo Unit

This unit is driven by the transmitter pulse from the PIM Modulator and generates pulses of variable width and amplitude, delayed from the input pulses by an adjustable amount of time. Two pulses can be produced for each input pulse representing echoes from two different targets.

Figure 9 is a block diagram of the Artificial Echo Unit and Figure 10 is the schematic diagram. The incoming pulse from the PIM Modulator is amplified and inverted in V1. After being amplified and inverted the pulse triggers a one-shot multivibrator (V2) which produces a pulse delayed from the input pulse by

---

[1] Signal Corps Contract No. DA-36039 SC-56696 Interim Report December 1953-January 1955, pp 42-43.

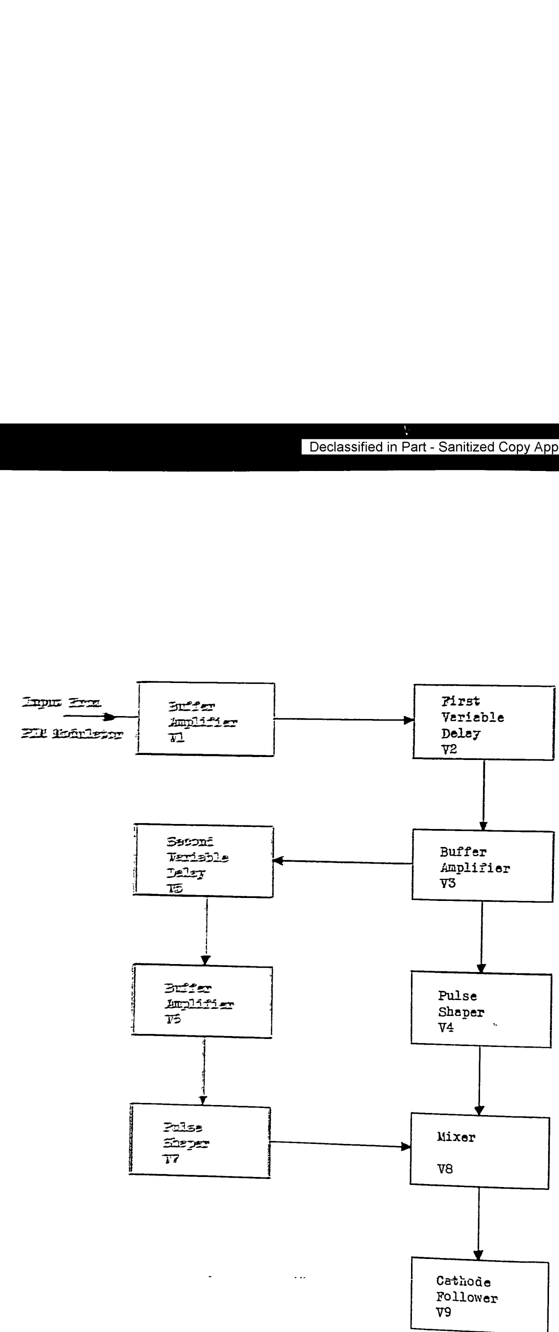

Artifical Echo Unit

Figure 9

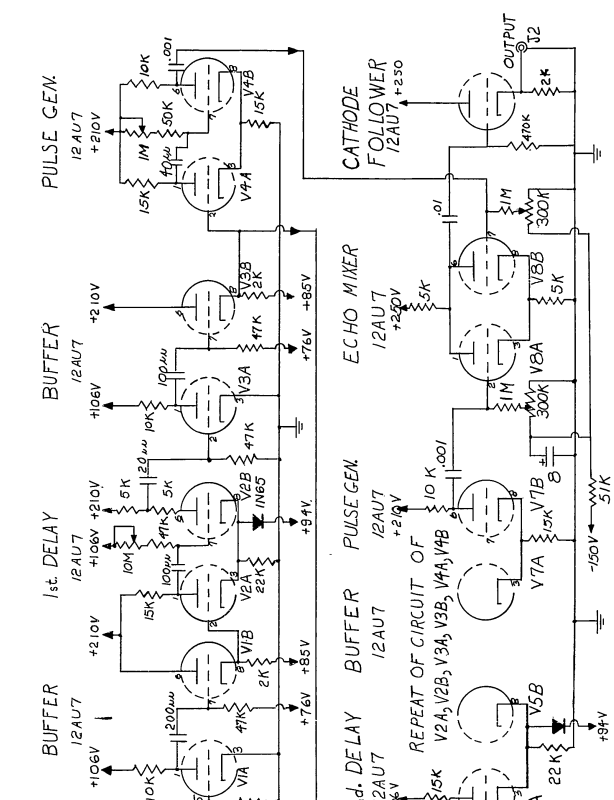

Artifical Echo Unit

Figure 10

Declassified in Part - Sanitized Copy Approved for Release @ 50-Yr 2014/01/31 : CIA-RDP81-01043R002900240002-8

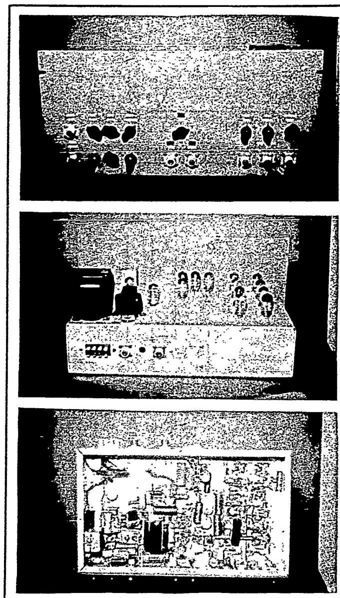

Panel View

Rear View.

Bottom View.

Artificial Echo Unit

Figure 11

20 to 500 microseconds. The output of the one-shot multivibrator is put through a buffer amplifier (V3) and applied to a pulse shaping circuit (V4) which generates a rectangular pulse whose duration can be varied between 1.3 and 10 microseconds. The pulse output of this stage is delayed from the transmitter pulse by the time determined in the 1st Delay Multivibrator V2. The output of the buffer amplifier (V3) is also applied to the 2nd Delay Multivibrator (V5) which is a one-shot multivibrator. The output of this one-shot multivibrator is applied to a pulse shaping circuit (V7) through a buffer amplifier (V6). The output of this pulse shaping circuit is a rectangular pulse similar to the output of V4 and is the second simulated target echo which is delayed from the transmitter pulse by the sum of the two delay multivibrator delay times.

The output of the pulse shaping circuits are mixed together in the Echo Mixer (V8). The output of the Echo Mixer is coupled to the output connector by a cathode follower (V9).

Figure 11 shows the Panel, Rear, and Bottom views of the Artificial Echo Unit. Also included on the chassis is some of the storage tube control circuitry.

Noise Generator

A General Radio Random Noise Generator Type No. 1390A is used along with its voltage divider. This noise generator has filters to provide random noise with band widths of 5 MC, 500 KC or 20 KC. The RMS value of noise across an 800 ohm load can be varied from zero to 2 volts, 800 ohms being the equivalent output impedance of the generator. Throughout the experimental work, except when otherwise mentioned, noise with 5 MC band width was used.

Noise and Echo Mixer

This unit mixes the output of the Artificial Echo Unit with the output of the Noise Generator.

Figure 12 is the schematic diagram of the Noise and Echo Mixer. The mixing of the signals is accomplished by the use of two cathode followers with a common cathode load. Adjustment of the signal to noise ratio is provided by the 10 K potentiometer in the cathode of the noise cathode follower.

Figure 13 is the Panel, Rear, and Bottom views of the rack unit consisting of the Noise Generator and the Noise and Echo Mixer.

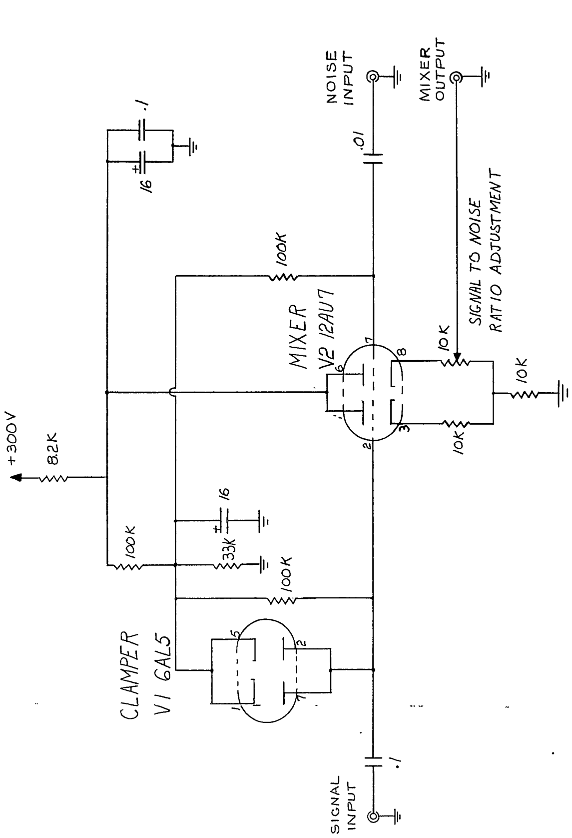

Noise and Echo Mixer

Figure 12

Declassified in Part - Sanitized Copy Approved for Release @ 50-Yr 2014/01/31 : CIA-RDP81-01043R002900240002-8

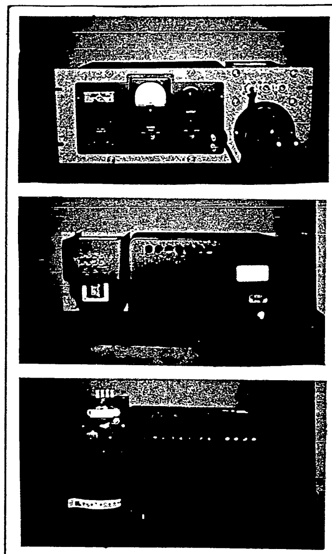

Panel View

Rear View

Bottom View

Noise Generator and Noise and Echo Mixer

Figure 13

OPTICAL-ELECTRONIC AMBIGUITY FILTER

Figure 14 is a block diagram of the Optical-Electronic Ambiguity Filter. The simulated radar response from the PIM Radar Simulator is applied as vertical deflection to the Primary Indicator. The sweep of the Primary Indicator is triggered by the transmitter pulse from the PIM Radar Simulator. The sweep length of the Primary Indicator is adjusted to be slightly less than the shortest interval between transmitter pulses.

A Tektronix Type 162 Waveform Generator is operated as a free running pulse generator to determine the repetition rate of the Dage TV Camera scanner. A second Type 162 Waveform Generator is operated as a triggered sawtooth generator to develop horizontal sweep voltage for the scanner. This sawtooth sweep voltage is amplified in the Horizontal Deflection Amplifier which drives the Horizontal Deflection Coil of the scanner with a sawtooth of current.

The scanner is a Dage Television Camera Model 100 B. Under this operation only the Vidicon, Video Amplifier, and Power Supplies are used. The Vidicon beam is not deflected vertically, but is deflected horizontally as discussed above.

The Secondary Indicator is a Tektronix Oscilloscope Type 535, triggered by the Waveform Generator which determines the repetition rate of the scanner. The Vidicon output is presented as vertical deflection on the Secondary Indicator.

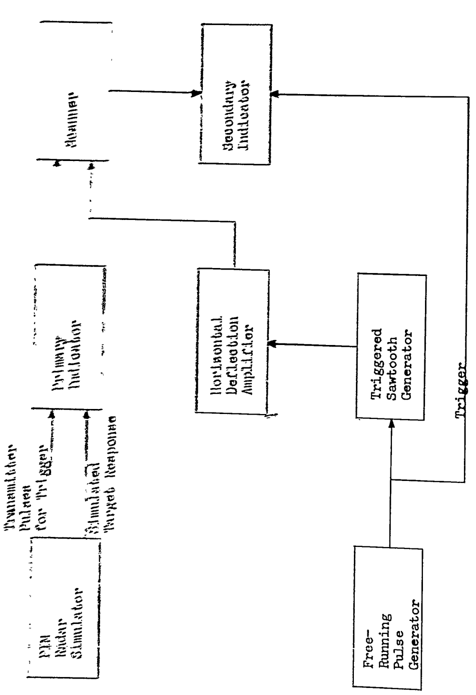

Optical-Electronic Ambiguity Filter System

Figure 14

Since the PIM radar presents the information in a number of sub-intervals, recombination of the sub-intervals is necessary. The recombination of subranges has been demonstrated with the Optical-Electronic Ambiguity Filter experimental equipment for the case of three sub-intervals.

Figure 15 is a block diagram of the recombing system. In recombining, the simulated radar response is presented as vertical deflection to the 5 Channel Oscilloscope which is the Primary Indicator. A 5 Channel Oscilloscope was constructed but due to the cost of the Tektronix pulse and sawtooth generation equipment required for sweep generation only three sub-intervals were recombined. Additional pulse and sawtooth generation equipment would allow the recombination of up to five sub-intervals with the existing Primary Indicator (5 Channel Oscilloscope) and Scanner. The horizontal sweeps of the 5 Channel Oscilloscope are delayed by slightly less than one pulse interval from each other. The scanner is caused to sweep the traces of the Primary Indicator in sequence and present the recombined information in one continuous sweep, eliminating the ambiguities of the false responses in the recombining operation.

To develop the sweep voltages for the 5 Channel Oscilloscope, Tektronix Type 162 Waveform Generators and Type 163 Pulse Generators are used.

The transmitter pulse from the PIM Radar Simulator

Declassified in Part - Sanitized Copy Approved for Release @ 50-Yr 2014/01/31 : CIA-RDP81-01043R002900240002-8

Optical-Electronic Ambiguity Filter Subrange Combining System

Figure 15

is applied to a Type 163 Pulse Generator which in turn triggers the first Type 162 Waveform Generator. The Waveform Generator generates a sawtooth voltage waveform with duration slightly less than the smallest interval between transmitter pulses. This sawtooth waveform is used to form the sweep voltage for the first beam in the 5 Channel Oscilloscope.

The sawtooth voltage from the first Waveform Generator is also used by the second Pulse Generator as a time delay before triggering. The output pulse from the second Pulse Generator can be delayed from 0 to 100 percent of the duration of the first sawtooth voltage. The second Pulse Generator triggers the second Waveform Generator which generates a sawtooth voltage for sweep of the second beam of the 5 Channel Oscilloscope. The sawtooth voltage of the Second Waveform Generator is coupled to the third Pulse Generator and the process is repeated for the third beam of the 5 Channel Oscilloscope.

The simulated radar response is amplified by the TIC Vertical Deflection Amplifier and applied to all of the traces of the 5 Channel Oscilloscope simultaneously.

An additional Tektronix Type 162 Waveform Generator is used to provide the sweep repetition frequency for the scanner. This Waveform Generator operates recurrently and provides a sawtooth voltage output which is applied to the sawtooth input of the Horizontal Deflection Amplifier. The Waveform Generator also provides a

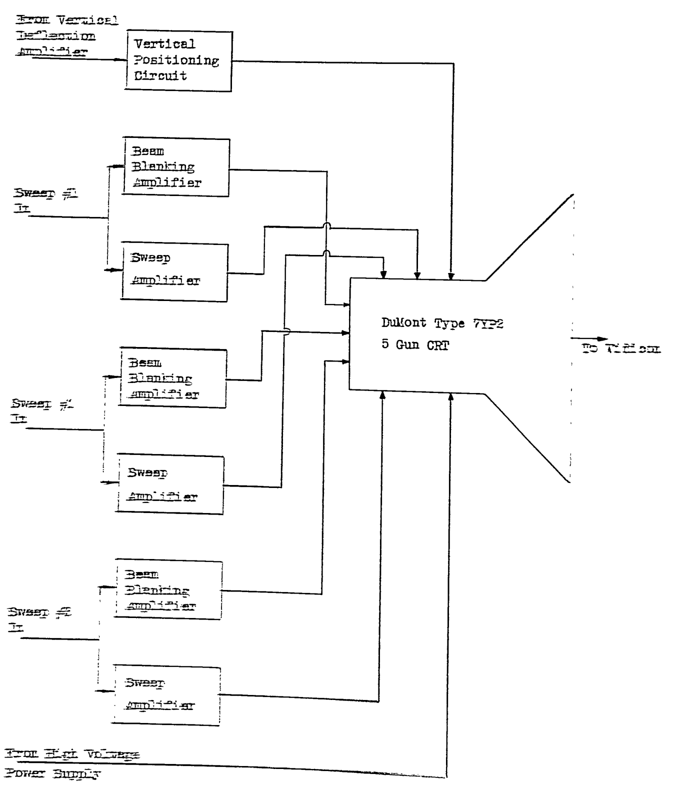

5 Channel Oscilloscope

Figure 16

pulse to trigger a Pulse Generator which is used as a pulse to operate the Staircase Voltage Generator. The pulse from the Pulse Generator is also applied to the Horizontal Deflection Amplifier to cause a more rapid retrace.

The Staircase Voltage Generator produces a staircase of voltage, the number of steps selected by the front panel switch each step initiated by a pulse from the Pulse Generator. This staircase voltage is amplified in the Vertical Deflection Amplifier and applied to the scanner as a staircase of current through the vertical deflection coil. The combination of the staircase on the vertical and sawtooth on the horizontal causes the scanner to scan the primary traces successively. The Secondary Indicator is triggered from the Staircase Generator and is sweep once for each staircase. The Vidicon output is applied as vertical deflection on the Secondary Indicator which presents the sub-ranges recombined in a total range display.

5 Channel Oscilloscope

Figure 16 is a block diagram of the 5 Channel Oscilloscope and Figures 17, 18, and 19 are the schematic diagrams.

The cathode ray tube used in this Oscilloscope is a 7YP2 which has five complete electron gun assemblies. Each electron gun as a complete set of deflection plates, allowing independent deflection of each beam.

Declassified in Part - Sanitized Copy Approved for Release @ 50-Yr 2014/01/31 : CIA-RDP81-01043R002900240002-8

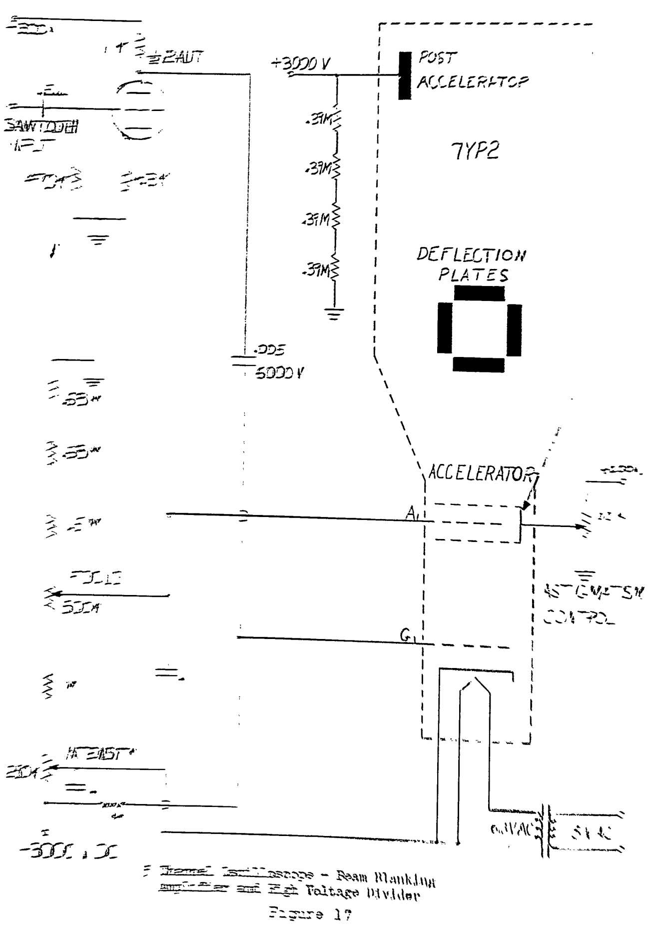

5 Channel Oscilloscope - Beam Blanking Amplifier and High Voltage Divider

Figure 17

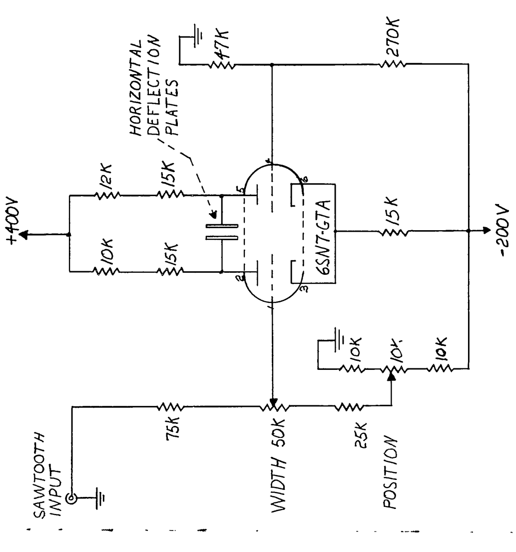

5 Channel Oscilloscope - Horizontal Sweep Amplifier

Figure 18

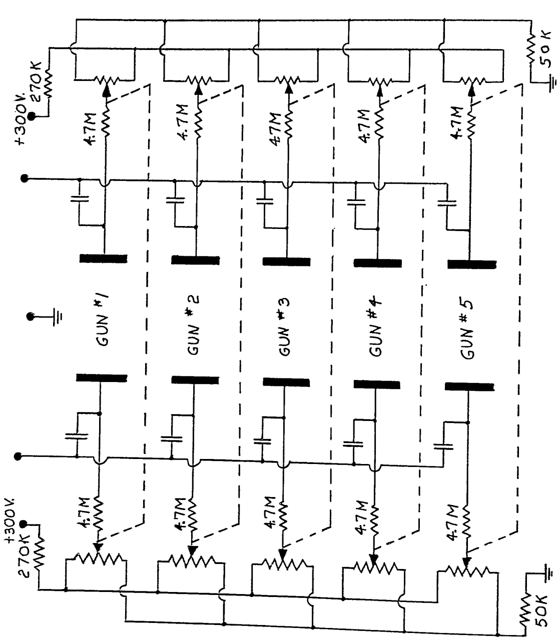

5 Channel Oscilloscope - Vertical Positioning Circuit

Figure 19

All Potentiometers are 500k dual sections.

All capacitors are 0.1 uf. at 600 volts.

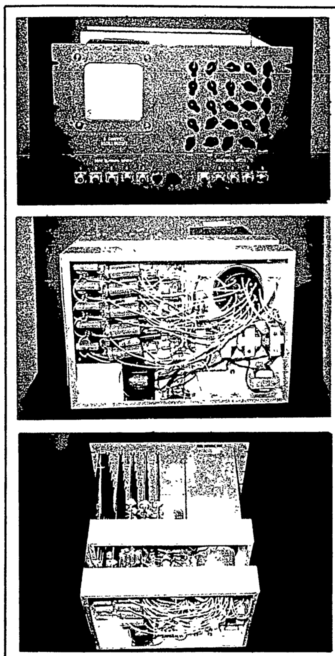

Panel View

Rear View

Top View

5 Channel Oscilloscope

Figure 20

Declassified in Part - Sanitized Copy Approved for Release @ 50-Yr 2014/01/31 : CIA-RDP81-01043R002900240002-8

The Sweep Voltage Amplifiers are dc coupled push-pull amplifiers. A total supply voltage of 600 volts is provided to allow full deflection of the beams at high accelerating voltages. The sawtooth voltage of [illegible] volts from the Waveform Generators is amplified to the (approximately [illegible] volts (push-pull) necessary for full horizontal deflection.

The blanking of the retrace of the sweeps is accomplished by the Beam Blanking Amplifiers. The horizontal sweep voltage is differentiated such that there is a positive pulse output during decay of the sawtooth. This pulse is amplified and inverted and applied to the grid of the respective cathode ray gun causing blanking of the beam during retrace.

All of the vertical deflection plates are capacitively coupled to the [illegible] Vertical Deflection Amplifier. For each pair of plates positioning is provided by a dual voltage divider.[1]

Figure [illegible] shows the Panel, Rear, and Top views of the [illegible] Channel Oscilloscope.

[illegible] Vertical Deflection Amplifier

This is a Telemeter Type 1000 amplifier built by Tel-Instruments Co., Inc. of Carlstadt, N. J.

[1]Signal Corps Contract No. DA-36-039 SC-56696 Sixth Q.P. [illegible] May [illegible] - June [illegible], pp 50-68.

Staircase Voltage Generator

The Staircase Voltage Generator is driven by pulses from the Tektronix Type 163 Pulse Generator. As each pulse enters, the output voltage of the Staircase Generator changes abruptly from its previous level to a new level. After a selected number of level changes, or steps, (between one and five) the level returns to the initial value and the cycle repeats.

Figure 21 is a block diagram of the Staircase Voltage Generator and Figures 22 , 23, 24, and 25 are the schematic diagrams. At the start of a cycle all the gates are closed (a pulse input to either input alone will not cause an output pulse), all the triggers (bi-stable Eccles-Jordan circuits) are in the same initial state (in this initial condition they will change state if a pulse is applied to the left side input but not if the pulse is applied to the right side input), the output-cathode-followers all have a positive dc potential at their input, and the reset-one-shot-multivibrator is in its stable condition. A train of positive pulses from the Tektronix Type 163 Pulse Generator is applied to the input-pulse-amplifier. Pulse No. 1 is amplified and fed to trigger No. 1 and one input of all the gate circuits. Since all the gates are closed, no output pulses are obtained from any of the gates. Trigger No. 1 is caused to change from its initial state to its other stable state. This

Declassified in Part - Sanitized Copy Approved for Release @ 50-Yr 2014/01/31 : CIA-RDP81-01043R002900240002-8

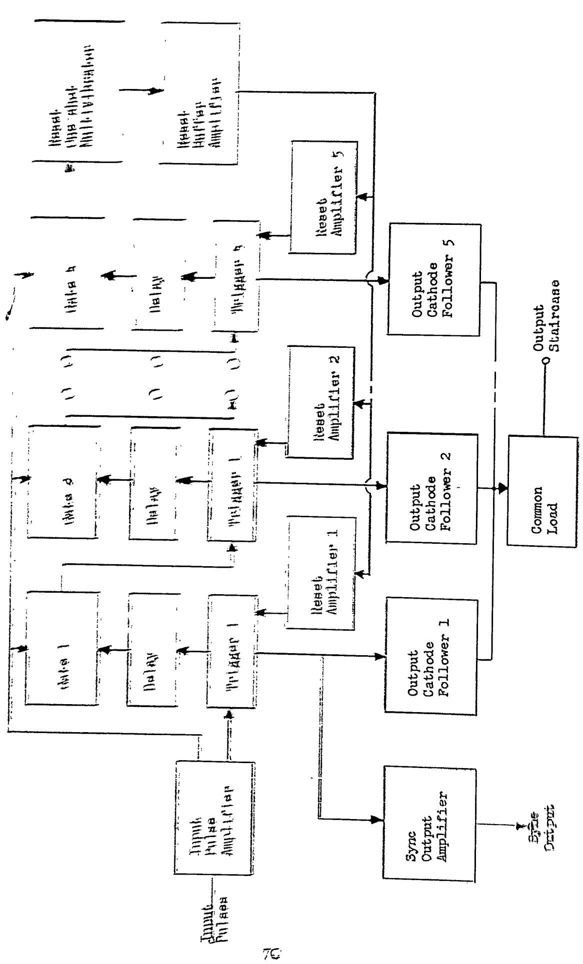

Staircase Voltage Generator

Figure 21

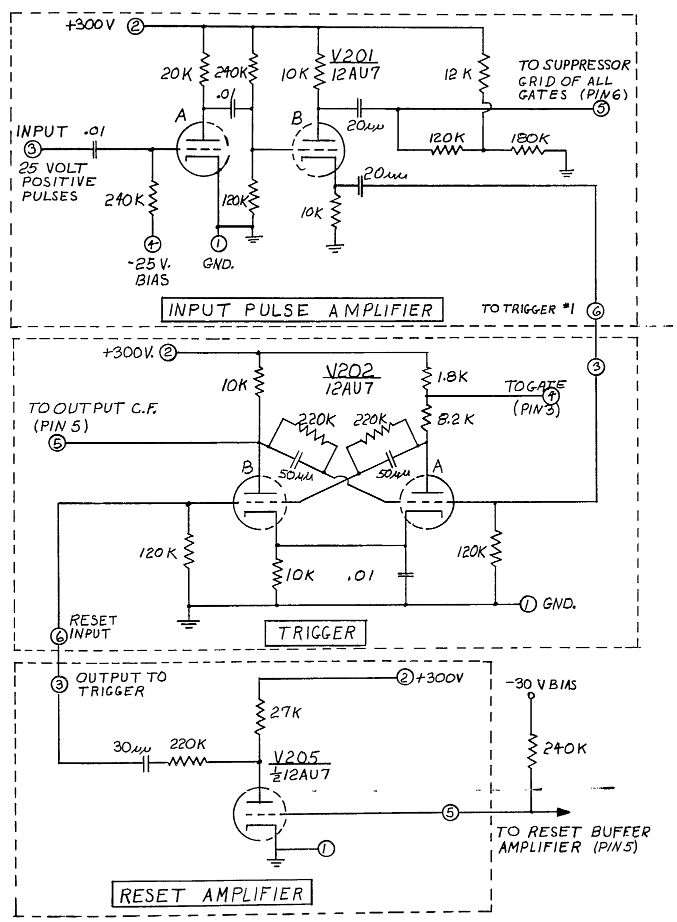

Figure 22 Staircase Voltage Generator - Input Pulse Amplifiers, Trigger No. 1 and Reset Amplifier

Declassified in Part - Sanitized Copy Approved for Release @ 50-Yr 2014/01/31 : CIA-RDP81-01043R002900240002-8

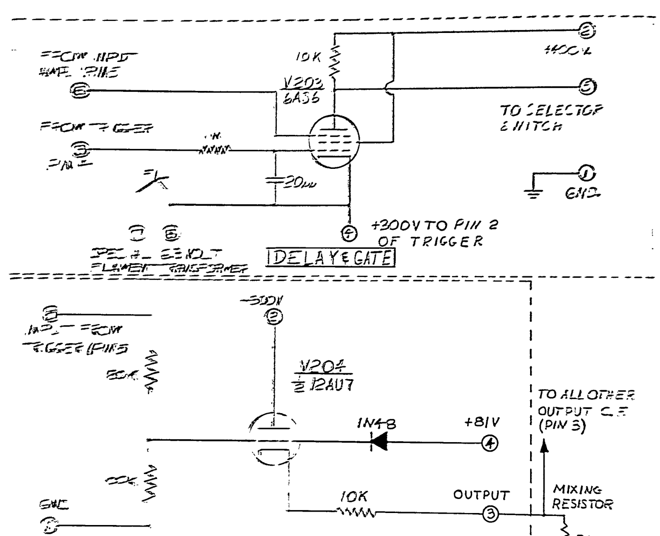

Figure 23 Staircase Voltage Generator - Delay and Gate No. 1, Output Cathode Follower No. 1, and Sync. Output Amplifier

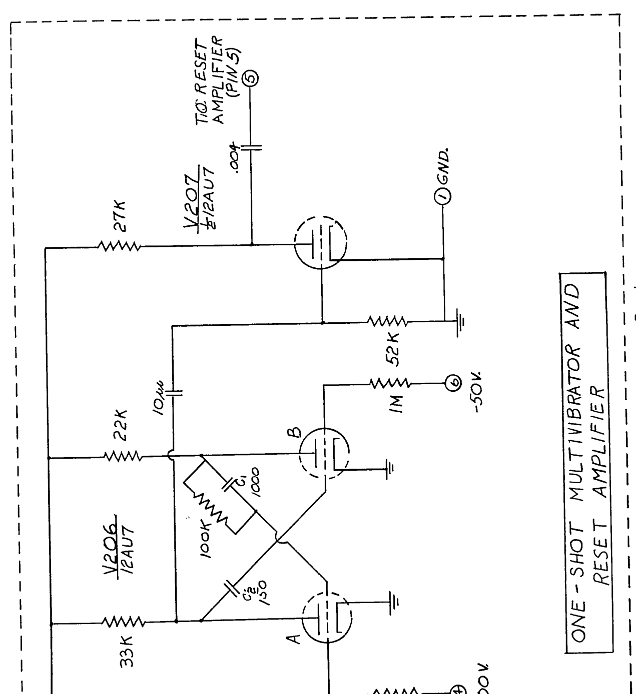

Staircase Voltage Generator - Reset one-shot Multivibrator and Reset Amplifier

Figure 24

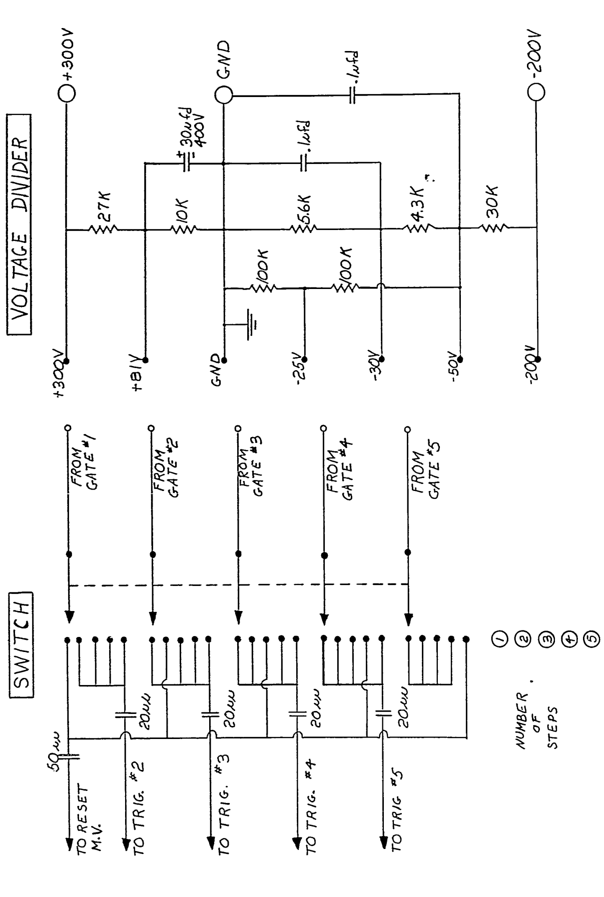

Staircase Voltage Generator - "Number of-Steps" Switch and Voltage Divider

Figure 25

change of state causes the dc level of the output of trigger No. 1, which goes to the delay circuit, to change, and after a short delay period this change of dc level is transferred to the input of gate No. 1. No output pulse is generated by gate No. 1, however, it is now open to pulses from the input-pulse-amplifier. Another output from trigger No. 1 changes the dc level at the input to output cathode follower No. 1, this change in dc level changes the current through the common load impedance and consequently the voltage across it which is the output voltage. This is the first step.

Pulse No. 2 is amplified and also fed to trigger No. 1 and one input of all the gate circuits. Since trigger No. 1 has already been triggered by pulse No. 1, no further action occurs here. At the gate circuits, all the gates are closed except gate No. 1. Thus gates No. 2, No. 3, No. 4, and No. 5 have no output pulses, but gate No. 1 has. This output pulse from gate No. 1 goes to the input of trigger No. 2 which changes state. This change of state unblocks gate No. 2 after a short time delay and changes the dc level at the input to output-cathode-follower No. 2 immediately. The change in level at the input of output-cathode-follower No. 2 changes the current through the common load impedance and consequently the voltages across it. This gives the second step in the output staircase.

As pulses No. 3, No. 4, and No. 5 enter, the process continues in similar fashion triggering triggers

Declassified in Part - Sanitized Copy Approved for Release @ 50-Yr 2014/01/31 : CIA-RDP81-01043R002900240002-8

No. 3, No. 4 and No. 5, opening gates No. 3, No. 4 and No. 5, and causing the output voltages to make the third, fourth, and fifth steps.

When pulse No. 6 enters the input-pulse-amplifier it is fed to trigger No. 1 and through gates No. 1, No. 2, No. 3, No. 4, and No. 5. No action occurs at these trigger circuits since they have all been triggered previously. Pulse No. 6 is also fed through gate No. 5 to the reset-one-shot-multivibrator. The reset-one-shot-multivibrator generates a single pulse whose duration is approximately one-half the minimum time interval between two successive input pulses. This pulse is differentiated and fed to the reset-buffer-amplifier which puts out a single pulse coinciding in time with the end of the square pulse generated by the reset-one-shot-multivibrator. This pulse is fed simultaneously to all the reset-amplifiers. These reset-amplifiers apply the pulses to the second input terminal of each of the triggers, causing them to revert to their original state, as at the beginning of the cycle. Pulse No. 7 will cause a second cycle to start and the entire procedure will repeat.

The number of steps in the output voltage can be varied by changing the number of triggers and their associated gates, output-cathode-followers, and reset amplifiers. The selector switch shown in Figure 25 is incorporated in the unit so as to change the effective number of triggers in operation between one and five.

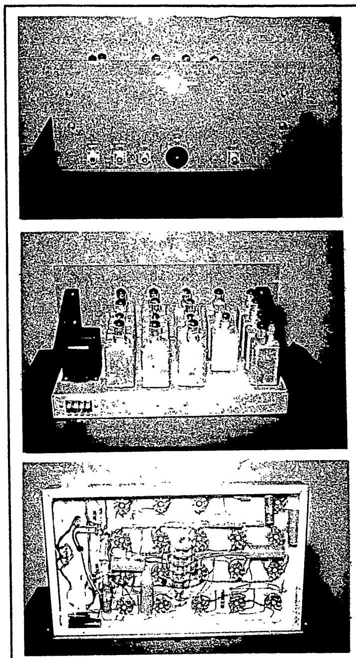

Panel View

Rear View

Bottom View

Staircase Voltage Generator

Figure 26

Declassified in Part - Sanitized Copy Approved for Release @ 50-Yr 2014/01/31 : CIA-RDP81-01043R002900240002-8

The sync.-pulse-output-amplifier shown in Figure 23 delivers an external sync pulse in synchronism with the first step in the staircase voltage output. This sync pulse is used to synchronize the sweep of the Secondary Indicator.[1]

Figure 26 shows the Panel, Rear, and Bottom views of the Staircase Voltage Generator.

Vertical Deflection Amplifier

Figure 27 is a block diagram of the Vertical Deflection Amplifier and Figure 28 is the schematic diagram. The Vertical Deflection Amplifier accepts the staircase voltage from the Staircase Voltage Generator and produces a current of the same waveform in the Vertical Deflection Coil of the Vidicon tube.

The Vertical Deflection Amplifier is essentially a power amplifier with a large amount of negative current feedback. The circuit is composed of two resistance coupled voltage amplifiers, (V1A and V2A), a power amplifier (V3), feedback voltage regulator (V4), feedback amplifier (V5), feedback cathode follower (V2B), and linearity control (V1B).

The input voltage is appliedto the cathode of V1A. Since the grid-to-cathode voltage of V1A is a function of not only theinput voltage but also of the

[1]Signal Corps Contract No. DA-36-039 SC-56696 Sixth Q.P. R. May 1955-July 1955, pp 80-103.

grid voltage which is controlled by the cathode voltage of V2B, the plate voltage of V1A is a function of both the input voltage and the cathode follower (V2B) current. The effect of the grid voltage on V1A may be such as to either increase or decrease the gain depending on the phase relation between the grid voltage and the input voltage. In this circuit, the two are 180 degrees out of phase, hence the voltage from V2B tends to reduce the gain of the first stage (V1A), providing that the deflection coil current has the same waveform as the input voltage. The ac components of the plate waveform of V1A are coupled to the grid of V2A. V2A is a linear voltage amplifier and the ac components of its plate voltage are coupled to the grid of V3. With no input signal at the grid of V3 the vertical position bias control provides the necessary bias to the grid of V3 so that the plate voltage of V3 is approximately 100 volts. The deflection coil is connected between point X and the plate of V3. Point X is maintained at 100 volts by V4 and under these conditions the voltage across the deflection coil is zero, consequently the coil current is zero. If a positive signal is applied at the input, the grid of V3 will be driven negative by the voltage amplifiers (V1A and V2B). The plate voltages of V3 will rise above 100 volts, impressing a voltage across the deflection coil from the plate of V3 to point X. This current flowing thru the 5.1 K ohm resistor in the

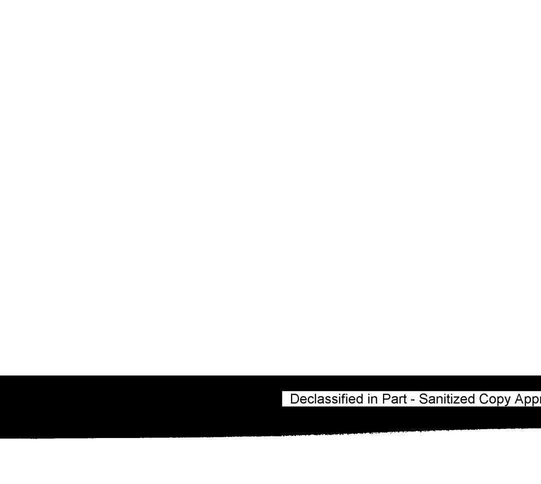

Vertical Deflection Amplifier

Figure 27

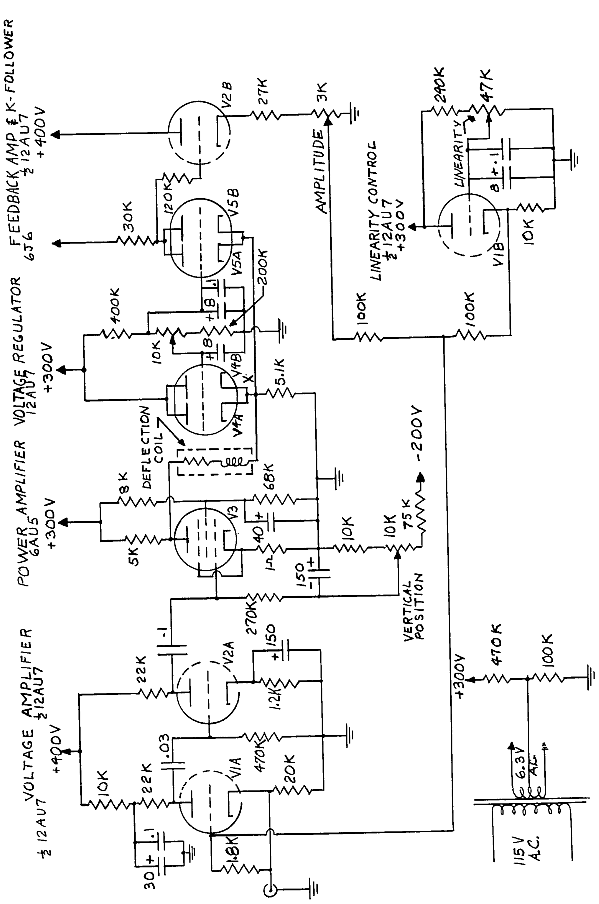

Vertical Deflection Amplifier

Figure 28

cathode circuit of V4 causes an additional voltage drop across the cathode resistor. This additional voltage drop is partially cancelled out by a decrease of current flow thru V4 since the grids of V4 are maintained at a fixed potential. The rise in voltage on the cathodes of V4 is also present on the cathodes of V5. The grids of V5 are also held at a fixed potential and the rise in voltage on the cathodes causes the plate voltage of V5 to increase. The plates of V5 are direct coupled to V2B which is a cathode follower. The cathode follower output which is a rise in voltages across the amplitude control is applied to the grid of V1A thru a resistive network. This resistive network in conjunction with V1B sets the reference level of the feedback voltage thereby controlling the linearity. If the above process proceeds instantaneously, the coil current follows the variations in the input voltage with no time lag. If the coil current does not follow instantaneously, the cancelling effect of the voltage from V2B fed back to V1A will lag and the gain of this first stage will be much greater than before. This increased gain will cause a much higher voltage to be applied to the deflection coil to accelerate the current change. When the change does occur, the feedback will reduce the gain of the input stage which removes the excess voltage from the deflection coil. Direct coupling in the feedback loop is employed to improve the low

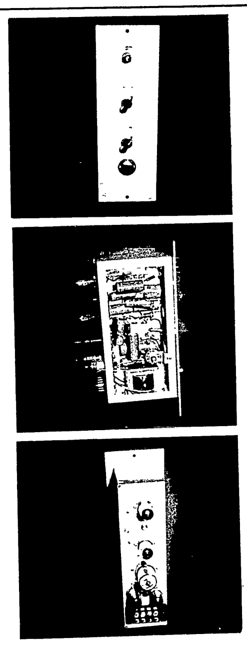

Vertical Deflection Amplifier

Figure 29

frequency response.[1]

Figure 29 shows the Panel, Side, and Rear views of the Vertical Deflection Amplifier.

Horizontal Deflection Amplifier

Figure 30 is a block diagram of the Horizontal Deflection Amplifier and Figure 31 is the schematic diagram.

The sawtooth voltage input from the Tektronix Type 162 Waveform Generator is amplified in V1A and mixed, in the common plate resistor, with the pulse from the type 163 Pulse Generator which is amplified in V1B. The output from V1, which is a sawtooth voltage with a rapid decay and negative overshoot, is coupled to V2, the power amplifier. V3 and V4 form a voltage regulator which maintains a constant voltage at point Y. The deflection voltage for the horizontal deflection coil is developed between the plate of V2 and point Y. Horizontal positioning is accomplished by adjusting the bias on V2 and thus the average plate voltage of V2 and average current thru the deflection coil.[2]

Figure 32 shows the Panel, Side, and Rear views of the Horizontal Deflection Amplifier.

[1]Signal Corps Contract No. DA-36-039 SC-56696 Sixth Q. P.R. May 1955-July 1955, pp 104-125.

[2]Signal Corps Contract No. DA-36-039 SC-56696 Sixth Q. P.R. May 1955-July 1955, pp 73-80.

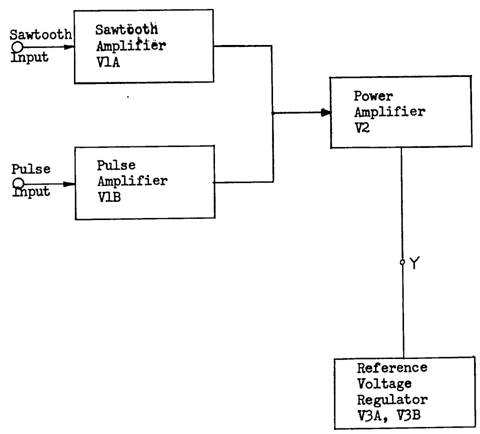

Horizontal Deflection Amplifier

Figure 30

Declassified in Part - Sanitized Copy Approved for Release @ 50-Yr 2014/01/31 : CIA-RDP81-01043R002900240002-8

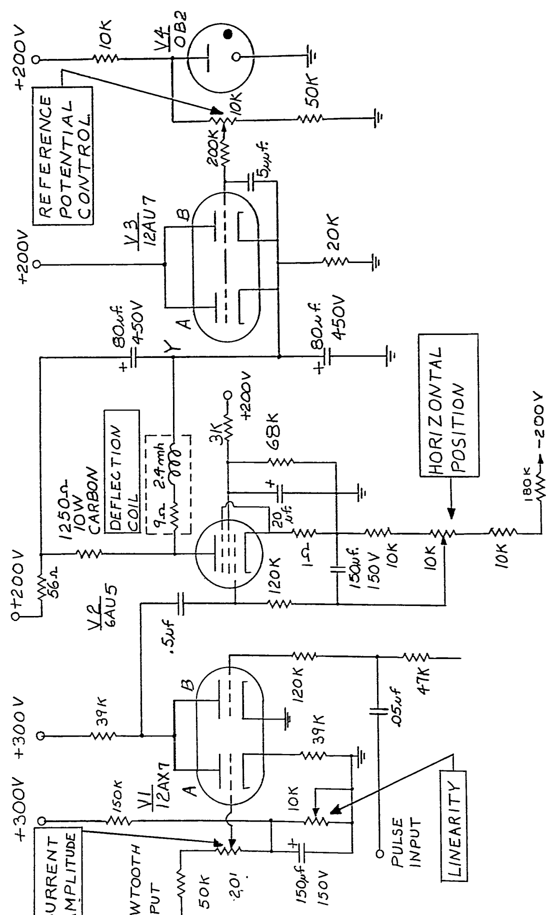

Horizontal Deflection Amplifier

Figure 31

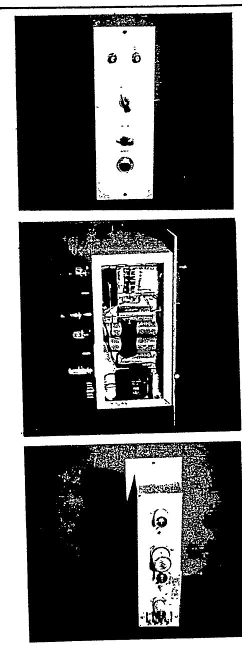

Panel View

Side View

Rear View

Horizontal Deflection Amplifier

Figure 32

Declassified in Part - Sanitized Copy Approved for Release @ 50-Yr 2014/01/31 : CIA-RDP81-01043R002900240002-8

STORAGE-TUBE AMBIGUITY FILTER

In the Storage-Tube Ambiguity Filter system the barrier grid storage-tube essentially replaces the Primary Indicator and the Scanner of the Optical-Electronic Ambiguity Filter system.

Figures 33 and 34 are block diagrams of the two Storage-Tube Ambiguity Filter systems which have been considered. They differ only in the method of writing the simulated radar response in the storage tube.

The PIM Radar Simulator provides the transmitter pulses for timing, simulated radar responses, and the counter output pulse. The counter output pulse triggers the Gate Generator which produces a gate of one pulse interval duration once in every modulation cycle. During this gate interval the information deposited in the storage tube during the other n-l pulse intervals in the modulation cycle is read out.

The Gate Generator's output is applied to the Write Amplifier to disable the Write Amplifier during the reading time. The Gate Generator's output is also applied to the Potential Shifter which shifts the voltage between the back plate and the barrier grid of the storage tube to change the storage tube from a write to a read condition. The output of the storage tube is amplified by the Read Amplifier and observed on the Secondary Indicator which is triggered by the Gate Generator.

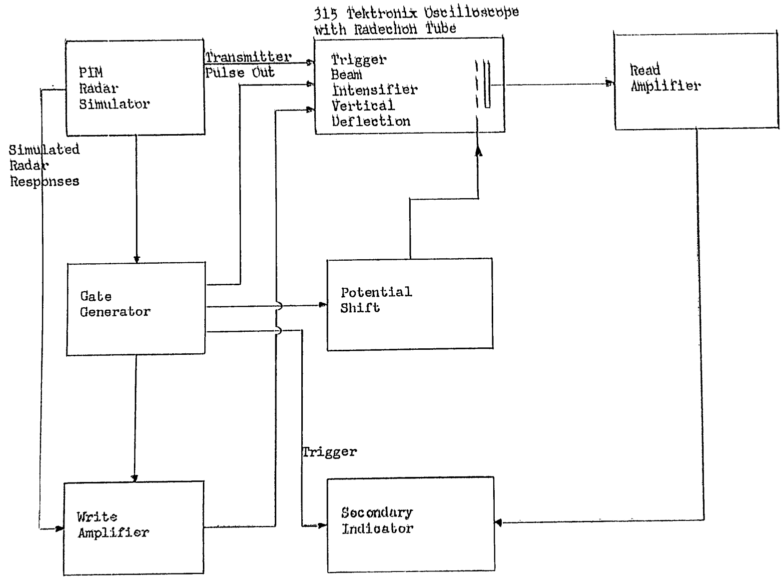

Storage Tube Ambiguity Filter System,
Deflection-Modulation, Base-Line-Scanning

Figure 33

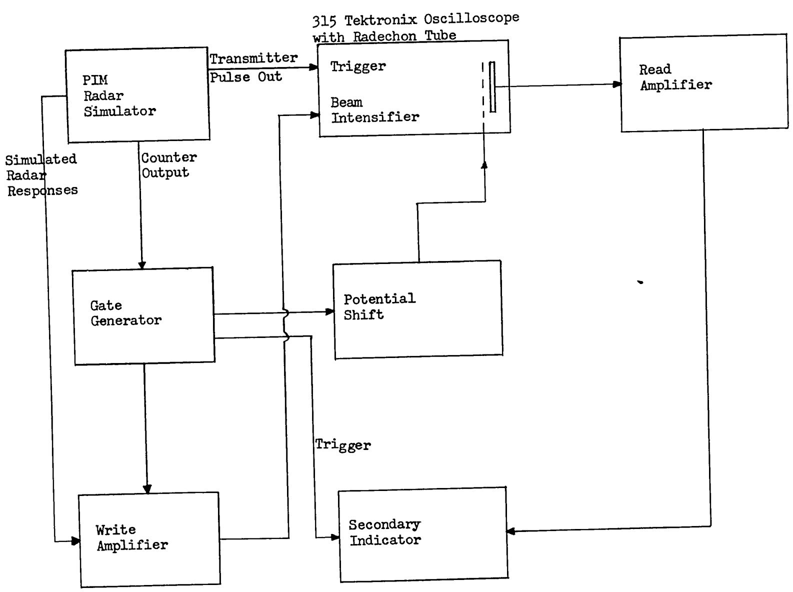

Storage Tube Ambiguity Filter System,
Negative-Intensity_Modualtion, Base-Line-Scanning

Figure 34

In Figure 33, with Deflection-Modulation, Base-Line-Scanning, the output of the Write Amplifier is applied to the vertical deflection circuit of the Storage Tube Unit. During reading, since the echo signal is eliminated by the disabled Write Amplifier, the base line of the stored response is scanned. Constant beam currents are used during reading and writing with the reading beam current being increased above the writing beam current for maximum signal output. This is accomplished by applying the Gate Generator's output to the intensifier input of the Storage Tube Unit.

In Figure 34 with Negative-Intensity-Modulation, Base-Line-Scanning, the output of the Write Amplifier is applied to the Intensifier input of the Storage-Tube Unit. The grid bias of the storage-tube is set such that echoes will cut off the storage-tube beam current. During reading the video is gated out by the Write Amplifier and the target swept with a constant beam current.

Gate Generator

Figure 35 is a block diagram of the Gate Generator and Figure 36 is the schematic diagram.

A positive trigger pulse from the Counter is applied to the Gate Generator's input. This pulse triggers the one-shot multivibrator (V1) which generates the gate pulse. The gate width is controlled by the 10 megohm potentiometer in the grid circuit of V1B. The gate width is adjusted to equal the smallest time interval

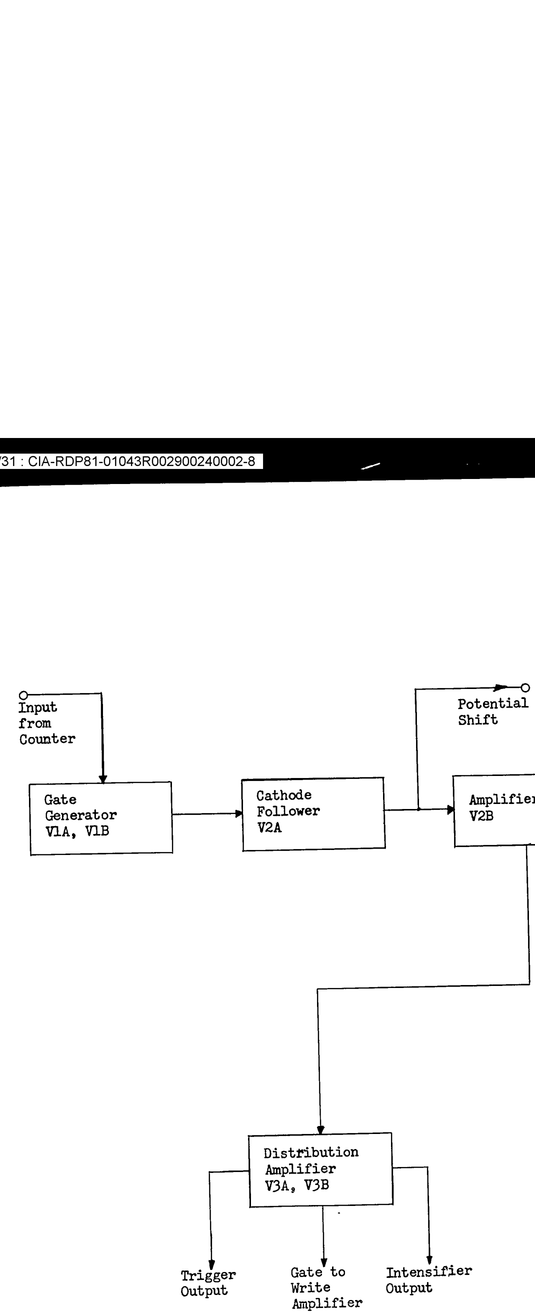

Gate Generator
Figure 35

Declassified in Part - Sanitized Copy Approved for Release @ 50-Yr 2014/01/31 : CIA-RDP81-01043R002900240002-8

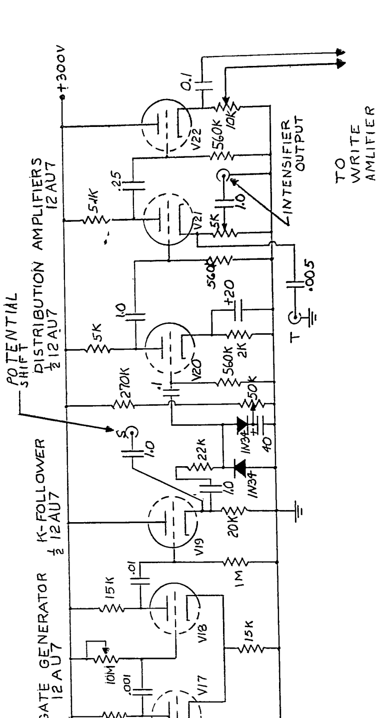

Gate Generator

Figure 36

between successive transmitter pulses. Tube V2A is a cathode follower whose output is clipped to obtain a flat topped gate. An output is taken from this cathode follower for the Potential Shifter. The gate pulse is amplified in V2B and distributed by the distribution amplifier (V3) with outputs taken from V3A (negative) and V3B (positive). The negative gate output is used for triggering purposes and beam intensifying and the positive gate output is used to gate the Write Amplifier.[1]

The circuitry of the Gate Generator is included on the Artificial Echo Unit chassis.

Write Amplifier

Figure 37 is a block diagram of the Write Amplifier and Figure 38 is the schematic diagram.

The simulated radar response is applied to the control grid of the gated video amplifier (V1). This video amplifier is gated off during the read interval by lowering the screen grid potential to below the cathode potential, thereby cutting the tube off. This is accomplished by connecting the screen grid of the gated video amplifier to the plate of the gate tube (V2) which is driven into heavy conduction during the read interval by the positive gate input from the Gate Generator.

[1] Signal Corps Contract No. DA-36-039 SC-56696 Fifth Q. P. R. February 1955-April 1955, pp 107-118.

Declassified in Part - Sanitized Copy Approved for Release @ 50-Yr 2014/01/31 : CIA-RDP81-01043R002900240002-8

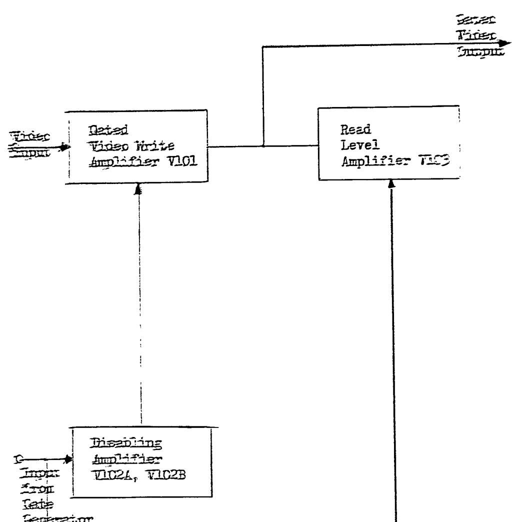

Write Amplifier

Figure 37

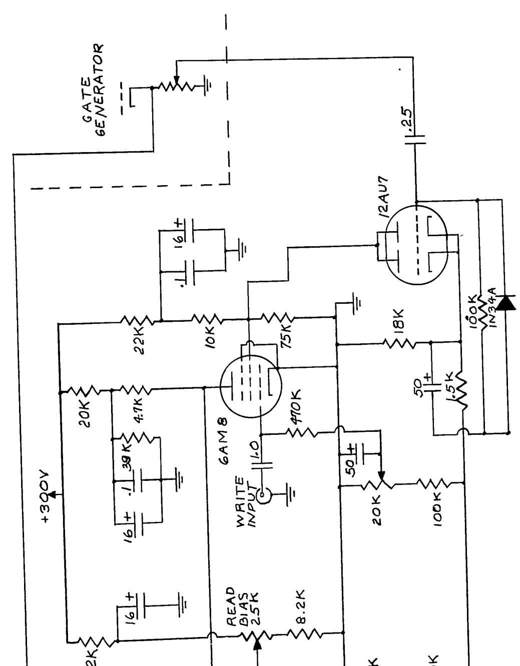

Write Amplifier

Figure 38

The positive gate voltage is also applied to the read level amplifier (V3) which is normally cut off. This tube having a common plate load resistance with the gated video amplifier determines the voltage output during the read interval when the gated video amplifier is cut off. This is controlled by the read bias control which controls the screen grid potential on the read level amplifier.

In Deflection-Modulation, Base-Line-Scanning the voltage level during reading must be the same as the base line voltage level during writing but in Negative-Intensity-Modulation, Base-Line-Scanning the voltage level during reading is decreased to increase the beam current in the storage-tube.

The circuitry of the Write Amplifier is included on the Artificial Echo Unit Chassis.

Potential Shifter

Figure 39 is a block diagram of the Potential Shifter and Figure 40 is the schematic diagram.

The Potential Shifter provides the necessary voltage between the back plate and barrier grid of the storage-tube to shift from a read to write condition. The Potential Shifter also provides a low impedance from the back plate to ground during writing and a high impedance from the back plate to ground during reading.

The positive gate input from the Gate Generator is applied to the phase splitter (V1B) which in turn applies the gate voltage to the two cathode followers (V2 and V3).

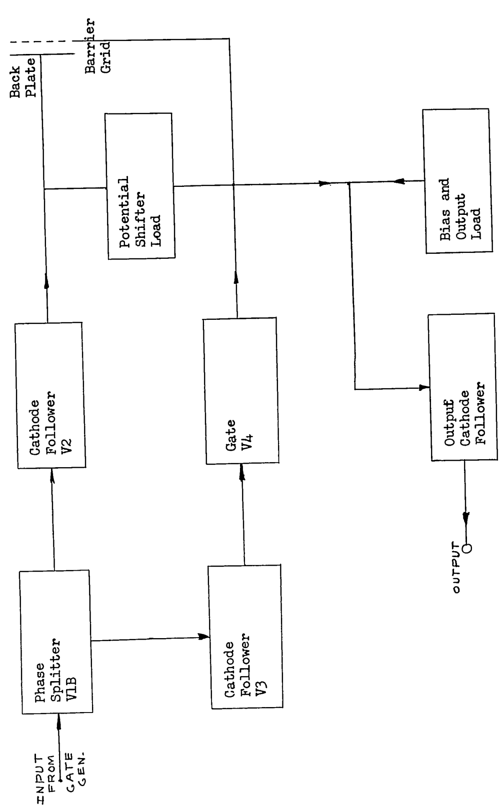

Potential Shifter

Figure 39

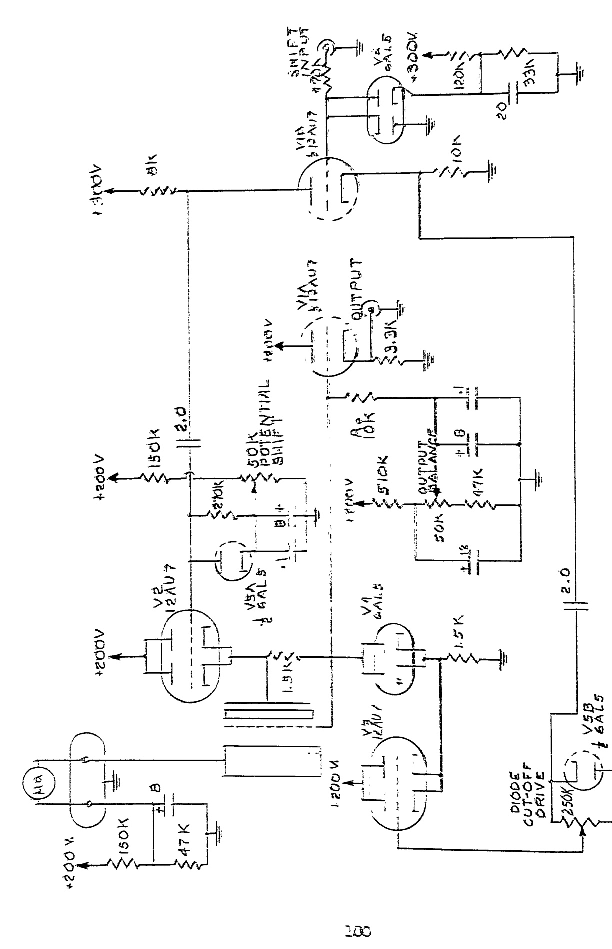

Potential Shifter

Figure 10

During writing V2 is in conduction and V3 is cut off. In this condition the diode gate (V4) is in conduction and current flows thru the potential shift load resistance. This current provides a voltage drop across the resistance which makes the back plate positive with respect to the barrier grid. The diode gate provides the low impedance to ground.

The positive input from the Gate Generator during the read time cuts V2 off and causes V3 to conduct. The additional voltage developed across the common cathode resistance of V3 and V4 opens the diode gate.

In this condition there is no current thru the potential shifter load resistor and the back plate and barrier grid are at the same potential. Since the diode gate has opened the back plate has a high impedance to common thru the output load impedance. A small amount of bias voltage is provided to compensate for the diode drop during writing and provide a constant level output over the entire cycle. The output signal developed across the output load impedance is cathode followed in V1A and applied to the Read Amplifier. The Potential Shifter can be seen mounted on the front of the Storage-Tube Unit which is the Type 315 Tektronix Scope in Figure 42

Storage-Tube Unit

This unit is a Type 315 Tektronix Scope with the CRT removed and replaced by the Radechon Type C 73405A storage-tube. The high voltage supply and the horizon-

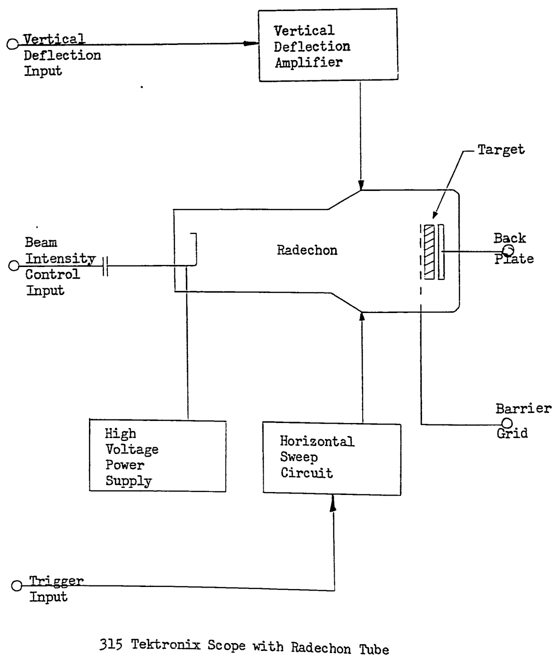

315 Tektronix Scope with Radechon Tube

Figure 41

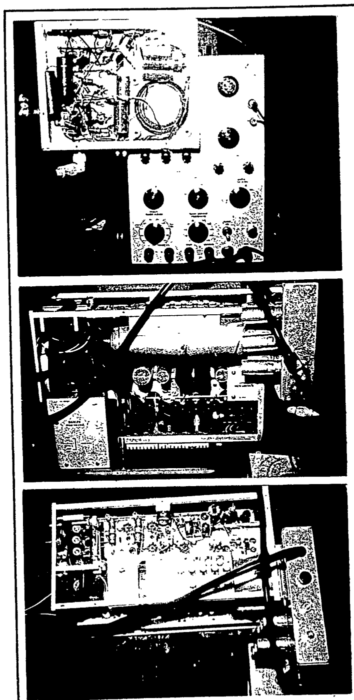

Storage-Tube Unit

Figure 42

Declassified in Part - Sanitized Copy Approved for Release @ 50-Yr 2014/01/31 : CIA-RDP81-01043R002900240002-8

tal and vertical deflection circuits of the oscilloscope are used with the storage-tube.

Figure 41 is a block diagram of the unit. The horizontal sweep is triggered by the transmitter pulses from the PIM Radar Simulator. The duration of the sweep is manually controlled to correspond to the smallest interval between two successive transmitter pulses.

The output of the Write Amplifier is applied to the vertical deflection amplifier's input for Deflection-Modulation, Base-Line-Scanning and to the cathode of the storage tube for Negative-Intensity-Modulation, Base-Line-Scanning.

The collector current of the storage tube is metered by a Simpson Type 268 meter.

The Potential Shifter chassis is mounted on the front of the Type 315 Tektronix scope to allow for the shortest lead connections to the barrier grid and the back plate.[1]

Figure 42 shows the Front, Top, and Side views of the Storage-Tube Unit.

Read Amplifier

This is a Tektronix Type 121 Wide Band Pre-Amplifier.

[1]Signal Corps Contract No. DA-36-039 SC-56696 Fifth Q.P. R. February 1955-April 1955, pp 107-118.

POWER SUPPLIES AND REGULATORS

D.C. Voltage Regulators

Three units of this type were constructed to provide the necessary plate supply and bias voltages with a minimum number of power supplies.

Figure 43 is the schematic diagram of the plug-in regulator unit constructed by Mega Research, Inc., of Dover, N.J., with the necessary modifications listed to determine the range of operation and the polarity of the output voltage.

Figure 44 is the schematic diagram of two of the DC Voltage Regulators constructed for positive-voltage regulation. Each regulator unit is capable of providing two regulated and metered output voltages from one power supply. The power supply output itself is also metered in the regulator unit and is also available at the output terminals of the regulator unit.

Figure 45 is the schematic diagram of the third DC Voltage Regulator. This unit was constructed to regulate the output two negative-voltage supplies.

Figure 46 shows the Panel, Rear, and Bottom views of the DC Voltage Regulator.

High Voltage Power Supply

Figure 47 is a schematic diagram of the High Voltage Power Supply which provides accelerating and post accelerating voltage to the 5 Channel Oscilloscope. The High Voltage Power Supply provides a positive 3500 volt output

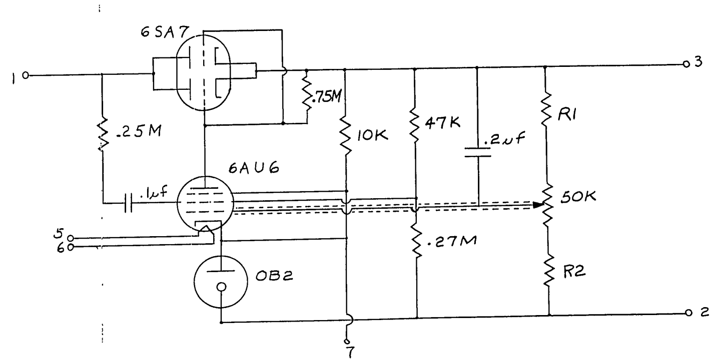

R_1 = 120k R_2 = 82k for 300-400 Volt Operation

R_1 = 75k R_2 = 27k for 200-300 Volt Operation

No. 327 case tied to pin 3
No. 321 case tied to pin 2

D. C. Voltage Regulator Plug-in Unit

Figure 43

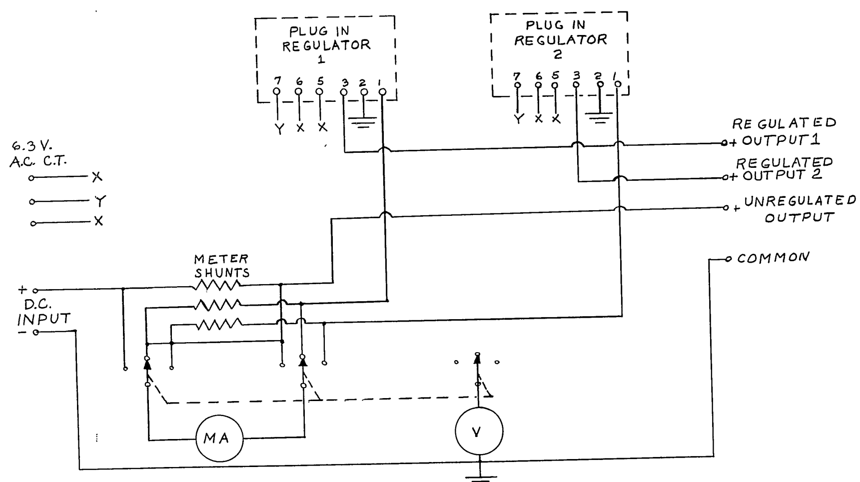

D. C. Voltage Regulator for Positive Voltage Operation

Figure 44

Declassified in Part - Sanitized Copy Approved for Release @ 50-Yr 2014/01/31 : CIA-RDP81-01043R002900240002-8

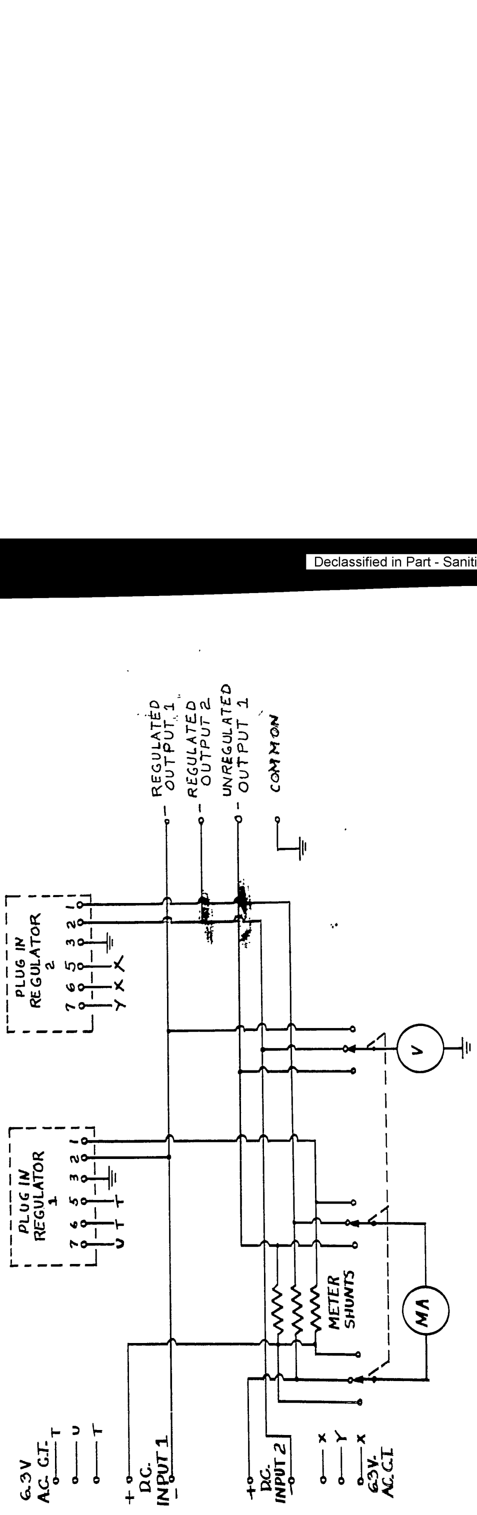

D. C. Voltage Regulator for Negative Voltage Operation

Figure 45

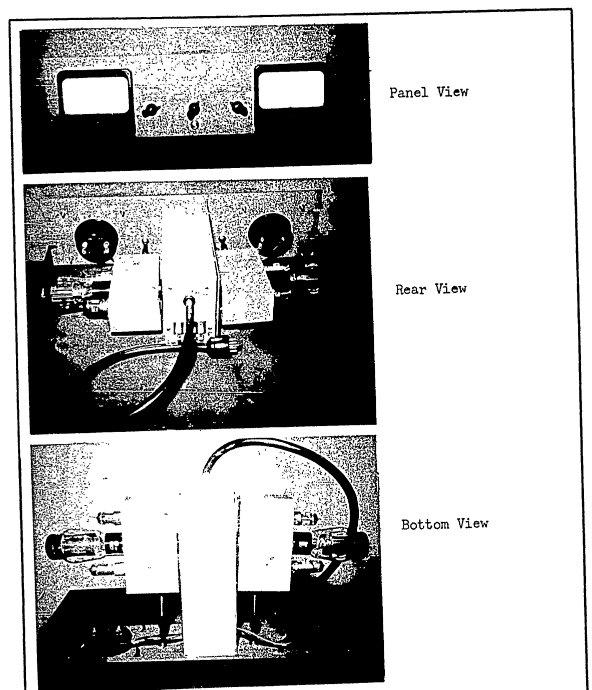

D C Voltage Regulator

Figure 46

Declassified in Part - Sanitized Copy Approved for Release @ 50-Yr 2014/01/31 : CIA-RDP81-01043R002900240002-8

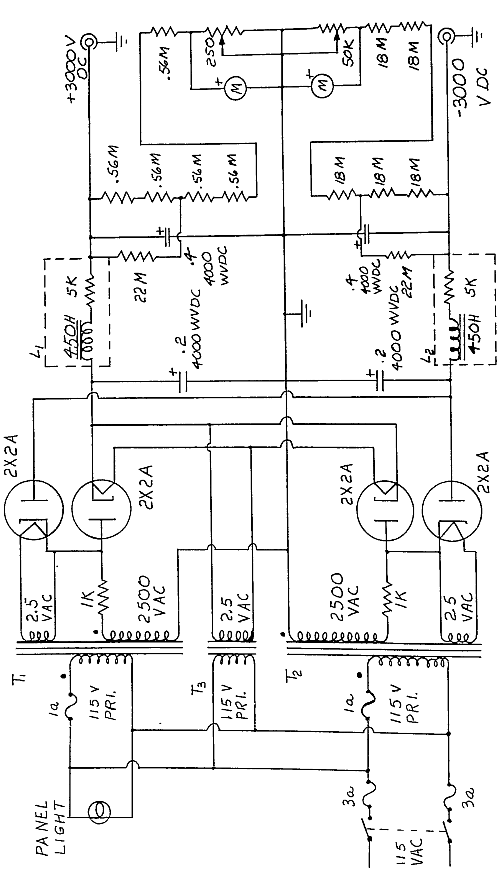

High Voltage Power Supply

Figure 47

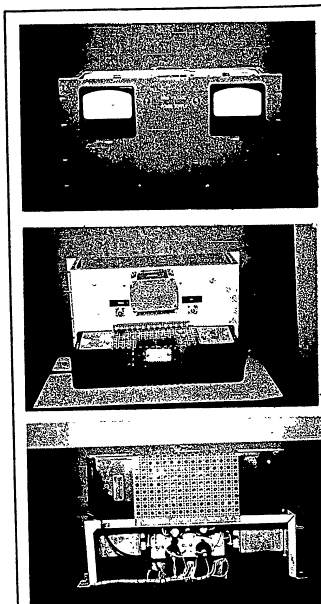

Panel View

Rear View

Bottom View

High Voltage Power Supply

Figure 48

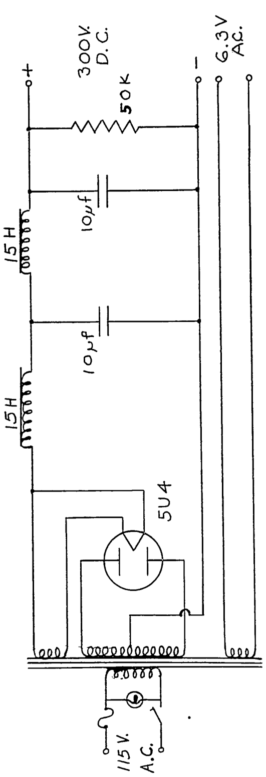

Dual D. C. Power Supply

Figure 49

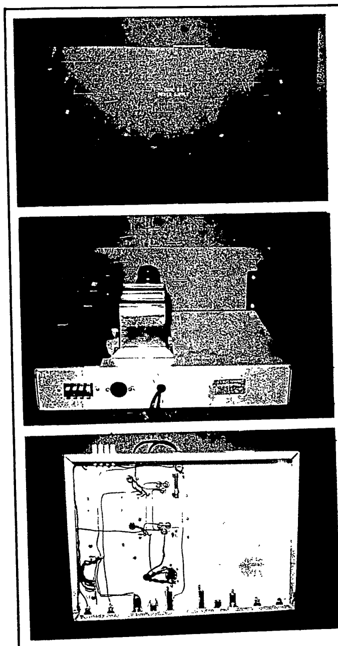

Panel View

Rear View

Bottom View

Dual D C Power Supply

Figure 50

and a negative [illegible] volt output.

Figure [illegible] shows the Panel, Rear, and Bottom views of the High Voltage Power Supply.[1]

Dual DC Power Supply

The panel and chassis for the Dual DC Power Supply were designed to accommodate two independent power supplies in the rack unit. Only one power supply was required at this time and hence only one has been constructed on the chassis. The power supply provides a 300 volt output which is used as the negative-voltage supply.

Figure [illegible] is the schematic diagram and Figure 50 shows the Panel, Rear, and Bottom views of the Dual DC Power Supply.

Positive-Voltage Power Supplies

Two Sorensen Power Supplies are used to provide the positive-voltage dc voltages. These power supplies are a Model [illegible] Nobatron and a Model [illegible] Nobatron.

Potential Shifter Ripple Filter Chassis

Figure 51 is a schematic diagram of the Potential Shifter Ripple Filter Chassis.

This additional filtering of the supply voltages was necessary in order not to mask the small output voltage from the storage-tube in the output circuits.

[1] Signal Corps Contract No. DA-36-039 SC-56696 Sixth Q.P. R. May [illegible]-July [illegible], p. [illegible].

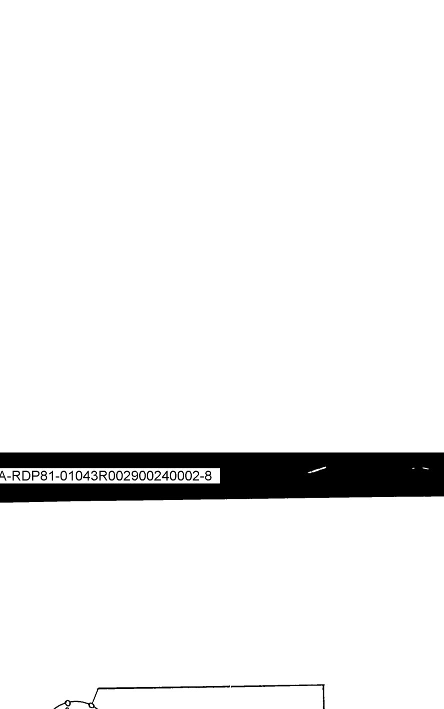

Potential Shifter Ripple Filter Chassis

Figure 51

TRANSIENT RESPONSE OF PHOSPHORS

THEORETICAL DERIVATION

Introduction

The operation of the Optical-Electronic Ambiguity Filter depends upon the brightness difference in the primary cathode ray tube trace baseline between the position of a TRI (true range indicating) echo and the remainder of the trace baseline. The brightness difference between the position of a FRI (false range indicating) echo and the remainder of the trace baseline should be minimized for optimum ambiguity suppression. Variations in the baseline brightness due to random noise should also be minimized for optimum noise suppression. In previous reports[1] a simplified analysis of the transient brightness variation and the experimental verification thereof were presented. Some discrepancies[2] between the theoretical and experimental results were noted and ascribed to inaccuracy of the simplifying assumptions made in the analysis under the particular conditions prevailing. A more comprehensive analysis of the

---

[1] Signal Corps Contract No. DA-36-039 SC-56696 Third Q. P.R. June 1954-August 1954, pp 13-67. Seventh Q.P.R. August 1955-October 1955, pp 8-32.

[2] The average brightness of the phosphor observed experimentally at very high and very low excitations was from 10 to 50 percent, respectively, different from the theoretically calculated average brightness.

transient behavior of phosphors is formulated here to form a basis for a more accurate theoretical determination of I_{E} and I_{NE} (ambiguity suppression and noise suppression figures-of-merit) for the Optical-Electronic Ambiguity Filter.

The majority of the expository material in the following analysis constitutes a tutorial review of the present theoretical descriptions of the transient behavior of phosphors. The approach to the quantitative analysis of the transient behavior in terms of probabilities as done here is believed to be novel. Simplifying assumptions applied to the quantitative results of the transient behavior derived here give the qualitative results found in the literature.

CRT Phosphors

Phosphors used on CRT screens are usually inorganic crystalline compounds containing trace quantities of foreign elements, and are classified as semiconductors. The most commonly used phosphors are the oxides, particularly of zinc; the sulfides of zinc and of cadmium; the silicates, particularly of zinc; the tungstates of calcium, magnesium, cadmium, and zinc; and the fluorides of zinc and magnesium. The foreign elements, some of which are added intentionally, have favorable or unfavorable effects on the luminescent behavior of the phosphor. The foreign elements giving favorable effects are called

activators, and the foreign elements giving unfavorable effects are called quenchers or killers. The activators may be metallic, such as zinc, copper, silver, or manganese, or non-metallic, such as uncombined sulfer in the sulfide phosphors. Quenching can be produced by metallic impurities, such as iron, nickel, or cobalt, or by an excess of the same elements that act as activators.[1]

The luminescent behavior of a phosphor depends upon its basic crystal type, the activators and quenchers present, and the crystalline structure as determined by manufacturing technique.

Phosphor Excitation and De-Excitation

When a phosphor is bombarded by a high energy electron beam the primary beam electrons penetrate the crystal structure. Electrons in the crystals may receive energy from the primary electrons by collision, and leave their normal energy levels. Several sequences of events may then occur, the exact and complete nature of which are not fully known and may differ from one phosphor to another. An over-all picture shows some electrons being raised from their normal energy levels to the conduction-band. The holes left by these electrons subsequently migrate thru the crystal structure until they are "trapped" by luminescent-centers or quencher-centers

[1]P. Pringsheim, Fluorenscence and Phosphorescence, Interscience Publishers, Inc., 1949.

Declassified in Part - Sanitized Copy Approved for Release @ 50-Yr 2014/01/31 : CIA-RDP81-01043R002900240002-8

located at the sites of activators and quenchers, respectively. Some electrons in the conduction-band drop to lower energy levels in the luminescent-centers which have holes trapped in them and radiate the energy difference as one photon (hf). Through vibrational energy loss some electrons in the conduction-band drop to lower energy levels in the quencher-centers which have holes trapped in them. By these radiative and non-radiative electron transitions the holes are filled. Some conduction-band electrons may lose a small quantity of energy and become trapped in high-energy-electron-traps slightly below the conduction-band. These high-energy-electron-traps are located at the sites of impurities or crystal structure defects. The absorption of energy by these electrons raises them from the high-energy-electron-traps to the conduction-band.

When the primary electron beam is removed, the phosphor is in an excited state, having both trapped electrons and trapped holes. Electrons from the conduction-band and electrons raised from the high-energy-electron-traps into the conduction-band make radiative transitions to the luminescent-centers and non-radiative transitions to the quencher-centers and thus fill the holes in these centers.

The mechanism of luminscence is the radiative transition of electrons from the conduction-band to the luminescent-centers containing holes. A luminescent-

center containing a hole is excited, and decays when the hole is filled by the radiative transition of an electron to the luminescent -center. The transient behavior of phosphors is couched in terms of the excitation and decay of luminescent-centers in the phosphor.

Decay of Luminescent-Centers

The transient response of a phosphor during decay is analyzed first because the number of factors involved in the decay mechanism is less than the number involved in the excitation mechanism, making the development more easily followed and facilitating the introduction of special notation.

The phosphor may contain several types of luminescent-centers, designated as types 1, 2, ... i ... . If a particular activator structure in the crystal lattice traps n holes, it is considered not as a single luminescent-center but rather as n distinct luminescent-centers. The multiple centers could be several centers of a single type or of different types. The number of luminescent-centers per unit area of the screen of each type are designated as N_1, N_2, ... N_i, ..., and the number of these which are excited are designated as N_{e1}, N_{e2}, ... N_{ei}, ... The probability time densitites of decay of the excited luminescent-centers (which are just the probabilities that electrons will make the transition from the conduction-band to the luminescent-centers in unit time) are denoted by p_{d1}, p_{d2}, ... p_{di} ....

Since the decay mechanism is the same for all types of luminescent-centers, the analysis is carried out for the i^{th} type to provide results applicable to all types.

The average change in the number of excited luminescent-centers per unit area of the screen of the i^{th} type (dN_{ei}) in a time interval dt is

(1) $$dN_{ei} = -p_{di} N_{ei} dt$$

In order to solve the differential equation in (1) the dependence of p_{di} on N_{ei} and t must be known explicitly. It should be pointed out that p_{di} may be a function of other variables, such as temperature, incident electromagnetic radiation, excess of electrons in the conduction band, and so forth. Radiation from the decay of luminescent-centers within the phosphor itself has negligible effect since most phosphors do not readily absorb their own radiation.[1]

The probability time density of decay of the luminescent-centers (p_{di}) depends upon where the transition-electrons (electrons that can ultimately make radiative transitions to the luminescent-centers) are, and how many are present. If all the transition-electrons are in the conduction-band, p_{di} is just the probability time density that electrons in the conduction-band will combine with holes trapped in the luminescent-

[1]T. Soller, M. Starr, G. Valley, Cathode Ray Tube Displays, McGraw-Hill Book Company, Inc., 1948.

centers (p_{ci}). In long persistence phosphors, an appreciable fraction of the electrons needed to fill the trapped holes are trapped in high-energy-electron-traps and must leave these traps and return to the conduction-band before they can make the radiative transitions to the luminescent-centers. In these phosphors, p_{di} will depend upon the probability time density that electrons in the conduction-band will become trapped in high-energy-electron-traps (p_{tt}) and the probability time density that electrons will escape from these traps to the conduction-band (p_{et}), as well as on the previously mentioned factors. The decay probability time density (p_{di}), in this case, is just the probability time density that electrons in the conduction-band will make the transition to luminescent-centers (p_{ci}), weighted by the fraction of the transition-electrons in the conduction-band, plus the probability time density that electrons in high-energy-electron-traps will leave the traps for the conduction-band and then leave the conduction-band in transitions to luminescent-centers, weighted by the fraction of the transition-electrons in the high-energy-electron-traps. This is

(2) $$p_{di} = \frac{p_{ci}}{N_C + N_T} (N_C + p_{et} N_T)$$

where

N_C = number of transition-electrons in the conduction-band per unit area of the screen.

Declassified in Part - Sanitized Copy Approved for Release @ 50-Yr 2014/01/31 : CIA-RDP81-01043R002900240002-8

N_T = number of transition-electrons in the high-energy-electron-traps per unit area of the screen.

Integrating (2) into (1) gives

(3) $dN_{ei} = -$ [illegible] $N_{ei}\,dt$

which shows that dN_{ei} depends upon the number of transition-electrons in the conduction-band and in the high-energy-electron-traps.

Since electrons are entering and leaving the high-energy-electron-traps, N_C and N_T are not constant. The average change in N_C (dN_C) in a time interval dt is

(4) $dN_C = ($[illegible]$N_T -$ [illegible]$N_C - \Sigma p_{ci} N_C)dt$

and the average change in N_T (dN_T) in a time interval dt is

(5) $dN_T = ($[illegible]$N_C -$ [illegible]$N_T)dt$

Equations (3), (4), and (5) form a system of simultaneous differential equations which must be solved for N_{ei}.

If the time variation of N_{ei} shortly after cessation of the primary bombarding electrom beam is of most interest, the system of differential equations can be reduced to a single differential equation by an appropriate approximation. The operating conditions of the [illegible] in the Optical-Electronic Ambiguity Filter are such that the time interval between successive excitations is small compared to the amount of time necessary for

the long persistence characteristic to manifest itself. Thus the phosphor is always in a relatively high state of excitation, with most of the transition-electrons in the conduction-band. This condition is expressed as

(6) $N_C >> N_T$

Applying the approximation given in (6) to (3) gives

(7) $dN_{ei} = -p_{ci} N_{ei}\,dt$

It is convenient to express p_{ci} as a constant (α_i) plus some function of the number of electrons per unit area of the screen in excess of the number of holes in the phosphor per unit area of the screen (N_{XS})

(8) $p_{ci} = \alpha_i + f_i(N_{XS})$

where

α_i = decay constant of type i luminescent-centers

$f_i(N_{XS})$ = a function of N_{XS}

Substitution of (8) into (7) gives

(9) $dN_{ei} = -\left[\alpha_i + f_i(N_{XS})\right] N_{ei}\,dt$

The excess electrons in the phosphor, due to the primary beam current, begin to dissipate as soon as the primary beam is removed. Therefore, during decay, N_{XS} is a function of the physical and electrical characteristics of the phosphor and time. Since the only variable of interest in (9) is time, $f_i(N_{XS})$ can be replaced by $g_i(t-t_o)$, where

(10) $f_i(N_{XS}) = g_i(t-t_o)$

Declassified in Part - Sanitized Copy Approved for Release @ 50-Yr 2014/01/31 : CIA-RDP81-01043R002900240002-8

and (9) becomes

(11) $$dN_{ei} = -\left[\alpha_i + g_i(t-t_o)\right] N_{ei}dt$$

whose solution is

(12) $$N_{ei} = N_{eio}\, e^{-\alpha_i(t-t_o)}\, e^{-\int_{t_o}^{t} g_i(t-t_o)dt}$$

where

N_{eio} = the value of N_{ei} at t_o

For conditions of excitation at which few excess electrons are in the phosphor, or those that are in the phosphor are dissipated in a very short time, the integral in (12) can be approximated by a constant for values of t greater than t_o. That is

(13) $$\int_{t_o}^{t} g_i(t-t_o)dt = K_i$$

where

K_i = constant

This modifies (12) to

(14) $$N_{ei} = N_{eio}\, e^{-\alpha_i(t-t_o)-K_i}$$

When the effect of excess electrons is negligible, that is, when

(15) $$\int_{t_o}^{t} g_i(t-t_o)dt \ll \alpha_i(t-t_o)$$

equation (12) can be simplified to

(16) $$N_{ei} = N_{eio}\, e^{-\alpha_i(t-t_o)}$$

Equation (16) shows that under the simplifying assumptions set forth in (6) and (15), the decay of excited luminescent-centers after removal of the primary electron beam follows an exponential decay law.

The energy released by the decay of a luminescent-center is radiated as one photon, or quanta of energy (hf). The frequency of the radiation (f) is not the same for all decaying luminescent-centers, even if they are all of the same type. This is due to the fact that the transition-electrons drop from different energy levels in the conduction-band to the luminescent-centers. The energy level distribution of the transition-electrons in the conduction band thus leads to a frequency distribution of the radiated energy from the decaying luminescent-centers. The frequency density of the radiation from the decay of i type luminescent-centers is denoted by $p_{fi}(f)$. A continuous function is assumed because the energy levels in the conduction-bands are so closely spaced that the energy can be considered to be a continuous variable.

The rate of energy radiation per unit area of the screen, or luminous power output per unit area of the screen, in the frequency increment df is the energy per photon multiplied by the rate of emission of photons in the frequency increment df per unit area of the screen. The rate of emission of photons is just the negative of the rate of change of the number of excited luminescent-centers. The incremental power output per unit area of the screen due to the decay of i type luminescent-centers ($d\pi_i$) is

$$(17) \qquad d\pi_i = -hf\, p_{fi}(f)\, df\, \frac{dN_{ei}}{dt}$$

Substituting from (12) into (17) gives

$$(18) \qquad d\pi_i = hf\, p_{fi}(f)\, df\, N_{eio}\, e^{-\alpha_i(t-t_o) - \int_{t_o}^{t} g_i(t-t_o)dt} \cdot \left[\alpha_i + g_i(t-t_o)\right]$$

and the total luminous power output per unit area of the screen due to i type luminescent-centers is

$$(19) \qquad \pi_i = N_{eio}\left[\alpha_i + g_i(t-t_o)\right] h \cdot e^{-\alpha_i(t-t_o) - \int_{t_o}^{t} g_i(t-t_o)dt} \int_0^{\infty} f\, p_{fi}(f)df$$

If the assumption embodied in (15) is used, (19) reduces to

$$(20) \qquad \pi_i = N_{eio}\alpha_i\, h\, e^{-\alpha_i(t-t_o)} \int_0^{\infty} f\, p_{fi}(f)\, df$$

Thus the luminous power output decreases exponentially after electron bombardment of the phosphor is stopped.

Common radiant energy detectors exhibit spectral sensitivity distributions, that is, the detector output is a function of the frequency of the radiation as well as the power. The human visual mechanism has an approximately Gaussian sensitivity distribution that peaks at about 5500 Angstroms. In the Optical-Electronic Ambiguity Filter the detector is a 6198 Vidicon camera-tube whose sensitivity peaks at about 5000 Angstroms. These sensitivity distributions are sketched in Figure 52 for comparison.

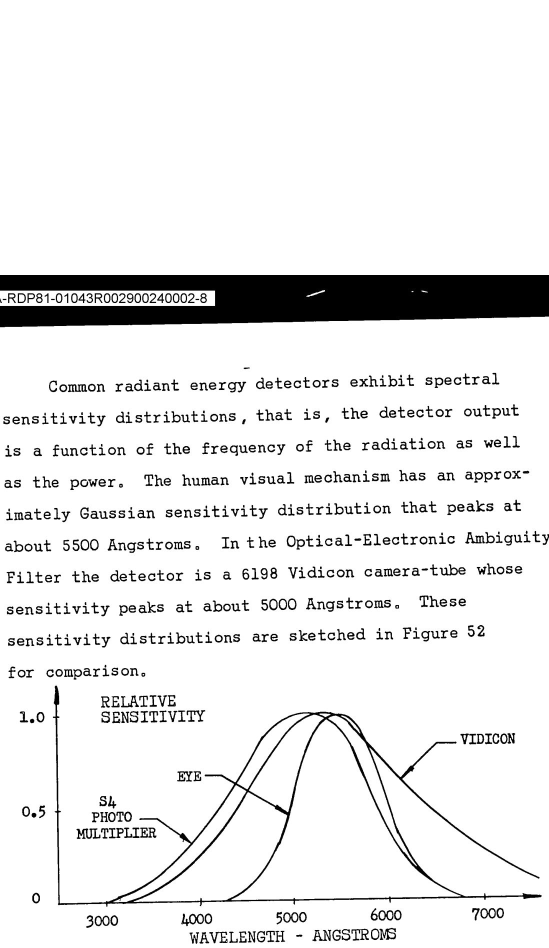

Figure 52 Spectral Sensitivity of Average Human Eye, 6198 Vidicon Tube, and Photomultiplier with S4 Response.

The spectral sensitivity distribution of the Vidicon tube is denoted by $s_v(f)$. The brightness (effective luminous power per unit area) due to luminous power in the frequency band df from i type luminous centers in the phosphor is, from (18),

Declassified in Part - Sanitized Copy Approved for Release @ 50-Yr 2014/01/31 : CIA-RDP81-01043R002900240002-8

(21) $$dB_i = hfp_{fi}(f)\ s_v(f)\ df\ N_{eio}\ \cdot$$

$$\left[\alpha_i + g_i(t-t_o)\right] e^{-\alpha_i(t-t_o) - \int_{t_o}^{t} g_i(t-t_o)dt}$$

The total contribution to the effective brightness seen by the Vidicon from i type luminous centers is

(22) $$B_i = N_{eio}\left[\alpha_i + g_i(t-t_o)\right] h\ e^{-\alpha_i(t-t_o) - \int_{t_o}^{t} g_i(t-t_o)dt}\ \cdot$$

$$\int_0^{\infty} f\ p_{fi}(f)\ s_v(f)\ df$$

If the assumption embodied in (15) is used, (22) reduces to

(23) $$B_i = N_{eio}\ \alpha_i h\ e^{-\alpha_i(t-t_o)} \int_0^{\infty} f\ p_{fi}(f)\ s_v(f)df$$

which can be more concisely expressed as

(24) $$B_i = B_{io}\ e^{-\alpha_i(t-t_o)}$$

where

B_{io} = the value of B_i at t_o

The total effective brightness seen by the Vidicon is the sum of the effects produced by each type of luminescent-center in the phosphor. If the spectral sensitivity is constant over the range of brightness encountered, then

(25) $$B = \sum_i B_i = \sum_i B_{io} e^{-\alpha_i(t-t_o)}$$

Thus, the brightness decay of a phosphor after electron bombardment can be expressed as the sum of several exponentially decreasing functions with different initial values and time constants for the conditions expressed in (6) and (15). The number of different exponential functions necessary to quantitatively describe the brightness decay depends upon the number of different types of luminescent-centers contributing significantly to the total radiant output.

<u>Excitation of Luminescent-Centers</u>

The luminescent-centers in a phosphor can be excited by several means, but excitation by electron bombardment is of most interest here. As was pointed out earlier, several types of luminescent-centers may exist in the phosphor, but they are considered to be mutually independent and capable of only single excitation. That is, once a luminescent-center is excited (has a trapped hole) it cannot be active in further excitation processes until after it decays (loses the trapped hole).

The probability time density that a luminescent-center will trap a hole is designated as p_{e1}, p_{e2}, ... p_{ei} ... . These excitation probability time densities are assumed to be mutually independent. The number of i type luminescent-centers per unit area of the screen available for excitation at any time is $(N_i - N_{ei})$. The average change in the number of excited i type luminescent-centers per unit area of the screen in a time interval dt during excitation is

(26) $dN_{ei} = p_{ei}\ (N_i - N_{ei})dt - p_{di}\ N_{ei}\ dt$

The nature of p_{ei} and p_{di} during excitation must be known in order to solve the differential equation in (26).

The decay probability time density (p_{di}) is given in (2).

The relation between p_{ei} and N_{ei} and time must be known explicitly. The excitation probability time density p_{ei} (which is just the probability time density that an i type luminescent-center will capture a hole) may be a function of temperature and the density of holes in the filled band. The hole density is a function of the incident electromagnetic radiation, primary beam current density, primary electron velocity, and time. If the primary beam current density and electron velocity are constant during excitation, and the effects of electromagnetic radiation from the phosphor itself are neglected due to the negligible absorption, the excitation probability time density can be considered as a function of time only. During constant, continuous, primary electron bombardment, the hole density approaches an equilibrium value. It is convenient to express p_{ei} as a constant plus some function of time to account for the initial time variation of the hole density.

(27) $p_{ei} = \eta_i + h_i(t-t_o)$

where

η_i = excitation constant of type i luminescent-centers

The excitation constant is a function of the temperature, primary beam current density, and primary electron velocity.

Substitution from (2) and (27) into (26) gives

$$(28) \qquad dN_{ei} = \left\{\left[\eta_i + h_i(t-t_o)\right](N_i - N_{ei}) - \frac{p_{ci}}{N_C + N_T}(N_C + p_{et}N_T)N_{ei}\right\} dt$$

which must be solved simultaneously with (4) and (5). Use of the assumption embodied in (6), and expansion of p_{ci} in the form indicated in (8), reduces the system to the form

$$(29) \qquad dN_{ei} = \left\{\left[\eta_i + h_i(t-t_o)\right](N_i - N_{ei}) - \left[\alpha_i + q_i(t-t_o)\right] N_{ei}\right\} dt$$

The solution of (29) is

$$(30) \qquad N_{ei} = \left\{\int_{t_o}^{t}\left[\eta_i + h_i(t-t_o)\right] N_i\, e^{\int_{t_o}^{t}\left[\eta_i + \alpha_i + h_i(t-t_o) + q_i(t-t_o)\right] dt}\, dt + N_{eio}\right\} e^{-\int_{t_o}^{t}\left[\eta_i + \alpha_i + h_i(t-t_o) + q_i(t-t_o)\right] dt}$$

The solution for the number of excited i type luminescent-centers per unit area of the screen during electron bombardment can be further simplified under certain conditions. If the number of excess conduction-band electrons in the phosphor does not affect the luminescent-center decay rate appreciably, that is, if

Declassified in Part - Sanitized Copy Approved for Release @ 50-Yr 2014/01/31 : CIA-RDP81-01043R002900240002-8

$$(31) \qquad \int_{t_o}^{t} q_i(t-t_o)\,dt << \alpha_i(t-t_o)$$

and if the hole density in the filled band of the phosphor reaches an equilibrium value in a very short time compared to the time required for the luminescent-centers to donate electrons to the holes, that is, if

$$(32) \qquad \int_{t_o}^{t} h_i(t-t_o)\,dt << \eta_i(t-t_o)$$

then (30) can be simplified to

$$(33) \qquad N_{ei} = \frac{\eta_i N_i}{\eta_i+\alpha_i}\left\{1 - \left[1 - \frac{N_{eio}(\eta_i+\alpha_i)}{\eta_i N_i}\right] e^{-(\eta_i+\alpha_i)(t-t_o)}\right\}$$

If no i type luminescent-centers are excited at the start of the primary electron bombardment, then N_{eio} is zero, and (33) reduces to

$$(34) \qquad N_{ei} = \frac{\eta_i N_i}{\eta_i+\alpha_i}\left\{1 - e^{-(\eta_i+\alpha_i)(t-t_o)}\right\}$$

which is a simple exponential build-up to a saturation value.

The radiated luminous power per unit area of the screen due to i type luminescent-centers during excitation is determined by the rate at which the i type luminescent-centers are decaying during excitation. This rate of decay during excitation is given in the second term of (26), and is $p_{di}\,N_{ei}$. Using the assumption set forth in (6) gives

$$(35) \qquad p_{di}N_{ei} = \left[\alpha_i + q_i(t-t_o)\right] N_{ei}$$

Using the general expression for the incremental radiated power per unit area of the screen due to i type luminescent-centers as expressed in (17) and the rate of decay of i type luminescent-centers during excitation as given in (35) gives

$$(36) \qquad d\pi_i = hfp_{fi}(f)\,df\left[\alpha_i + q_i(t-t_o)\right] N_{ei}$$

The expression for N_{ei} is given in (30). Substituting (30) in (36) and integrating over all frequencies gives the total radiated luminous power per unit area of the screen due to i type luminescent-centers.

$$(37) \qquad \pi_i = \left[\alpha_i + q_i(t-t_o)\right] h \left\{N_{eio} + \int_{t_o}^{t}\left[\eta_i + h_i(t-t_o)\right] N_i\, e^{\int_{t_o}^{t}\left[\eta_i+\alpha_i+h_i(t-t_o)+q_i(t-t_o)\right]dt}\, dt\right\} e^{-\int_{t_o}^{t}\left[\eta_i+\alpha_i+h_i(t-t_o)+q_i(t-t_o)\right]dt} \int_{o}^{\infty} fp_{fi}(f)\,df$$

The effective brightness of the screen, as seen by the Vidicon, during electron bombardment of the phosphor is determined by a development parallel to the one used to obtain (22) from (18). The brightness of the screen during excitation due to i type luminescent-centers is

Declassified in Part - Sanitized Copy Approved for Release @ 50-Yr 2014/01/31 : CIA-RDP81-01043R002900240002-8

(38) $$B_i = \left[\alpha_i + q_i(t-t_o)\right] h \left\{ N_{eio} + \int_{t_o}^{t} \left[\eta_i + h_i(t-t_o)\right] N_i \, e^{\int_{t_o}^{t}\left[\eta_i+\alpha_i+h_i(t-t_o)+ q_i(t-t_o)\right] dt} \, dt \right\}$$

$$e^{-\int_{t_o}^{t}\left[\eta_i+\alpha_i+h_i(t-t_o)+q_i(t-t_o)\right] dt} \int_o^{\infty} f p_{fi}(f) s_v(f)\, df$$

If the assumptions embodied in (31) and (32) are applied to (38), a simplified expression for B_i results.

(39) $$B_i = \left\{ 1 - \left[1 - \frac{N_{eio}(\eta_i+\alpha_i)}{\eta_i \; N_i} \right] e^{-(\eta_i+\alpha_i)(t-t_o)} \right\} .$$

$$\frac{h\alpha_i \eta_i N_i}{\eta_i+\alpha_i} \int_o^{\infty} f p_{fi}(f) s_v(f)\, df$$

Equation (39) can be more concisely expressed in the form

(40) $$B_i = B_{imax} \left\{ 1 - \left[1 - \frac{B_{io}}{B_{imax}} \right] e^{-(\alpha_i + \eta_i)(t-t_o)} \right\}$$

where

B_{imax} = saturation brightness of the phosphor caused by i type luminescent-centers under the excitation conditions present

B_{io} = brightness of the phosphor due to i type luminescent-centers at the start of excitation ($t = t_o$).

The total effective brightness seen by the Vidicon is the sum of the effects produced by each type of

luminescent-center in the phosphor. If the spectral sensitivity is constant over the range of brightness encountered, then

(41) $$B = \sum_i B_i$$

$$= \sum_i B_{imax} \left\{ 1 - \left[1 - \frac{B_{io}}{B_{imax}} \right] e^{-(\alpha_i + \eta_i)(t-t_o)} \right\}$$

Thus, the brightness build-up of a phosphor during electron bombardment can be expressed as the sum of several exponentially increasing functions with different initial and saturation values and time constants for the excitation conditions expressed in (6), (31) and (32). The number of different exponential functions necessary to quantitatively describe the brightness build-up depends upon the number of different types of luminescent-centers contributing significantly to the total radiant output.

Declassified in Part - Sanitized Copy Approved for Release @ 50-Yr 2014/01/31 : CIA-RDP81-01043R002900240002-8

EXPERIMENTAL VERIFICATION

Introduction

Experiments were performed in order to determine how accurately the results of the theoretical analysis of the transient behavior of phosphors represent the actual behavior. Several different types of phosphors were used in the experimental work to give a broader verification of the analysis than would be possible with a single phosphor. Phosphors with the RMA designations P1, P2, and P11 were used. The primary detector of the phosphors radiant energy in the Optical-Electronic Ambiguity Filter is a 6198 Vidicon tube. A detector having the same spectral sensitivity distribution combined with a transient response faster than that of the phosphor is necessary to measure the transient brightness variations as seen by a Vidicon tube. A 931-A photomultiplier with an S4 sensitivity distribution met this requirement. The S4 spectral sensitivity distribution is shown in Figure , along with the spectral energy distributions of the phosphors.

Declassified in Part - Sanitized Copy Approved for Release @ 50-Yr 2014/01/31 : CIA-RDP81-01043R002900240002-8

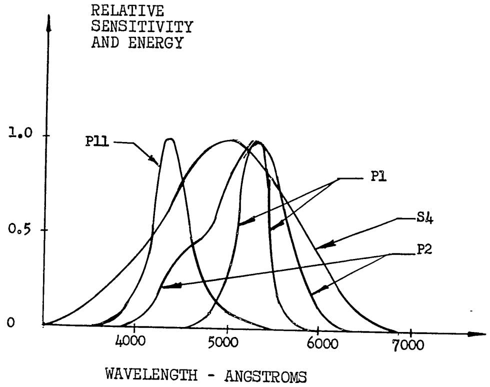

Figure 53 Relative Spectral Energy Distributions of P1, P2, and P11 Phosphors and S4 Spectral Sensitivity Distribution

An experimental determination of the build-up and decay constants of the P2 phosphor was reported in a previous report on this project[1]. These constants were determined on the a priori assumption of simple single exponential transient variations of brightness in the phosphor.

Experimental Equipment

A block diagram of the essential elements of the system employed to measure the transient brightness

[1]Signal Corps Contract No. DA-36-039 SC-56696 Seventh Q.P.R. August 1955-October 1955, pp 8-32.

variations is shown in Figure 54 . The CRT containing the phosphor under investigation was adjusted for no vertical or horizontal deflection (stationary spot) and the intensity control was adjusted so that the electron beam was just cut off. Positive pulses from the triggered pulse generator, of adjustable amplitude and duration, were coupled to the first grid of the CRT with negligible overshoot or droop and rise and decay times of one microsecond each. The interval between these pulses was controlled by the repetition rate of the free-running pulse generator. This rate was adjusted so that the luminous power output from one pulse was no longer discernable before the next pulse was applied.

The spot of light formed on the screen of the CRT was well focused and approximately 0.030 inch in diameter. An opaque mask with a small pin hole in it was fastened to the face of the CRT so as to block off all light from the phosphor except that from the center portion of the spot. In order to obtain the brightness under uniform excitation conditions the pin hole must expose only the center portion of the spot where the beam current density is approximately constant. The finite thickness of the glass faceplate of the CRT and lateral diffusion of light within the phosphor layer allows some light from the phosphor area around the center of the spot to

Declassified in Part - Sanitized Copy Approved for Release @ 50-Yr 2014/01/31 : CIA-RDP81-01043R002900240002-8

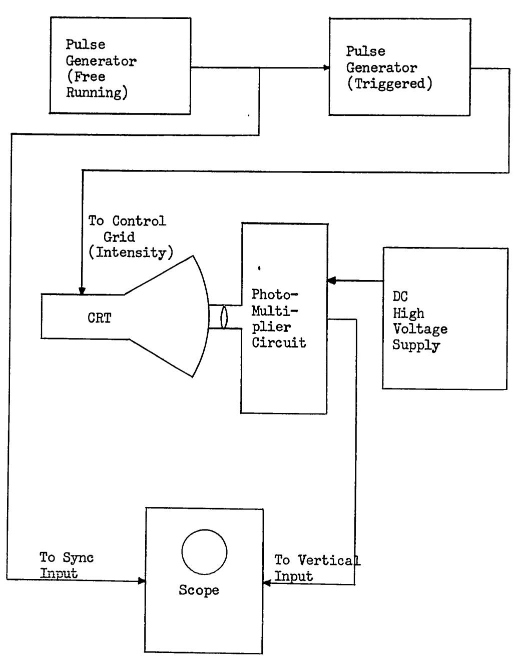

Equipment to Measure Transient Brightness Variation in CRT Phosphors

Figure 54

emerge from the pin hole. This effect on the results is minimized if the area around the portion of the spot exposed by the pin hole has the same brightness as the center of the spot. The brightness variation across the spot, due to non-uniform current density and lateral diffusion of light in the phosphor, appears to be Gaussian.[1] This requires as small a pin hole diameter to spot diameter ratio as practical. The pin hole has to be large enough to pass sufficient light to the detector to obtain an easily measured response. A 0.010 inch diameter pin hole was the best compromise experimentally obtainable.

A lens system (in the block marked "Photomultiplier Circuit") was used to focus the light from the pin hole onto the photocathode of the 931-A photomultiplier. The circuit for the photomultiplier is shown in Figure 55. The rise and decay times of this circuit are approximately 30 microseconds each. An adjustable high voltage dc supply with less than 50 millivolts of ripple and noise at the output supplied the power to the photomultiplier circuit.

The output of the photomultiplier circuit was displayed on a Tektronix Type 535 oscilloscope, in order to obtain time and amplitude measurements. In order to facilitate comparison of experimental and theoretical

[1] W.R. Beam, "A New Method for Magnifying Electron Beam Images", RCA Review, Vol. 16, No. 2, June 1955, pp 242-250.

Declassified in Part - Sanitized Copy Approved for Release @ 50-Yr 2014/01/31 : CIA-RDP81-01043R002900240002-8

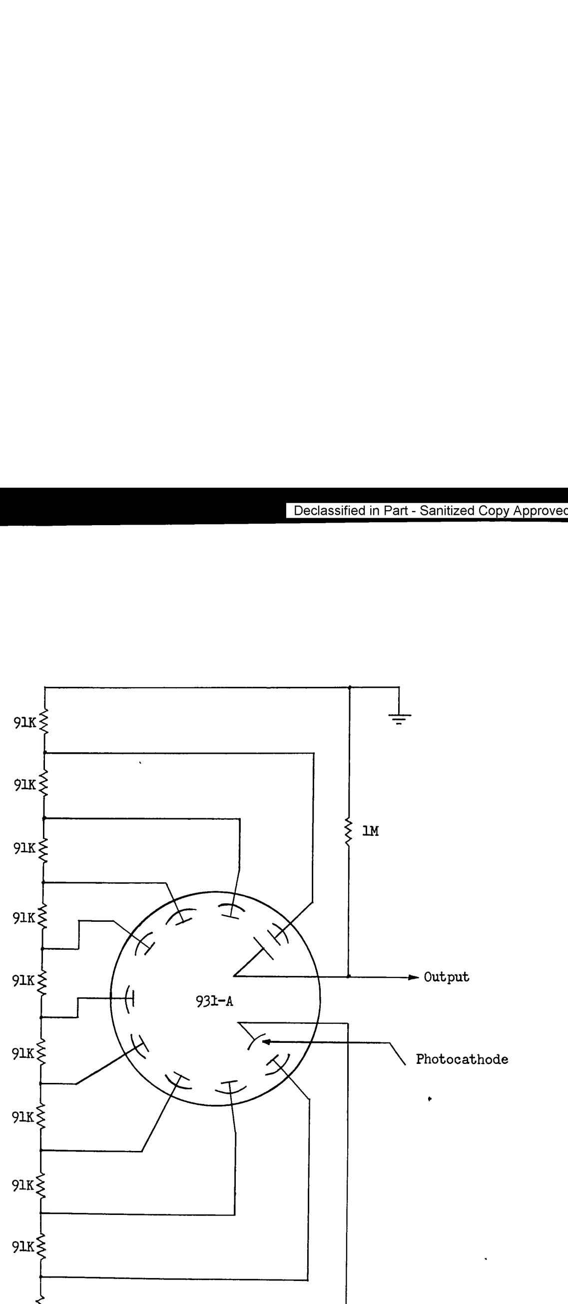

Photomultiplier Circuit

Figure 55

waveforms, the data on the oscilloscope were photographed and enlarged. This allowed more accurate plotting of theoretical curves on the experimental curves for comparison than could be obtained by comparisons made on the oscilloscope directly.

Experimental Results

Representative samples of the data obtained and the theoretical curves chosen to fit the data are shown for the various phosphors investigated. The effects of all the possible variables in the system were not extensively studied, since much work of this type has been reported in the literature[1] and the time allocated to this study was limited.

Figures 56 and 57 show the experimental data and theoretical curves for the type P1 phosphor at two different values of primary beam current density. It was not possible to measure the value of the current density at the center of the spot but data on the 5JP1 tube used shows that the third anode currents were 2 and 20 micro-amperes respectively, giving an approximately ten to one ratio of current densities.

Good correlation between the experimental data and the theoretical curves is obtained by considering only

---

[1] G.R. Fonda and F. Seitz, Solid Luminescent Materials, John Wiley and Sons, Inc., 1948. H. W. Leverenz, Luminescence of Solids, John Wiley and Sons, Inc., 1950. P. Pringsheim, Fluorescence and Phosphorescence, Interscience Publishers, Inc., 1949.

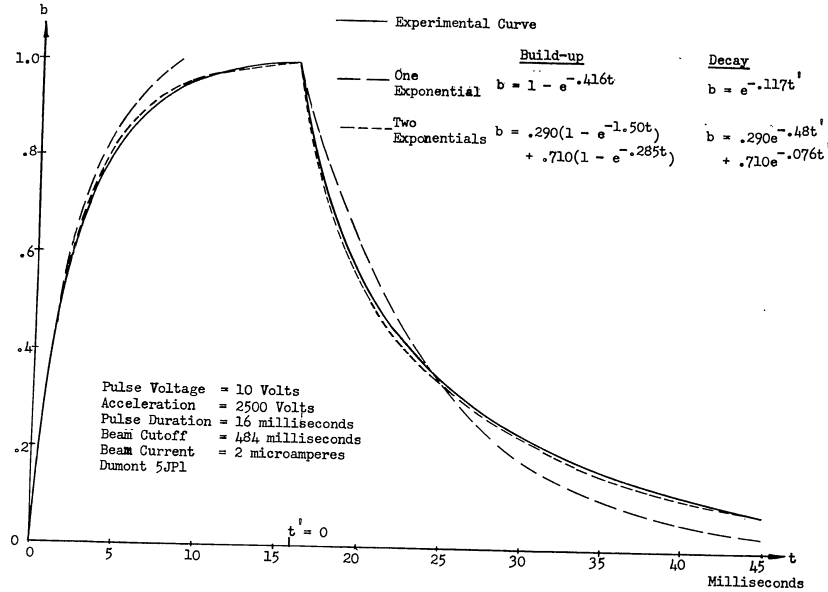

Normalized Brightness Build-up and Decay in Type P1 Phosphor

Figure 56

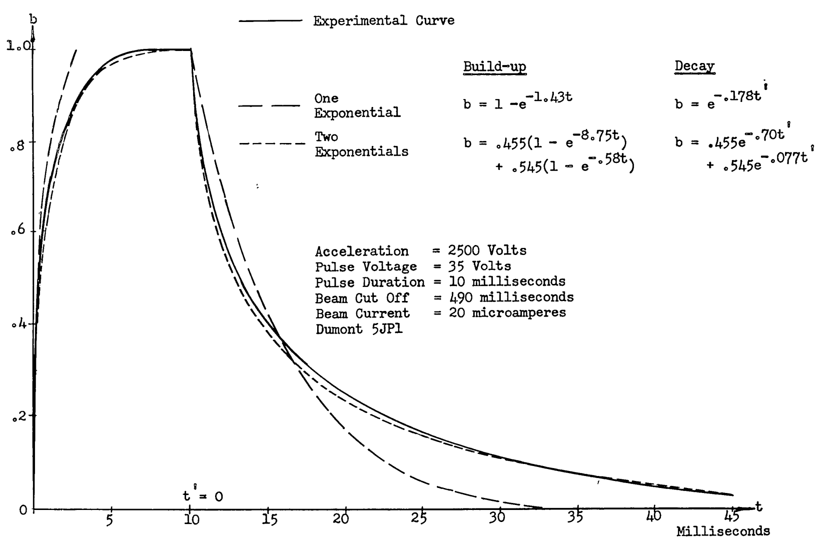

Normalized Brightness Build-up and Decay in Type P1 Phosphor

Figure 57

Declassified in Part - Sanitized Copy Approved for Release @ 50-Yr 2014/01/31 : CIA-RDP81-01043R002900240002-8

the two most active types of luminescent-centers as contributing significantly to the brightness. This gives double exponential brightness build-up and decay curves. The excellent experimental agreement indicates that the other types of luminescent-centers which may be present have a relatively small contribution to the total brightness.

The behavior of the excitation and decay probability time densities (as reflected in the exponents) for different values of excitation intensity agrees with the behavior predicted by equations (27) and (8), respectively. The decay probability time density of the more slowly decaying type of luminescent-centers is not highly dependent on the excitation intensity. A similar comparison for the faster decaying type of luminescent-centers shows that the presence of excess electrons in the phosphor at high excitation intensity increases the decay probability time density. This increase in decay probability time density also accounts for the larger relative contribution to the total brightness by the faster decaying type of luminescent-centers at high excitation intensity, as predicted by equation (22). The brightness build-up exponents are larger than the corresponding brightness decay exponents, and they increase with increasing beam current density, as predicted by equation (38). This may be seen by comparison of the build-up exponents in Figures 56 and 57.

Figure 58 shows a single brightness build-up and decay transient in a type P2 phosphor, sketched from the display on the Tektronix Type 535 oscilloscope. Several difficulties could not be easily resolved in the time allocated to this investigation, and consequently no photographs were made for the P2 phosphor. The chief difficulty encountered was excessive drifting of the spot on the phosphor screen due to instability of the deflection amplifiers in the oscilloscope containing the CRT with the P2 phosphor. The values indicated on the sketch in Figure 58 were measured directly from the Tektronix Type 535 oscilloscope presentation by assuming the brightness build-up and decay each consisted of only two exponentials of widely different time constants, which appears justifiable by the shape of the curve. The measurements were made by measuring the time required for the brightness to build-up to 63 percent of the saturation value and decay to 37 percent of the saturation value.

From Figure 58 it may readily be seen that the relative contribution to the total brightness from each of the two types of luminescent-centers is widely different at different times in the transient. During electron bombardment, the luminescent-centers with the high decay probability time density (large α) contribute the major portion of the total brightness. During decay, the brightness from the luminescent-centers

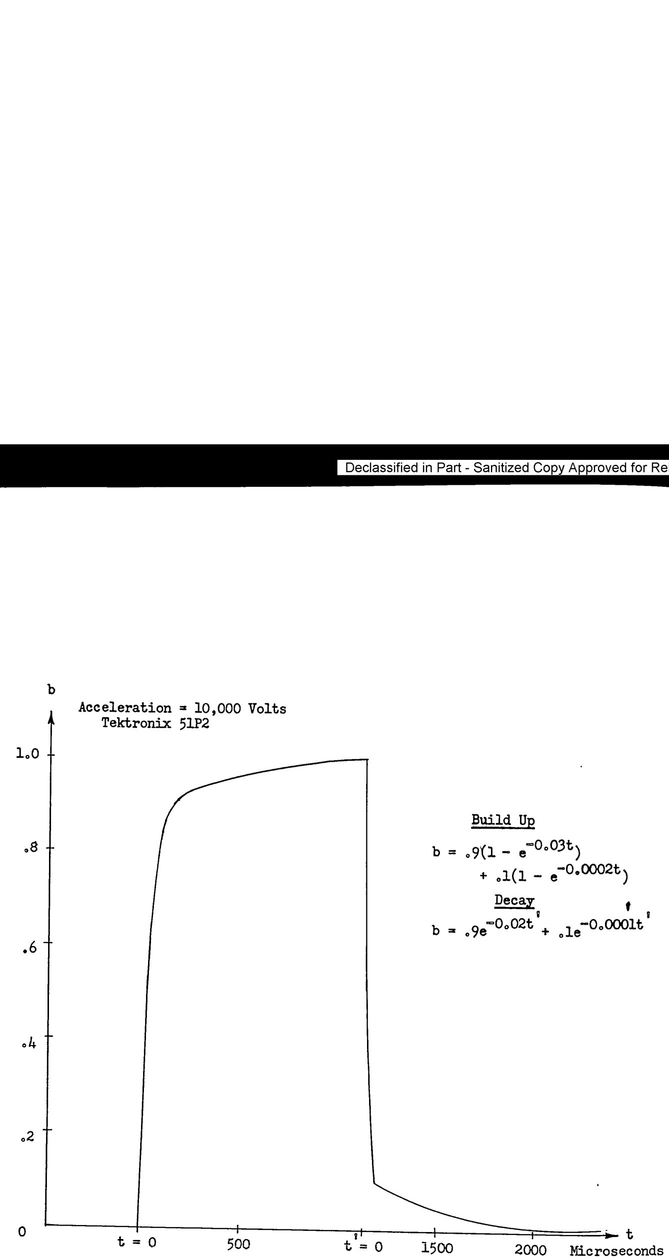

Normalized Brightness Build-up and Decay in Type P2 Phosphor

Figure 58

with the large α decreases very rapidly and the total brightness becomes more nearly that due to the slowly decaying luminescent-centers. It may be expected that the relative contributions to the total brightness during excitation from each of the two types of luminescent-centers will change for different values of primary beam current density, as in the case of the P1 phosphor. The brightness build-up exponents are larger than the corresponding brightness decay exponents, as predicted by the theory.

Figure 59 shows a representative sample of the experimental data and theoretical curves obtained for a type P11 phosphor. Equipment difficulties encountered in obtaining the experimental data make the transient waveforms which were photographed open to question. The oscilloscope in which the CRT with the P11 phosphor was located suffered from cross-coupling between the intensity modulation circuit and the deflection circuits. When the excitation pulse was applied to the intensity modulation circuit, the spot jumped away from the pin hole approximately one-half spot diameter and then drifted back. As the excitation was cut off, the spot jumped again. Since the beam current density is not constant over the whole spot, the data obtained does not correspond to constant uniform excitation current density. The nature of the cross-coupling could not be found and removed in the time allocated to this work, and consequently the data can be considered as a crude

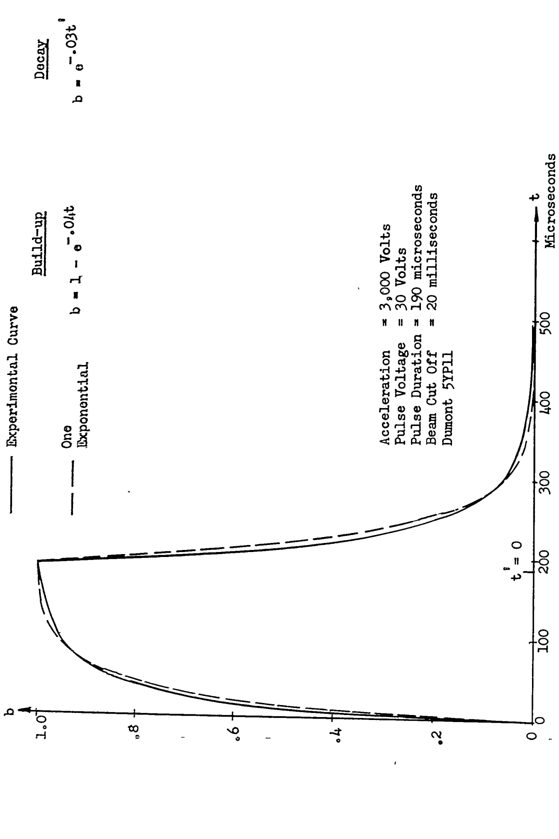

Normalized Brightness Build-up and Decay in Type P11 Phosphor

Figure 59

approximation to the actual physical conditions desired to verify the theory.

The data in Figure 59 was used to determine single exponential build-up and decay characteristics for the P11 phosphor, in order to give approximate time constants for comparison with the P1 and P2 phosphors. As predicted by the theory, the brightness build-up exponent is larger than the brightness decay exponent.

A summary of the experimental data obtained for the three types of phosphors is given below.

PHOSPHOR TYPE	BUILD-UP TIME CONSTANTS SECONDS	DECAY TIME CONSTANTS SECONDS
P1	0.66×10^{-3} to 0.11×10^{-3}	2.1×10^{-3} to 1.4×10^{-3}
	and	and
	3.6×10^{-3} to 1.7×10^{-3}	13×10^{-3}
P2	0.03×10^{-3}	0.05×10^{-3}
	and	and
	5×10^{-3}	10×10^{-3}
P11	0.02×10^{-3}	0.03×10^{-3}

Conclusions

The theory of several independent types of luminescent-centers contributing to the overall luminescent behavior of a phosphor appears to adequately describe the experimental data obtained here. While some small discrepancies may exist between the theoretical and experimental values, the use of this theory allows the quantitative description of brightness variation in phosphors, which is necessary in the analysis of systems employing a phosphor as an intermediate link.

Previous analysis on the Optical-Electronic Ambiguity Filter was based on the assumption that the brightness transients could be described by single exponential functions during build-up and decay. The more extensive analysis made here shows that this assumption provides a rough approximation to the actual behavior of the phosphor. In a simplified analysis, or in the case of a phosphor with only one predominant type of luminescent-center, this assumption may be adequate.

The exponential constants found for the three types of phosphors investigated depend upon the excitation conditions existing in the experimental work, and hence they do not represent constant characteristics of the phosphors under all operating conditions. In the Seventh Quarterly Progress Report, August-October, 1955, the build-up and decay exponential constants for a P 2 phosphor were determined on the assumption that only one type of luminescent-center was present. These constants are tabulated below with the approximate values of the double exponential constants found in the experimental work done here.

	SINGLE EXPONENTIAL	DOUBLE EXPONENTIAL
$\alpha =$	800 sec^{-1}	20,000 and 100 sec^{-1}
$\beta =$	6000 sec^{-1}	30,000 and 200 sec^{-1}

The exponential constants for a single exponential approximation to the actual transient behavior lie between the corresponding values of the constants of a double exponential approximation, as would be expected.

An examination of the discrepancies which occurred in some of the data of the Seventh Quarterly Progress Report shows that the double exponential build-up and decay of brightness gives a better theoretical - experimental correlation. A complete re-analysis of the Optical-Electronic Ambiguity Filter using the double exponentials is not done here, but any further analysis on this system should make use of the double exponential variation if a P2 phosphor is used.

OPTICAL-ELECTRONIC AMBIGUITY FILTER
SUBRANGE COMBINING SYSTEM

Introduction

It has been pointed out that the Optical-Electronic Ambiguity Filter used with the PIM radar system presents the echo information of the entire range in n subrange displays. The system operation is enhanced by recombining the subrange displays into one single display of the entire range. The method used to accomplish this has been presented in detail in several previous reports,[1] and the equipment and its operation are described in the section entitled DESCRIPTION OF EXPERIMENTAL EQUIPMENT of this report.

Subrange Combining System

The Subrange Combining System for use with the Optical-Electronic Ambiguity Filter is shown in block diagram form in Figure 15. The subrange displays are presented on the 5 Channel Oscilloscope (Primary Indicator) with common vertical deflection-modulation of all the electron beams and sequentially triggered simultaneously running horizontal sweeps. Oscillograms of the primary display on the CRT of the Primary Indicator, for the first three subranges, are shown in Figures 60 and 61. The display on the Primary Indicator is focused on the target of the camera tube

[1] Signal Corps Contract No. DA-36-039 SC-56696 Fifth Q.P.R. February 1955-April 1955, pp 73-106. Sixth Q.P.R. May 1955-July 1955, pp 46-125.

Optical Combining
First Three Subranges
n = 4

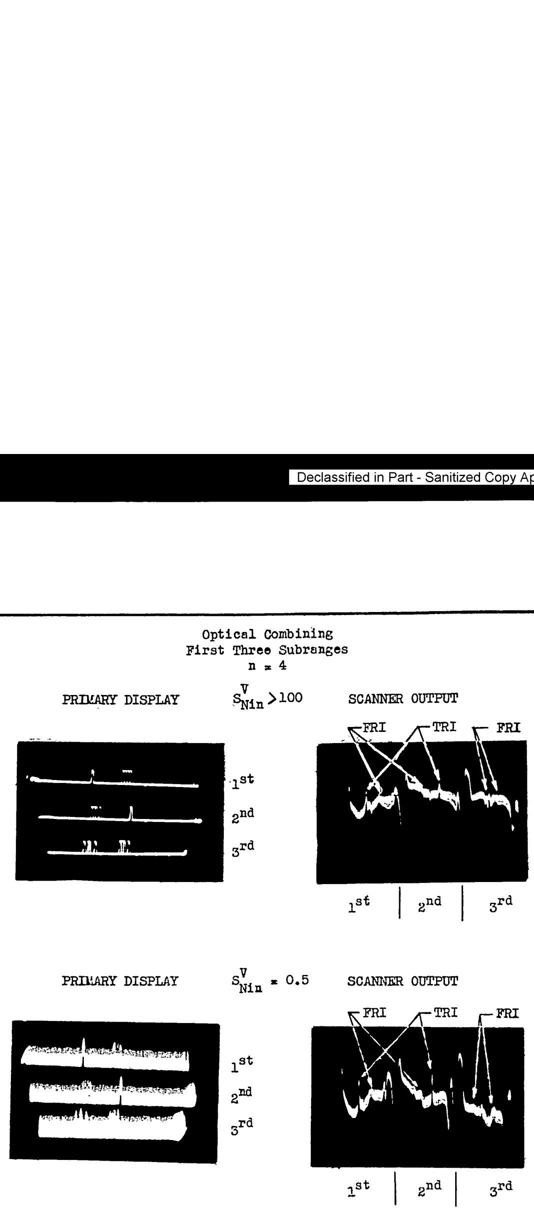

Optical-Electronic Ambiguity Filter
Deflection-Modulation, Baseline Break Detection

Figure 60

Optical Combining
First Three Subranges
n = 10

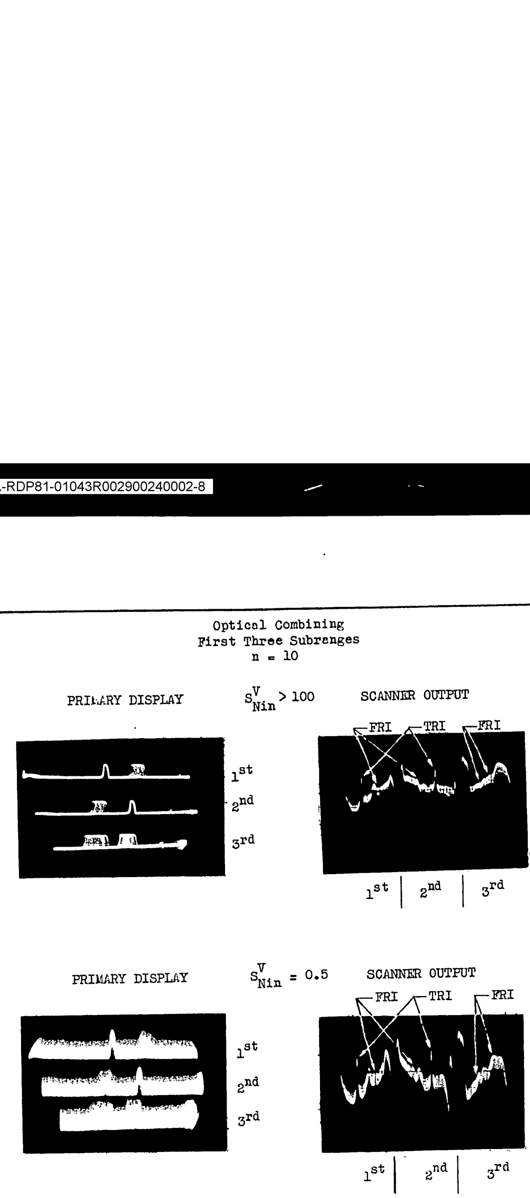

Optical-Electronic Ambiguity Filter
Deflection-Modulation, Baseline Break Detection

Figure 61

Declassified in Part - Sanitized Copy Approved for Release @ 50-Yr 2014/01/31 : CIA-RDP81-01043R002900240002-8

(Vidicon) in the scanner, creating a charge pattern on the target similar to the brightness pattern on the primary CRT. The baselines of this charge pattern are swept sequentially by the electron beam of the camera tube, thus reading out the baseline break information. The output of the scanner thus combines the information of the subrange displays into one sequential display, as shown in the oscillograms in Figures 60 and 61.

Experimental Results

The equipment assembled and built to form the Subrange Combining System combines only the first three subranges. This was considered adequate to demonstrate the operation of the system with minimum equipment cost. Provision was made to combine up to five subranges by the addition of more sweep generators to the system.

Representative examples of the system operation are shown in the oscillograms in Figures 60 and 61. These oscillograms show the primary displays for noiseless and noisy operation at two different values of n. The FRI echoes and the random noise appearing in the primary displays are greatly suppressed in the scanner output. The two large negative pulses that appear in each of the scanner output oscillograms are the switching transients developed as the scanner electron beam jumps from one baseline to another. The non-horizontal baselines of the scanner output oscillograms are due to slight non-

linearity in the camera tube sweep and ac ripple in the camera tube electron beam current. Further refinements must be incorporated in the circuitry to reduce these undesirable effects.

The figures-of-merit for the Optical-Electronic Ambiguity Filter with Subrange Combining were verified to be substantially the same as the figures-of-merit obtained with single subrange operation.[1]

Conclusions

The feasibility of recombining the subrange displays in the Optical-Electronic Ambiguity Filter has been experimentally demonstrated. Considerable care in the design of the circuitry is necessary to keep noise and ripple from degrading the output signal. Alignment between the primary CRT and the camera tube is critical. Drift in the positions of the primary traces and the scanning raster of the camera tube must be kept less than the thickness of the traces. These considerations indicate that considerable development work remains to be done before the Optical-Electronic Ambiguity Filter Subrange Combining System would be practical. Some of the newer schemes (for ambiguity elimination) directly present the entire range, thereby obviating the necessity for extra subrange combining equipment. If the figures-of-merit of

[1]Signal Corps Contract No. DA-36-039 SC-56696 Seventh Q.P.R. August 1955-October 1955, pp 8-97.

these schemes are comparable to the figures-of-merit of the Optical-Electronic Ambiguity Filter, it is recommended that work on the Optical-Electronic Ambiguity Filter be discontinued.

STORAGE-TUBE AMBIGUITY FILTER

Introduction

The ability of an electrostatic barrier-grid storage-tube, such as the RCA Radechon Type C73405A, to store and integrate information leads to several applications in the systems devised to eliminate range ambiguities in high repetition rate radars. These applications are divided into two categories; those that primarily utilize only the storage ability, and those that primarily utilize the integration ability.

In the Mixed PRF System, comb filters are used to discriminate and suppress false range indicating (FRI) echoes and random noise.[1] Comb filters for this purpose can be synthesized from linear amplifiers, constant time delay devices, and linear adders.[2] A storage-tube device, operating with a linear input-output relationship primarily as a storage device, could form the time delay element in such a comb filter. Linear operation of the Radechon, primarily as a storage device, has been described in the literature.[3,4]

[1] Signal Corps Contract No. DA-36-039 SC-56696, Fifth Q.P. R. February 1955-April 1955, pp 55-72.

[2] Ibid, pp 119-170.

[3] A.S. Jensen, "The Radechon, A Barrier Grid Storage Tube", RCA Review, Vol. 16, No.2, June 1955, pp 197-215.

[4] A.S. Jensen and G.W. Gray, "Radechon Storage Tube Circuits", RCA Review, Vol. 16, No.2, June 1955, pp 234-241.

Declassified in Part - Sanitized Copy Approved for Release @ 50-Yr 2014/01/31 : CIA-RDP81-01043R002900240002-8

In the PIM System the discrimination of the FRI echoes is accomplished simply by modulation of the time interval between successive transmitter pulses, as explained in the section entitled METHODS FOR DISCRIMINATING FALSE RANGE INDICATING ECHOES. The discriminated FRI echoes have the same amplitude as the true range indicating (TRI) echoes, and no signal-to-noise improvement is accomplished thru the pulse interval modulation alone. An ambiguity filter is necessary to suppress the FRI echoes and random noise. Storage-tube ambiguity filters utilize the integration ability of the storage-tube as the primary mechanism for suppression of the FRI echoes and random noise.[1,2]

Two variations of the basic Storage-Tube Ambiguity Filter, using an RCA Radechon Type C73405A barrier-grid storage-tube, have been designed, assembled and operated. Conventional intensity modulation of the electron beam in the storage tube by the video signals to be stored and integrated is not used in either variation of the filter. Deflection-modulation and negative-intensity-modulation are used to obtain much better ambiguity and random noise suppression than possible with conventional intensity modulation. A description of the equipment used in each of these filters is given in the section entitled DESCRIPTION OF EXPERIMENTAL EQUIPMENT.

[1]Signal Corps Contract No. DA-36-039 SC-56696, Second Q.P.R., March 1954-June 1954, pp 124-142. Third Q.P.R. June 1954-August 1954, pp 103-128. Interim Report December 1953-January 1955, pp 110-155. Fifth Q.P.R. February 1955-April 1955, pp 15-54.

[2]J.V. Harrington and T.F. Rogers, "Signal-to-Noise Improvement Through Integration in a Storage Tube", Proceedings of the IRE, Vol. 38, October 1950, pp 1197-1203.

Deflection-Modulation

The deflection-modulation Storage-Tube Ambiguity Filter is shown in block diagram form in Figure 33. The echo information is written on the storage area (target) of the storage-tube by an electron beam with constant beam current, uniform sweep speed, and vertical deflection by the echo information to be stored and integrated. The echo information received during the n pulse intervals of the PIM modulation cycle is superimposed (integrated) on the target with a common baseline and uniform sweeps triggered by each transmitter pulse in the modulation cycle. This means that every part of the baseline (where no echoes appear) is swept n times by the electron beam. The baseline under any one of the multiple FRI echoes is swept n-1 times and the baseline under the TRI echoes is not touched by the electron beam. Figure 62A shows the relative charge density on the target after three sweeps of the electron beam. The density of the lines indicates the relative charge density.

After a complete modulation cycle has been written on the target (n sweeps), the vertical deflection of the electron beam is clamped at the baseline level, the

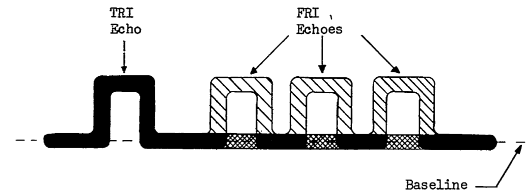

A. Deflection-Modulation

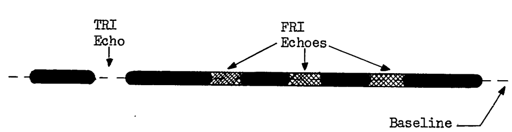

B. Negative-Intensity-Modulation

Relative Charge Density on Target After Three Sweeps By Electron Beam Writing Echo Information

Figure 62

necessary changes in the storage-tube electrode potentials are made, and the electron beam is swept along the baseline with constant beam current, thus reading out the integrated information in the baseline. This information consists of the baseline "breaks" due to TRI and FRI echoes. The output signal of the storage-tube during the reading operation is a function of the charge density on the target. With baseline scan during the reading operation, the output for a FRI echo is the difference between the baseline signal (where no echoes appear) and the signal due to the baseline under the FRI echoes. The output for a TRI echo is the difference between the baseline signal (where no echoes appear) and the signal due to the baseline under the TRI echo. This difference (or output) is greater for the TRI echoes than for the FRI echoes, and hence the FRI echoes are suppressed. The amount of suppression obtained depends upon the operating parameters of the storage-tube during both the writing and reading operations.

When the signal-to-noise ratio is low (less than 0.5), the operation of the filter becomes impaired by the spreading-out of the baseline and the filling-in of the baseline breaks under the TRI echoes. These effects reduce the output signal amplitude and the ambiguity suppression, respectively.

Negative-Intensity-Modulation

The negative-intensity-modulation Storage-Tube

Declassified in Part - Sanitized Copy Approved for Release @ 50-Yr 2014/01/31 : CIA-RDP81-01043R002900240002-8

Ambiguity Filter is shown in block diagram form in Figure 34 The echo information is written on the storage-tube target by an electron beam with uniform sweep speed, no vertical deflection, and negative-intensity-modulation of the beam current. Conventional intensity modulation of beam current usually means that the current is increased to write an echo. In negative-intensity-modulation the beam current is driven toward cut off in order to write an echo. The fraction of the echo duration that the beam current can be completely cut off, on the average, depends upon the input signal-to-noise ratio. The percent of the echo duration for which complete cut off is possible, on the average, is 99.99, 97.73, 84.13, and 69.15 percent for voltage signal-to-noise ratios of 5, 2, 1, and 0.5 respectively with a Gaussian noise amplitude distribution. The echo information received during the n pulse intervals of the PIM modulation cycle is superimposed (integrated) on the target along a common baseline. This means that every part of the baseline (where no echoes appear) is swept n times by the electron beam. The baseline at the position of any one of the multiple FRI echoes is swept n-1 times and the baseline at the position of a TRI echo is not touched by the electron beam (for large signal-to-noise ratios). Figure 62B shows the relative charge density on the target after three sweeps of the electron beam. The density of the line indicates the relative charge density.

Comparison of the charge distribution along the baseline obtained with deflection-modulation to that obtained with negative-intensity-modulation shows that for baseline break detection the two are equivalent when no noise is present. Consequently, the reading operation in the negative-intensity-modulation system is the same as in the deflection-modulation system.

The negative-intensity-modulation system has an advantage (as shown in Figures 62A, B) over the deflection-modulation system when the input signal-to-noise ratio is low. The baseline in negative-intensity-modulation is not spread out, but rather tends to fill in and become more uniform as the number of writing sweeps increases which improves the output signal-to-noise ratio.

Radechon Characteristics

The ambiguity suppression and signal-to-noise ratio improvement obtained in the Storage-Tube Ambiguity Filter are dependent primarily on the storage-tube characteristics. The operational mechanism of the Radechon storage-tube has been described in previous reports[1] and theoretical derivations of the characteristics have appeared in the literature.[2,3] The mathematical expressions for

[1] Signal Corps Contract No. DA-36-039 SC-56696, Fifth Q.P. R. February 1955-April 1955, pp 15-54.

[2] J.V. Harrington, "Storage of Small Signals on a Dielectric Surface", Journal of Applied Physics, Vol. 21, October 1950, pp 1048-1053.

[3] A.S. Jensen, "Discharging an Insulator Surface by Secondary Emission Without Redistribution", RCA Review, Vol. 16, No. 2, June 1955, pp 216-233.

Declassified in Part - Sanitized Copy Approved for Release @ 50-Yr 2014/01/31 : CIA-RDP81-01043R002900240002-8

the Radechon characteristics developed by A.S. Jensen are most suitable for use in determining the figures-of-merit for the Storage-Tube Ambiguity Filter since they can be made to incorporate all the pertinent system parameters.

A simplified schematic diagram of a Radechon storage-tube circuit is shown in Figure 63. If the back plate and barrier grid are connected together (switch in "R" position) and the target is repetitively swept by the electron beam, charge is deposited on the target until an equilibrium voltage between the target and the barrier grid is reached. At this equilibrium voltage the beam current impinging on the target is equal to the secondary emission current leaving the target. It is convenient to use this equilibrium voltage as a reference level to which all target to barrier grid voltages are referred. That is

(1) $$V_{tb} = V_{TB} - V_{EQ}$$

where

V_{tb} = target-to-barrier grid charging voltage

V_{TB} = actual target-to-barrier grid voltage

V_{EQ} = equilibrium target-to-barrier grid voltage

which makes the value of V_{tb} equal to zero at equilibrium.

For the writing operation, a fixed voltage (V_{sh}) is applied between the back plate and the barrier grid (switch in "W" position). Because of the large capacitive coupling between the back plate and the target, almost all of this voltage shift appears between the

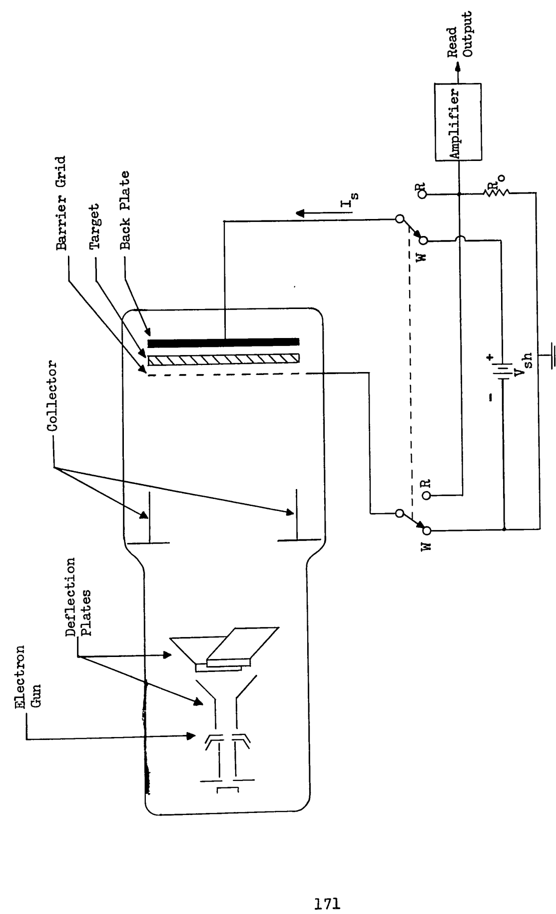

Simplified Radechon Storage-Tube Circuit

Figure 63

Declassified in Part - Sanitized Copy Approved for Release @ 50-Yr 2014/01/31 : CIA-RDP81-01043R002900240002-8

target and the barrier grid.[1] As charge is deposited on the target by the writing electron beam the charging voltage between the target and the barrier grid changes from this initial value (V_{tboW}) towards the equilibrium value. The charging voltage between the target and the barrier grid after n passages of the writing electron beam (V_{tbnW}) is[2]

$$V_{tbnW} = V_{tboW} + V_{se} \ln \left[\left(1 - e^{-\frac{V_{tboW}}{V_{se}}}\right) e^{-nJ_{bW}} + e^{-\frac{V_{tboW}}{V_{se}}} \right] \qquad (2)$$

where

V_{tboW} = charging voltage between target and barrier grid at start of write operation

V_{se} = average secondary electron energy in electron volts

n = number of write sweeps

J_{bW} = relative beam current during writing operation

The relative beam current during the writing operation (J_{bW}) is

$$J_{bW} = \frac{r\, I_{bW}}{C_x b\, V_{se} v_W} \qquad (3)$$

where

r = barrier grid transmission ratio

I_{bW} = electron beam current during writing operation

C_x = target capacitance per unit area

b = diameter of the electron beam

v_W = scan speed during writing operation

---

[1] Signal Corps Contract No. DA-36-039 SC-56696 Fifth Q.P.R. February 1955-April 1955, p 46.

[2] A.S. Jensen, Op. Cit.

When the writing operation is completed the external voltage (V_{sh}) between the back plate and the barrier grid is removed and an output load impedance (R_o) is connected between the back plate and ground (switch in "R" position). Removal of the external voltage (V_{sh}) causes another shift in the target to barrier grid charging voltage approximately equal to V_{sh}. This establishes the new initial conditions for the start of the read operation. The charging voltage between the target and barrier grid at the start of the read operation (V_{tboR}) is

$$V_{tboR} = V_{tbnW} - V_{tboW} \qquad (4)$$

which, by the use of (2), becomes

$$V_{tboR} = V_{se} \ln \left[\left(1 - e^{-\frac{V_{tboW}}{V_{se}}}\right) e^{-nJ_{bW}} + e^{-\frac{V_{tboW}}{V_{se}}} \right] \qquad (5)$$

As the electron beam sweeps the target in the reading operation, the target to barrier grid charging voltage changes toward the equilibrium value. Portions of the target which have not been written on by the electron beam during the writing operation are at equilibrium and hence no net charge is transferred to or from the target and the signal current (I_s) is zero at these places. Portions of the target on which charge was deposited during writing lose that charge during reading in order to reach the equilibrium voltage, producing a signal. The net charge flow, or current, perpendicular to the target surface induces a signal current I_s into the back plate, due to the capacitive coupling.

Declassified in Part - Sanitized Copy Approved for Release @ 50-Yr 2014/01/31 : CIA-RDP81-01043R002900240002-8

The signal current is a function of the target to barrier grid charging voltage at the start of the read operation (V_{tboR}). Three different expressions for the signal current are obtained, depending upon the value of V_{tboR}.[1] Case I results when the target is always positive with respect to the barrier grid. Case II results when the target is initially negative with respect to the barrier grid but is finally positive with respect to the barrier grid after the read sweep. Case III results when the target is always negative with respect to the barrier grid. These three cases are marked on the storage-tube characteristics of Figures 64 and 65.

Case I: $\left[-V_{se}\ln\delta \leq V_{tboR}\right]$

The relative signal current during reading (J_{sR}) is

$$(6) \qquad J_{sR} = -\ln\left[\left(1-e^{-\frac{V_{tboR}}{V_{se}}}\right) e^{-J_{bR}} + e^{-\frac{V_{tboR}}{V_{se}}}\right]$$

and the actual signal current (I_{sR}) is

$$(7) \qquad I_{sR} = C_x b\, V_{se} v_R J_{sR}$$

where

δ = secondary emission ratio of the target

J_{bR} = relative beam current during reading operation

v_R = scan speed during reading operation

[1] A.S. Jensen, Op. Cit.

The relative beam current during the reading operation (J_{bR}) is

$$(8) \qquad J_{bR} = \frac{r\, I_{bR}}{C_x b\, V_{se} v_R}$$

where

I_{bR} = electron beam current during reading operation

The charging voltage between the target and the barrier grid after the reading sweep is

$$(9) \qquad V_{tb1r} = V_{tboR} + V_{se}\ln\left[\left(1-e^{-\frac{V_{tboR}}{V_{se}}}\right) e^{-J_{bR}} + e^{-\frac{V_{tboR}}{V_{se}}}\right]$$

Case II: $\left[J_{bR}V_{se}(1-\delta)-V_{se}\ln\delta \leq V_{tboR} \leq -V_{se}\ln\delta\right]$

The relative signal current during reading (J_{sR}) is

$$(10) \qquad J_{sR} = -\ln\left[(1-\delta)e^{-J_{bR} + \frac{\delta}{1-\delta}\left(\frac{V_{tboR}}{V_{se}} + \ln\delta\right)} + e^{-\frac{V_{tboR}}{V_{se}}}\right]$$

The charging voltage between the target and the barrier grid after the reading sweep is

$$(11) \qquad V_{tb1R} = V_{tboR} + V_{se}\ln\left[e^{-\frac{V_{tboR}}{V_{se}}} + (1-\delta)e^{-J_{bR} + \frac{\delta}{1-\delta}\left(\frac{V_{tboR}}{V_{se}} + \ln\delta\right)}\right]$$

Case III: $\left[V_{tboR} \leq J_{bR}V_{se}(1-\delta) - V_{se}\ln\delta\right]$

The relative signal current during reading (J_{sR}) is

$$(12) \qquad J_{sR} = (1-\delta)\, J_{bR}$$

The charging voltage between the target and the barrier grid after the reading sweep is

$$(13) \qquad V_{tb1R} = V_{tboR} - J_{bR}(1-\delta)\, V_{se}$$

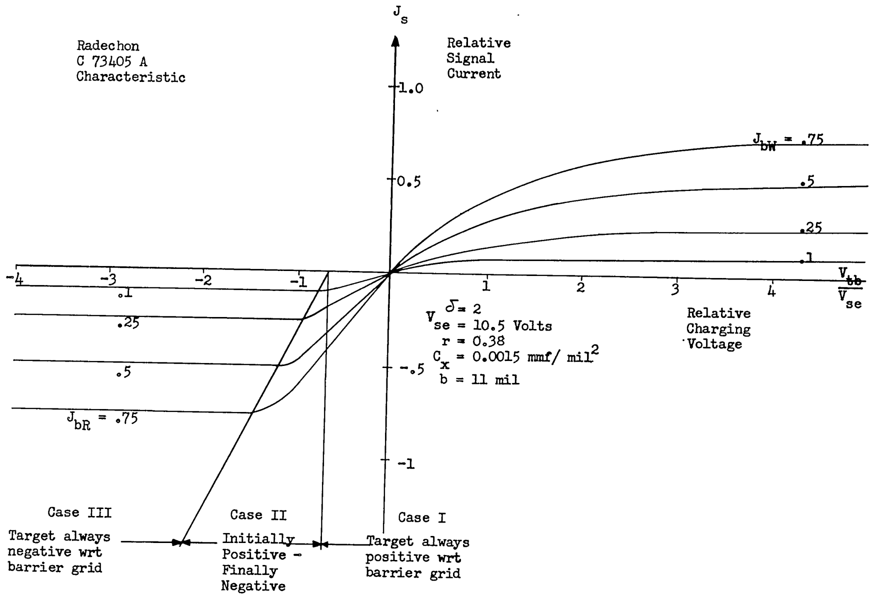

Radechon Characteristic

Figure 64

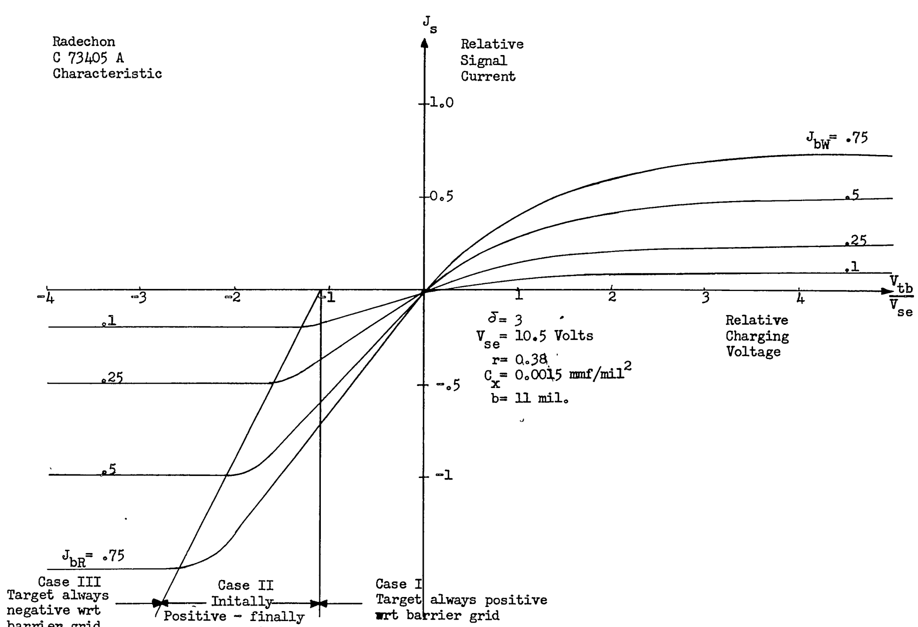

Radechon Characteristic

Figure 65

Equations (6), (10), and (12) are the storage-tube characteristics. These are plotted for two different values of δ (2 and 3), corresponding to high and low acceleration voltages (approximately 2000 volts and 1200 volts) respectively, in Figures 64 and 65. Equation (5) shows in which of the three regions of the characteristics the reading operation takes place when numerical values are substituted into the equation and the value obtained is compared to the numerical values of the limits of each of the three regions. The relative charging voltage at the start of the read operation (V_{tboR}/V_{se}) is plotted as a function of the cumulative relative beam current during the writing operation (nJ_{bW}) for two values of relative charging voltage at the start of the write operation (V_{tboW}/V_{se}) in Figure 66, from (5).

Figures-of-Merit

The ambiguity suppression figure-of-merit (F_{AS}) and the noise suppression figure-of-merit (F_{NS}) characterize the operation of the Storage-Tube Ambiguity Filter. Two types of modulation (deflection and negative-intensity) are possible, thus giving two variations of the basic filter for which the figures-of-merit must be determined. When no random noise is present in the input to the filter, only the ambiguity suppression figure-of-merit is applicable. The addition of random noise to the input of the filter makes the noise suppression figure-of-merit significant as well as modifying the ambiguity suppression

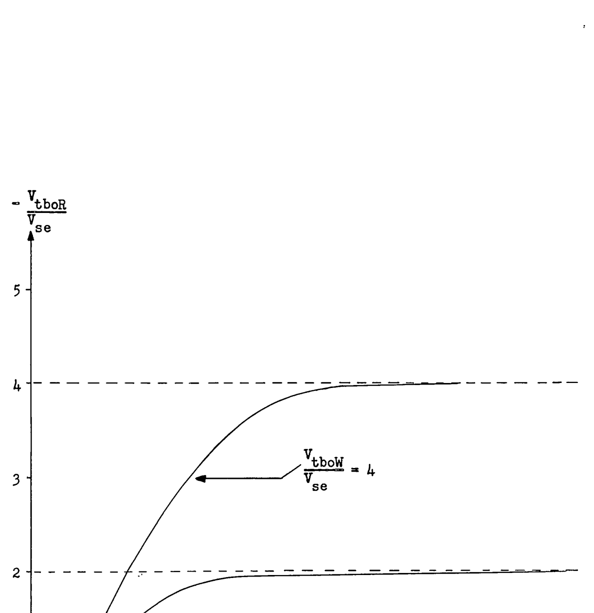

Target Charging Characteristics

Figure 66

figure-of-merit. It is desirable that the random noise degrade the ambiguity suppression as little as possible. The method of approach in determining the figures-of-merit is to first determine the idealized (no random noise present) ambiguity suppression figure-of-merit for each type of modulation. The amount of degradation of this figure-of-merit by random noise must then be determined for each type of modulation. The noise suppression figure-of-merit for each type of modulation is determined last. In the absence of noise the idealized ambiguity suppression figure-of-merit is the same for both deflection-modulation and negative-intensity-modulation when base line break detection is employed. This is readily seen from Figure 62 and previous discussion of the operation of the two modulation schemes.

The baseline (where no echoes appear) is swept by the writing electron beam n times, where n is the number of intervals in the PIM modulation cycle. At the start of the read operation the target to barrier grid charging voltage is, from (5),

$$(14) \qquad V_{tboRB} = V_{se} \ln \left[\left(1 - e^{-\frac{V_{tboW}}{V_{se}}}\right) e^{-nJ_{bW}} + e^{-\frac{V_{tboW}}{V_{se}}} \right]$$

The relative signal current due to the baseline during the reading operation (J_{sRB}) is determined by V_{tboRB} and the relative beam current during reading (J_{bR}). The reading operation may be in any one of the three regions of the storage-tube characteristics, depending upon the value of

V_{tboRB}.

Case I: $\left[-V_{se} \ln \delta \leq V_{tboRB} \right]$

$$(15) \qquad J_{sRB} = -\ln \left[\left(1 - e^{-\frac{V_{tboRB}}{V_{se}}}\right) e^{-J_{bR}} + e^{-\frac{V_{tboRB}}{V_{se}}} \right]$$

Case II: $\left[J_{bR} V_{se} (1-\delta) - V_{se} \ln \delta \leq V_{tboRB} \leq -V_{se} \ln \delta \right]$

$$(16) \qquad J_{sRB} = -\ln \left[(1-\delta) e^{-J_{bR} + \frac{\delta}{1-\delta}\left(\frac{V_{tboRB}}{V_{se}} + \ln \delta\right)} + e^{-\frac{V_{tboRB}}{V_{se}}} \right]$$

Case III: $\left[V_{tboRB} \leq J_{bR} V_{se} (1-\delta) - V_{se} \ln \delta \right]$

$$(17) \qquad J_{sRB} = (1-\delta) J_{bR}$$

The baseline under any one of the multiple FRI echoes is swept by the writing electron beam n-1 times. At the start of the read operation the target to barrier grid charging voltage is

$$(18) \qquad V_{tboRFRI} = V_{se} \ln \left[\left(1 - e^{-\frac{V_{tboW}}{V_{se}}}\right) e^{-(n-1)J_{bW}} + e^{-\frac{V_{tboW}}{V_{se}}} \right]$$

The relative signal current due to the FRI echoes during the reading operation (J_{sRFRI}) is given by (19), (20), or (21), depending upon the value of $V_{tboRFRI}$.

Case I: $\left[-V_{se} \ln \delta \leq V_{tboRFRI} \right]$

Declassified in Part - Sanitized Copy Approved for Release @ 50-Yr 2014/01/31 : CIA-RDP81-01043R002900240002-8

(19) $$J_{sRFRI} = -\ln\left[\left(1-e^{-\frac{V_{tboRFRI}}{V_{se}}}\right) e^{-J_{bR}} + e^{-\frac{V_{tboRFRI}}{V_{se}}}\right]$$

Case II: $\left[J_{bR}V_{se}(1-\delta)-V_{se}\ln\delta \leq V_{tboRFRI} \leq -V_{se}\ln\delta\right]$

(20) $$J_{sRFRI} = -\ln\left[(1-\delta)e^{-J_{bR}+\frac{\delta}{1-\delta}\left(\frac{V_{tboRFRI}}{V_{se}}+\ln\delta\right)} + e^{-\frac{V_{tboRFRI}}{V_{se}}}\right]$$

Case III: $\left[V_{tboRFRI} \leq J_{bR}V_{se}(1-\delta)-V_{se}\ln\delta\right]$

(21) $$J_{sRFRI} = (1-\delta)\,J_{bR}$$

The baseline under the TRI echoes is not touched by the writing electron beam. At the start of the read operation the target to barrier grid charging voltage is

(22) $$V_{tboRTRI} = 0$$

and the relative signal current during the reading operation is

(23) $$J_{sRTRI} = 0$$

The storage-tube output during the reading operation with baseline break detection for the echo signal shown in Figure 62 is shown in Figure 67.

Considering only the relative amplitudes of the storage-tube output signal, the relative TRI signal (J_{TRI}) becomes

(24) $$J_{TRI} = J_{sRTRI} - J_{sRB} = -J_{sRB}$$

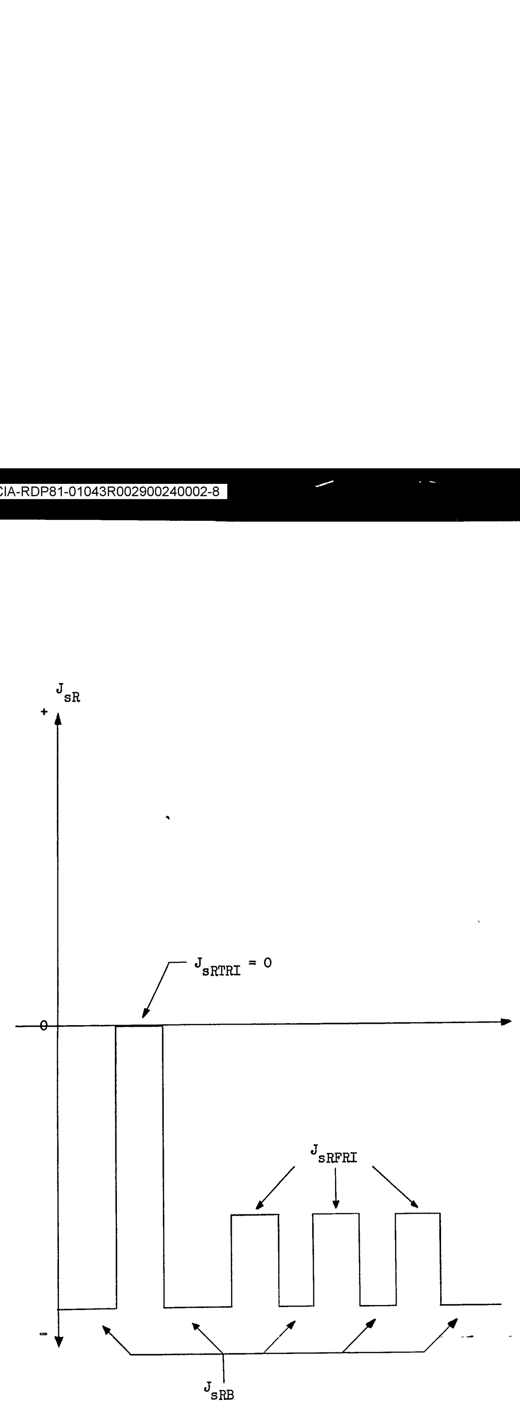

Storage-Tube Output Signal

Figure 67

and the relative FRI signal (J_{FRI}) becomes

(25) $$J_{FRI} = J_{sRFRI} - J_{sRB}$$

The ambiguity suppression figure-of-merit (F_{AS}) defined as

(26) $$F_{AS} = \frac{V_{TRI\ out}}{V_{FRI\ out}}$$

can be expressed as

(27) $$F_{AS} = \frac{J_{TRI\ out}}{J_{FRI\ out}}$$

Substitution of (24) and (25) into (27) gives the ambiguity suppression figure-of-merit as

(28) $$F_{AS} = \frac{J_{sRB}}{J_{sRB} - J_{sRFRI}}$$

Unfortunately, no further substitution for J_{sRB} or J_{sRFRI} can be made until the values of V_{tboRB} and $V_{tboRFRI}$ are known, since these charging voltages determine in which region of the characteristics the reading operation takes place and consequently the form of the equations for the relative signal currents. Further complication arises due to the fact that two different regions can be specified by the two charging voltages. In order to gain an insight of how F_{AS} varies with the various system parameters, the set of calculated curves shown in Figures 68 and 69 are presented. All of these curves are shown for $\delta = 3$ (approximately 1200 volts acceleration) but the same trend of variation occurs for smaller values of δ

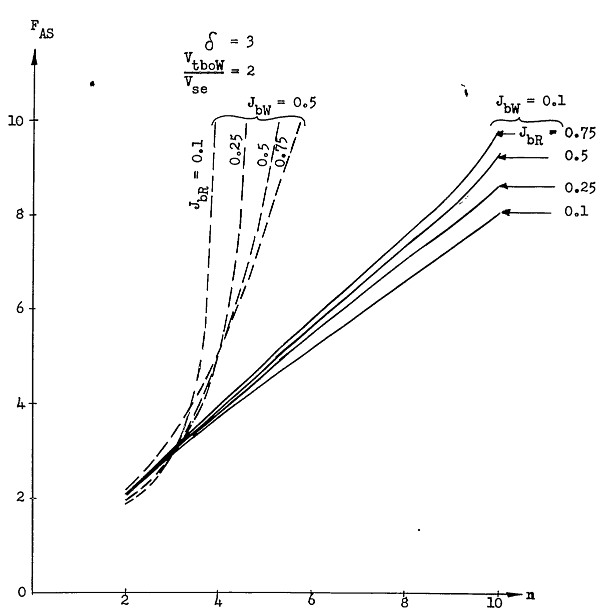

Theoretically Determined Ambiguity Suppression Figure-of-Merit

Figure 68

Declassified in Part - Sanitized Copy Approved for Release @ 50-Yr 2014/01/31 : CIA-RDP81-01043R002900240002-8

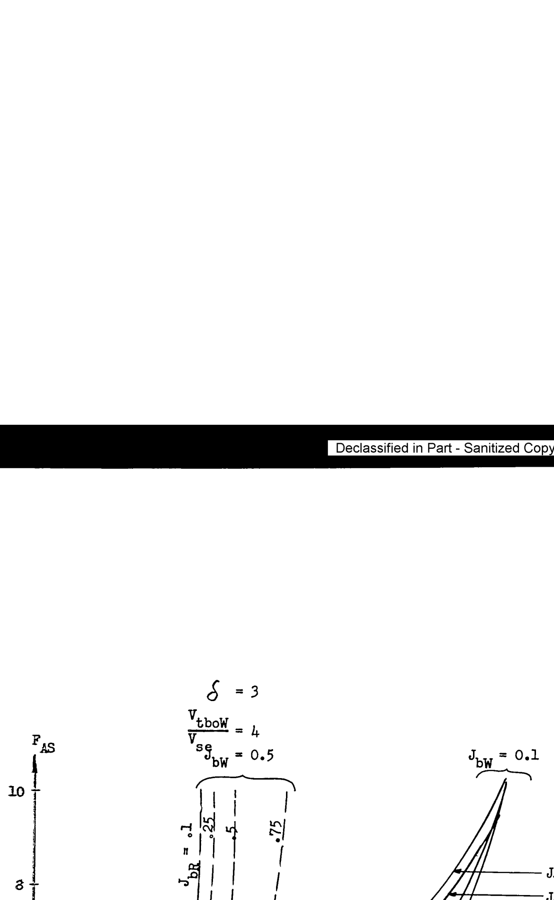

Theoretically Determined Ambiguity Suppression Figure-of-Merit

Figure 69

(higher acceleration voltages).

Equation (28) shows that when J_{sRFRI} is equal to J_{sRB} the ambiguity suppression figure-of-merit is infinitely large. This means that the FRI echoes are completely eliminated by the filter. If the reading operation for either the baseline or the FRI echoes occurs in regions I or II of the storage-tube characteristics, F_{AS} becomes infinitely large only when n (the number of writing sweeps) becomes infinitely large. If, however, the reading operations for both the baseline and the FRI echoes fall in region III of the storage-tube characteristics, n need not be infinitely large to yield an infinitely large value of F_{AS} for the idealized situation with no random noise at the input of the filter. For this condition to be met, it is necessary that

(29) $$V_{tboRFRI} \le J_{bR}V_{se}(1-\delta)-V_{se}\ln\delta$$

Using the equation for $V_{tboRFRI}$ (equation (18)) in (29) gives

(30) $$\ln\left[(1-e^{-\frac{V_{tboW}}{V_{se}}})\, e^{-(n-1)J_{bW}} + e^{-\frac{V_{tboW}}{V_{se}}}\right] \le J_{bR}(1-\delta)-\ln\delta$$

which can be manipulated into the form

(31) $$(n-1)J_{bW} \ge \ln\left[\frac{\delta(1-e^{-\frac{V_{tboW}}{V_{se}}})}{e^{J_{bR}(1-\delta)} - \delta e^{-\frac{V_{tboW}}{V_{se}}}}\right]$$

In order for $(n-1)J_{bW}$ to be real, it is necessary that

(32) $$e^{J_{bR}(1-\delta)} \geq \delta e^{-\frac{V_{tboW}}{V_{se}}}$$

which gives

(33) $$\frac{V_{tboW}}{V_{se}} \geq \ln\delta - J_{bR}(1-\delta)$$

Equation (33) establishes the minimum value of the initial writing target to barrier grid relative charging voltage that will allow an infinitely large value of F_{AS} to be attained. This is

(34) $$\frac{V_{tboW\ min\infty}}{V_{se}} = \ln\delta - J_{bR}(1-\delta)$$

which is plotted in Figure 70. Substitution of (34) into (31) establishes the condition

(35) $$(n-1)J_{bW} \geq \left[\ln \frac{\delta e^{-J_{bR}(1-\delta)} - e^{-\frac{V_{tboW} - V_{tboW\ min\infty}}{V_{se}}}}{1 - e^{-\frac{V_{tboW} - V_{tboW\ min\infty}}{V_{se}}}} \right]$$

Equation (35) establishes the minimum cumulative relative writing beam current required for an infinitely large value of F_{AS}, which is

(36) $$(n-1)J_{bW\ min\infty} = \left[\ln \frac{\delta e^{-J_{bR}(1-\delta)} - e^{-\frac{V_{tboW} - V_{tboW\ min\infty}}{V_{se}}}}{1 - e^{-\frac{V_{tboW} - V_{tboW\ min\infty}}{V_{se}}}} \right]$$

Equation (36) is plotted in Figures 71 and 72 for two values of δ.

From the preceding analysis it can be seen that the Storage-Tube Ambiguity Filter, under idealized operating

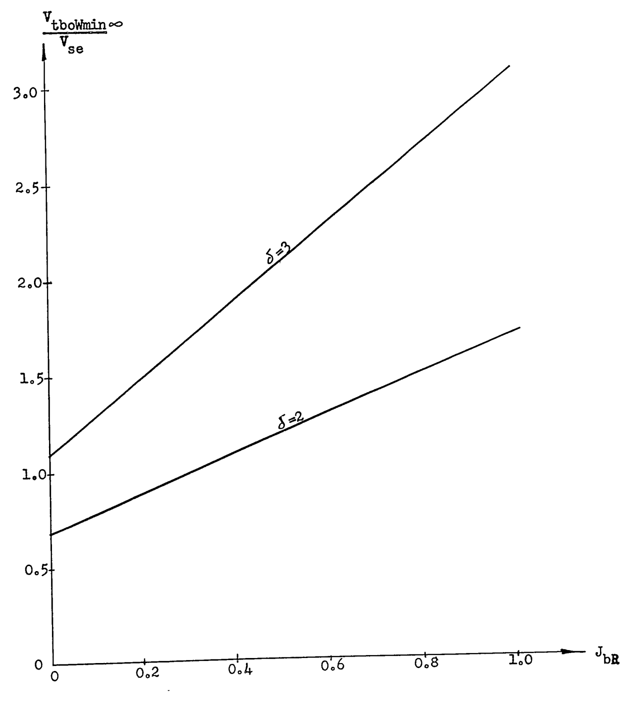

Theoretical Minimum Relative Charging Voltage For Infinite Ambiguity Suppression

Figure 70

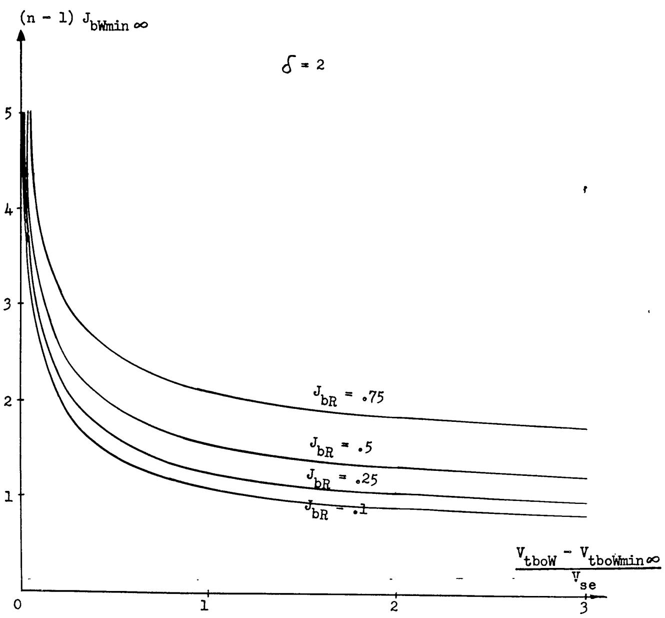

Theoretical Minimum Cumulative Relative Writing
Beam Current For Infinite Ambiguity Suppression

Figure 71

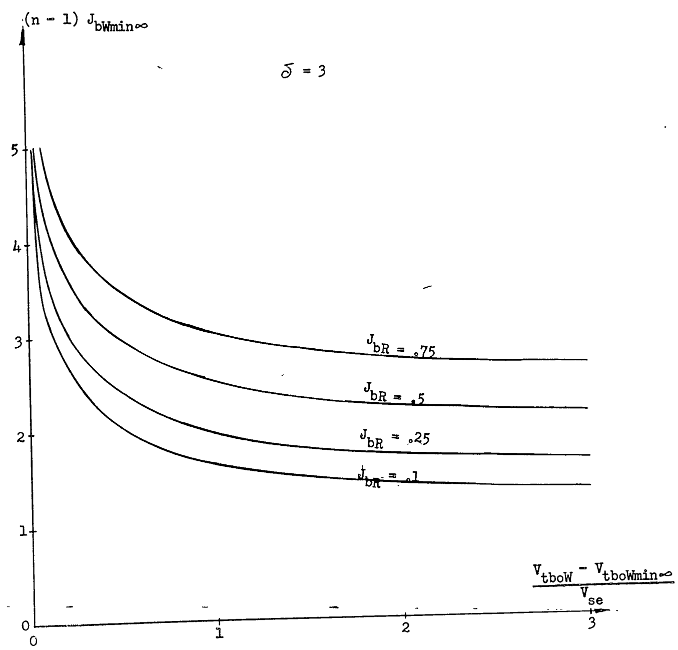

Theoretical Minimum Cumulative Relative Writing
Beam Current For Infinite Ambiguity Suppression

Figure 72

conditions, is capable of completely eliminating FRI echoes due to high pulse repetition rates when the operating parameters are suitably chosen. These optimum operating conditions for the Storage-Tube Ambiguity Filter are given by equations (33) and (35).

When random noise is present at the input to the filter the ambiguity suppression figure-of-merit may be affected. The noise suppression figure-of-merit also becomes significant in determining the effectiveness of the filter. The effects of random noise are to decrease the average amount of charge deposited at the baseline during writing (only with deflection-modulation), to make the charge density non-uniform along the baseline (where no echoes appear), and to partially fill in the baseline breaks due to TRI and FRI echoes. The first effect decreases the size of the output signals from the storage-tube. The second effect causes random noise to appear in the output of the storage-tube (in addition to the noise generated by the storage-tube itself). The third effect may alter the ambiguity suppression figure-of-merit. Since the baseline breaks under both the TRI and the FRI echoes are partially filled in by the random noise, a significant decrease in the ambiguity suppression figure-of-merit is not anticipated. It has been pointed out earlier that the negative-intensity-modulation scheme is expected to have a higher noise suppression figure-of-merit than the

deflection-modulation scheme. The theoretical figures-of-merit for the Storage-Tube Ambiguity Filter operating with low input signal-to-noise ratios remain to be found. A preliminary theoretical investigation has been made[1] but the results are inadequate because no provision was allowed for operation in region III of the storage-tube characteristics.

Experimental Results

The equipment used to determine the figures-of-merit of the Storage-Tube Ambiguity Filter experimentally is described in the section entitled DESCRIPTION OF EXPERIMENTAL EQUIPMENT. Unfortunately, the equipment was not versatile enough to permit a direct verification of the theoretical curves shown in Figures 68 thru 72. The target secondary emission ratio (δ), which depends upon the electron beam acceleration voltage, was not readily measurable. The electron beam current during writing and reading could not be directly measured.

In order to obtain representative values for the figures-of-merit the following procedure was used.

(1) The length of the modulation cycle was set at 2000 microseconds (equivalent to a maximum range of approximately 200 miles).

[1]Signal Corps Contract No. DA-36-039 SC-56696, Interim Report, December 1953-January 1955, pp 110-155.

Declassified in Part - Sanitized Copy Approved for Release @ 50-Yr 2014/01/31 : CIA-RDP81-01043R002900240002-8

(2) The read-write relative potential shift applied between the back plate and the barrier grid of the Radechon storage-tube was set at approximately 2. This was approximately the maximum value that could be produced in the potential shifting circuit without exceeding component ratings.

(3) Values of n between 4 and 15 were used (corresponding to 3 to 14 writing sweeps since one subinterval of the modulation cycle was used to read out the stored signals).

(4) For each value of n the writing and reading relative beam currents were adjusted to obtain the best compromise between the maximization of both F_{AS} and F_{NS} with one read sweep returning the target to as near equilibrium as possible. Both F_{AS} and F_{NS} did not consistently maximize simultaneously. One could be improved a little (above the compromise values obtained) at the expense of greatly reducing the other. Return of the target to equilibrium by one read sweep is not consistent with operation in region III of the storage-tube characteristics, as seen from equation (13), and hence the conditions for an infinitely large ambiguity suppression figure-of-merit were not attained in the experimental work.

(5) Several input voltage signal-to-noise ratios (S^V_{Nin}) were used.

(6) Two different acceleration voltages were used to verify the expected effects of δ on the figures-of-merit.

The results of the above experimental procedure are summarized in the curves in Figures 73 thru 76. A qualitative picture of the operation of the Storage-Tube Ambiguity Filter can be obtained from the oscillograms in Figures 77 thru 80.

Reference to the experimental curves of Figures 73 thru 76 verifies and/or justifies the theoretical analysis and assumptions of the preceding section. The ambiguity suppression figure-of-merit does not appear to be highly dependent upon the input signal-to-noise ratio for either negative-intensity-modulation or deflection-modulation when the input signal-to-noise ratio is greater than 0.5. The ambiguity suppression figure-of-merit for the negative-intensity-modulation scheme is higher than for the deflection-modulation scheme (theory indicates they should be the same with $S^V_{Nin}=\infty$) because of a slight spreading out of the baseline due to hum and extraneous fields which affects the deflection-modulation scheme more severely. The noise suppression figure-of-merit for the negative-intensity-modulation scheme is substantially greater than for the deflection-modulation scheme, as expected.

Declassified in Part - Sanitized Copy Approved for Release @ 50-Yr 2014/01/31 : CIA-RDP81-01043R002900240002-8

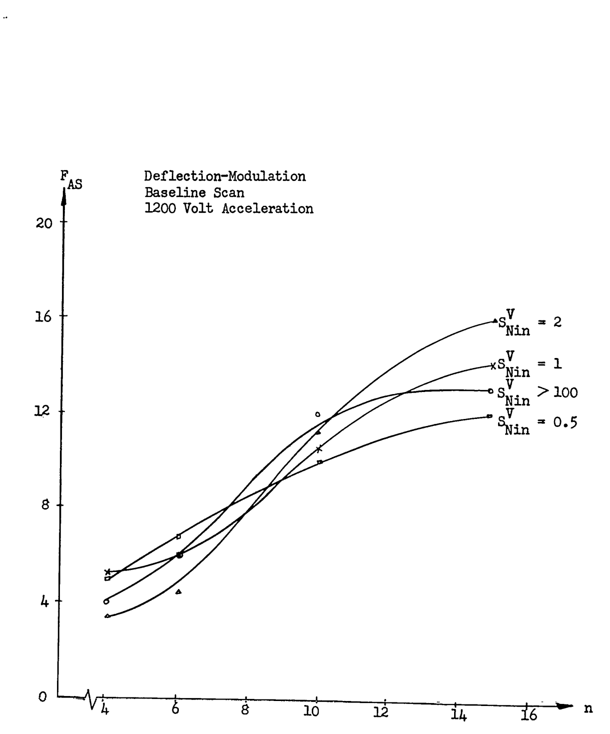

Storage-Tube Ambiguity Filter Experimental Ambiguity Suppression Figure-of-Merit

Figure 73

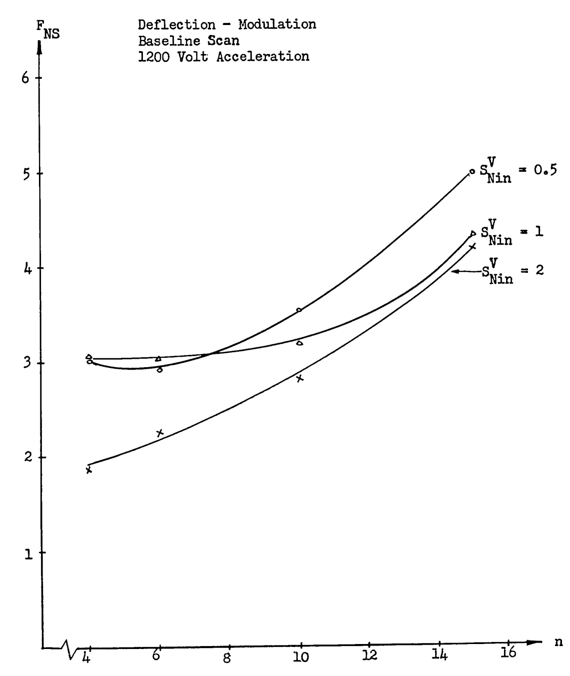

Storage-Tube Ambiguity Filter Experimental Noise-Suppression Figure-of-Merit

Figure 74

Declassified in Part - Sanitized Copy Approved for Release @ 50-Yr 2014/01/31 : CIA-RDP81-01043R002900240002-8

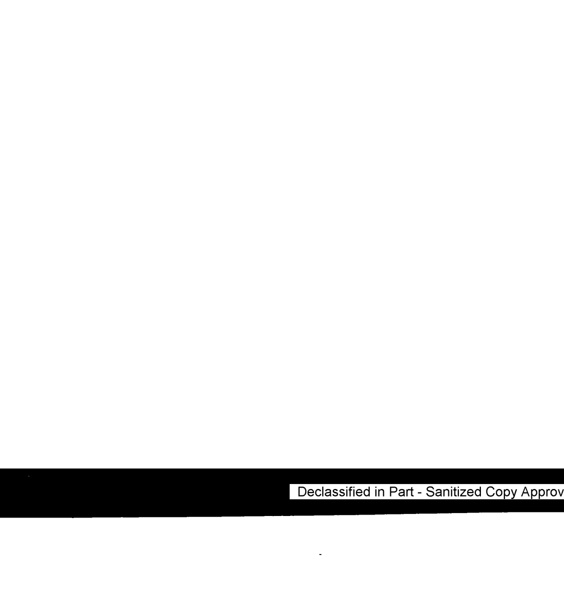

Storage-Tube Ambiguity Filter Expermental
Ambiguity Suppression Figure-of-Merit

Figure 75

Storage-Tube Ambiguity Filter Expermental
Noise-Suppression Figure-of-Merit

Figure 76

Declassified in Part - Sanitized Copy Approved for Release @ 50-Yr 2014/01/31 : CIA-RDP81-01043R002900240002-8

[illegible] VOLT [illegible]
[illegible]

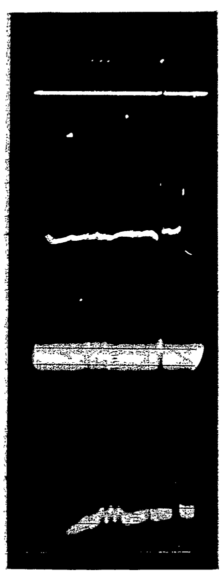

[illegible]
$S^V_{Nin} > 100$

[illegible]
$S^V_{Nin} > 100$

[illegible]
$S^V_{Nin} = 0.5$

[illegible]
$S^V_{Nin} = 0.5$

[illegible]-Tube [illegible] Filter Operation,
[illegible], Baseline Break Detection

Figure [illegible]

1200 VOLT ACCELERATION
n = 10

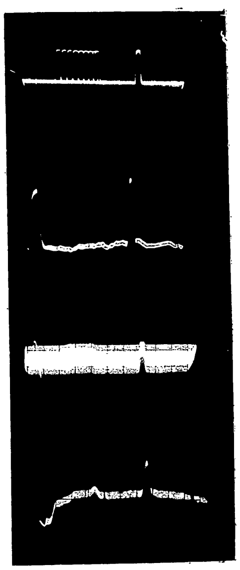

INPUT
$S^V_{Nin} > 100$

OUTPUT
$S^V_{Nin} > 100$

INPUT
$S^V_{Nin} = 0.5$

OUTPUT
$S^V_{Nin} = 0.5$

Storage-Tube Ambiguity Filter Operation,
Deflection-Modulation, Baseline Break Detection

Figure 78

Declassified in Part - Sanitized Copy Approved for Release @ 50-Yr 2014/01/31 : CIA-RDP81-01043R002900240002-8

1200 VOLT ACCELERATION
$n = 4$

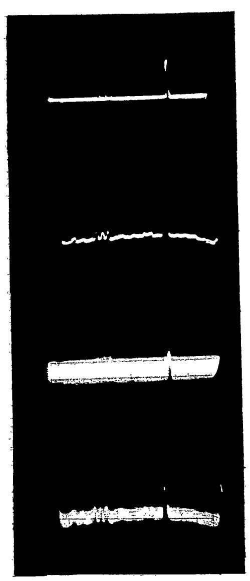

INPUT
$S^{V}_{Nin} > 100$

OUTPUT
$S^{V}_{Nin} > 100$

INPUT
$S^{V}_{Nin} = 0.5$

OUTPUT
$S^{V}_{Nin} = 0.5$

Storage-Tube Ambiguity Filter Operation,
Negative-Intensity-Modulation, Baseline Break Detection

Figure 79

1200 VOLT ACCELERATION
$n = 10$

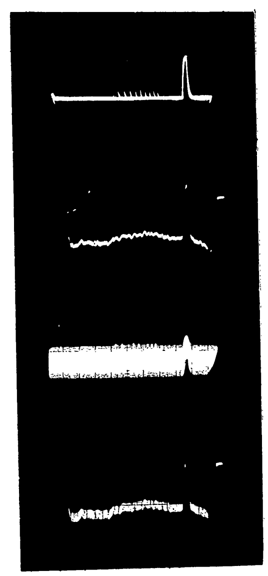

INPUT
$S^{V}_{Nin} > 100$

OUTPUT
$S^{V}_{Nin} > 100$

INPUT
$S^{V}_{Nin} = 0.5$

OUTPUT
$S^{V}_{Nin} = 0.5$

Storage-Tube Ambiguity Filter Operation,
Negative-Intensity-Modulation, Baseline Break Detection

Figure 80

The experimental noise suppression figure-of-merit at high acceleration voltage (2000 volts) appears to be approximately independent of n. This is because the random noise generated internally by the storage-tube is approximately the same at both low and high acceleration voltages, however, at high acceleration voltage the suppression of the input random noise is so great that its contribution to the total noise at the output of the filter is negligible even for small values of n. Since the total noise at the output of the filter at high acceleration voltage is substantially only the noise generated by the storage-tube and associated circuits, decreasing the signal-to-noise ratio at the input does not appreciably decrease the signal-to-noise ratio at the output and hence F_{NS} appears to increase as the input signal-to-noise ratio decreases (see definition of F_{NS} in the section entitled INTRODUCTION). Higher beam acceleration voltages increase the ambiguity suppression figure-of-merit but do not have such a simply related effect on the noise suppression figure-of-merit.

The accuracy of the data presented in Figures 73 thru 76 is such as to make these curves representative of the minimum trend of variation of the figures-of-merit. Measurement of the output of the storage-tube was extremely difficult and consequently the numerical values presented represent estimates of such

quantities as the rms value of the output noise and the amplitude of the FRI echoes buried in random noise several times their amplitude. These estimates were consistently made so as to yield conservative values for the figures-of-merit. At an n of 4, the possible errors involved are of the order of 20 to 30 percent. For values of n greater than 10 the possible errors involved are of the order of 50 to 100 percent in the direction such as to make the figures-of-merit presented in the curves too small.

The oscillograms of Figures 77 thru 80 may, in some respects, give a clearer impression of the operation of the Storage-Tube Ambiguity Filter with the two different types of modulation. Two comparisons can be made; first, between the two modulation systems for the same value of n in each, second, between the two values of n for each of the modulation systems. The first comparison shows that, at 1200 volts acceleration, the ambiguity and noise suppression of the negative-intensity-modulation system is better than that of the deflection-modulation system at large values of n. The second comparison shows that the ambiguity and noise suppression increases as n is increased.

Conclusions

Of all the Ambiguity Filters experimentally investigated, the Storage-Tube Ambiguity Filter with negative-intensity-modulation and baseline break detection appears to be the most versatile and practical. A simplified theoretical analysis indicates that an infinitely large value of F_{AS} is attainable under the assumption that there is no random noise in the input and the storage-tube has the idealized characteristics presented in this report. Under very restrictive experimental conditions, values of F_{AS} up to approximately 50 have been attained (FRI echoes 34 db down from TRI echoes). The noise suppression figure-of-merit of the filter under the same conditions was between 5 and 15 (signal-to-noise ratio increased 14 db to 23 db, depending upon the operating parameters).

A careful redesign of the negative-intensity-modulation, baseline break detection Storage-Tube Ambiguity Filter with particular emphasis on low noise input and output circuits, high acceleration voltage, large external back plate to barrier grid read-write potential shift, multiple read-out sweeps, and a sharp cut off electron gun in the storage-tube will result in a filter with higher figures-of-merit than those obtained with the present equipment.

MAGNETIC-STORAGE AMBIGUITY FILTER

Introduction

The performance of PIM and Mixed PRF systems in eliminating range ambiguities due to high pulse repetition rates is enhanced by ambiguity filters which suppress the false range indicating (FRI) echoes after they have been discriminated from the true range indicating (TRI) echoes, and which increase the signal-to-noise ratio.

In the Mixed PRF system the discrimination and suppression are performed simultaneously in comb filters. It has been pointed out that effective comb filters can be synthesized from linear amplifiers, constant time delay devices, and linear adders.[1] A magnetic-storage device could form the constant time delay mechanism in such a comb filter. In this capacity, the magnetic-storage device would operate with a linear input-output amplitude relationship. Thus, the device would operate in the manner of conventional magnetic recording devices. Such operation has been extensively described in the literature.

In the PIM system, the magnetic-storage device could be operated either linearly, or non-linearly, that is, the magnetic-storage media and/or the associated circuitry could be operated either within their linear range or outside their linear range.

[1]Signal Corps Contract No. DA36-039 SC-56696, Fifth Q.P.R. February 1955-April 1955, pp 119-170.

Magnetic-Storage Ambiguity Filter

A magnetic-storage ambiguity filter system (Series-Read System) is shown in Figure 81. The principle of operation can be most easily understood by considering linear operation of all the system elements.

Information is recorded on two tracks on the magnetic-storage media which moves under the writing and reading heads at a speed v. One track (trigger-track) is used to provide the timing of the interval modulated trigger pulses for the transmitter. The video output of the receiver is recorded on the second track (echo-track). Each track has one write-head and n read-heads spaced at non-equal intervals, where n is the number of intervals in the PIM modulation cycle. The magnetic write-head and read-heads along the echo-track have reversed spacing compared to the trigger-track head spacing, as shown in Figure 81.

The triggering of the transmitter is accomplished as follows. A trigger-pulse is recorded on the trigger-track by the write-head. After a time interval $T_{0,1}$

(1) $$T_{0,1} = \frac{x_1}{v}$$

the pulse reaches the first read-head and the signal is amplified and used to trigger the transmitter. After an additional time interval $T_{1,2}$ has elapsed,

(2) $$T_{1,2} = \frac{x_2}{v}$$

the pulse reaches the second read-head and the signal is amplified

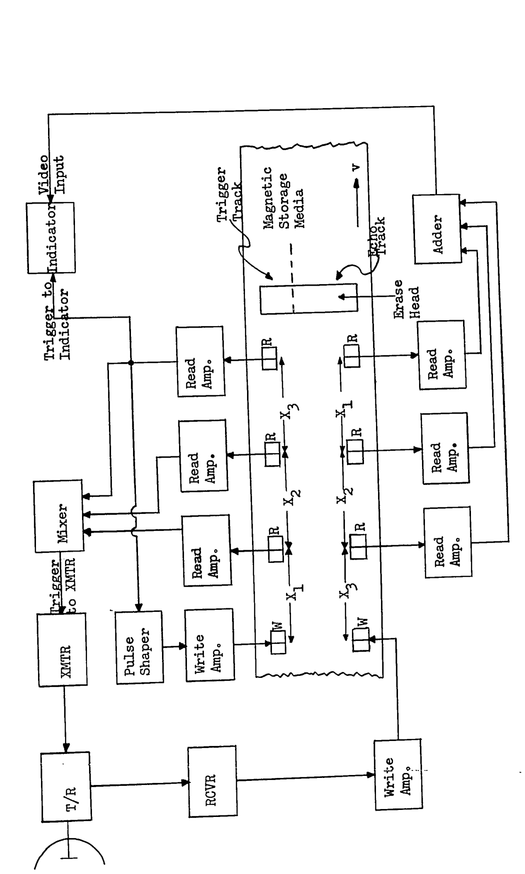

Series-Read Magnetic-Storage Ambiguity Filter System

Figure 81

and used to trigger the transmitter again. This is repeated until the pulse reaches the last read-head on the trigger-track. The signal here is not only used to trigger the transmitter but also to trigger the indicator sweep and record a new trigger-pulse on the trigger-track. The entire modulation cycle is repeated as the new trigger-pulse travels along the read-heads.

During the entire modulation cycle the video output of the receiver is continuously recorded on the echo-track. After one complete modulation cycle the echoes are recorded on the echo-track of the magnetic-storage media between the write-head and the last read-head. The read-head spacing causes TRI echoes to appear under all the read-heads simultaneously as the magnetic-storage media moves past the heads. FRI echoes do not appear under all read-heads simultaneously and hence no integration of FRI echoes occurs. The integrated TRI echoes and the non-integrated FRI echoes are displayed on the indicator. The indicator sweep duration is

$$T_M = \frac{(x_1 + x_2 + \ldots + x_n)}{v} \qquad (3)$$

so that the entire range is presented. The result is a presentation of the entire radar range with TRI echoes integrated to a higher degree than the FRI echoes and random noise.

As an example, consider a system with n equal to three, and three targets located so that their echoes are first, second, and third time-around echoes. Figure

82A shows the head spacing along the two tracks. Figure 82B shows the equivalent range positions of the three targets. Figure 82C shows the echoes due to the three targets (a, b and c) and the transmitter pulses (T) recorded on the echo-track after several modulation cycles have elapsed, along with the positions of the echo-track read-heads at the start of the indicator sweep. Figure 82D shows the conditions after the magnetic-storage media has moved a distance x_a. The recorded echoes due to the first target are all under read-heads, and the output of the three read-heads is added to give the echo at x_a on the indicator. A similar addition of outputs occurs as the second and third echoes appear simultaneously under the three read-heads after the magnetic-storage media has moved distances of x_b and x_c, respectively. The FRI echoes recorded on the echo-track appear as small responses between the TRI echoes on the indicator display, as shown in Figure 82E.

The common moving magnetic-storage media for generating the PIM modulation pulses and storing the echo information prior to integration alleviates the necessity for extreme long-time (more than 10 modulation cycles) stability and accuracy in the speed of the magnetic-storage media. Short-time (less than 10 modulation cycles) stability must be sufficiently good so as not to degrade the integration of TRI echoes. Ten modulation cycles, or less, is chosen as the basic short-time

Declassified in Part - Sanitized Copy Approved for Release @ 50-Yr 2014/01/31 : CIA-RDP81-01043R002900240002-8

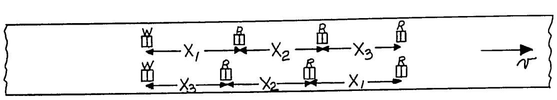

A. Head Spacing Along Tracks

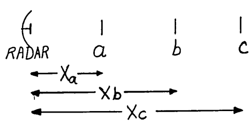

B. Equivalent Target Ranges

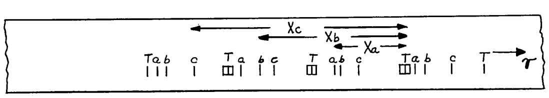

C. Conditions at Start of Indicator Sweep

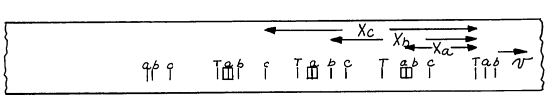

D. Conditions After Movement of Distance X_1

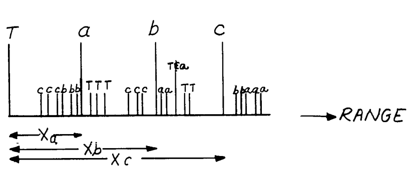

E. A - Scope Display After Movement of Distance $X_1 + X_2 + X_3$

Operation of Series - Read Magnetic - Storage Ambiguity Filter System

Figure 82

interval because under most practical search conditions a target is illuminated by the antenna beam for approximately ten, or less, modulation cycles.[1] Short-time stability is provided primarily by the momentum of the mechanical parts in the system.

Another magnetic-storage ambiguity filter system (Series-Write System) is shown in Figure 83. The operation of this system is similar to the operation of the Series-Read System. Transmitter triggering is accomplished in exactly the same manner in both systems. The Series-Write System uses n write-heads on n separate echo-tracks to record the echo information from the receiver. The distance between adjacent heads along the tracks is non-uniform, but the spacing is the same along each of the tracks. This eliminates the problem of obtaining reverse head-spacing accuracy which occurs in the Series-Read System. The positioning of the write-heads and read-heads along the echo-tracks causes TRI echoes to appear simultaneously under the read-heads as the magnetic-storage media moves. FRI echoes do not appear under the read-heads simultaneously and consequently are not integrated. The indicator sweep displays the entire radar range with TRI echoes integrated to a higher degree than FRI echoes and random noise, similarly to the Series-Read System.

[1]Signal Corps Contract No. DA-36-039 SC-56696 Seventh Q. P.R., August 1955-October 1955, pp 98-148.

Declassified in Part - Sanitized Copy Approved for Release @ 50-Yr 2014/01/31 : CIA-RDP81-01043R002900240002-8

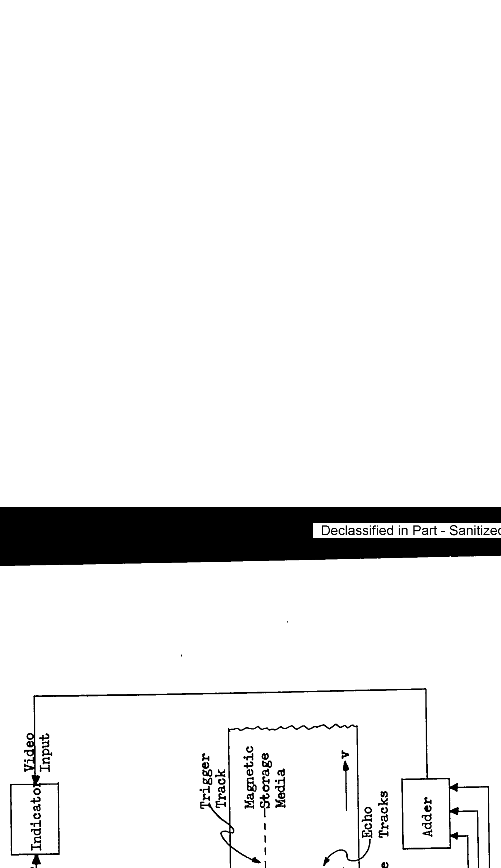

Figure 83

Series-Write Magnetic-Storage Ambiguity Filter System

A third magnetic-storage ambiguity filter system, which is a variation of the Series-Write System, involves integration of the echo information in the magnetic-storage media. The system is the same as the Series-Write System shown in Figure 83, except that the n write-heads are arranged in-line on one echo-track and only one read-head and read amplifier are used. This eliminates n-1 read-heads and read amplifiers and the adder in addition to requiring only one echo-track on the magnetic-storage media. This system is most applicable for use of the non-linearity (magnetic saturation) of the magnetic-storage media to increase the ambiguity suppression and signal-to-noise ratio improvement.

Magnetic-Storage Media Speed

The minimum allowable speed of the magnetic-storage media is dependent upon the highest frequency to be recorded and read out, the effective air-gap widths of the recording and reading heads, and the granularity of the magnetic-storage media.

The average particle size of currently used magnetic-storage coatings is approximately 0.015 mil, and particles rarely exceed 0.025 mil in size. This theoretically limits the shortest wavelength that can be recorded to approximately 0.05 mil. Recorded wavelengths as short as one mil have been achieved practically, with signal-to-noise ratios as high as 60 db.[1]

The finite size air-gaps of the heads have an averaging effect on the signal during both recording and reading. The write-head air-gap in addition to averaging the signal causes a complex distortion due to the magnetic hysteresis of the magnetic-storage media. An approximate relation between the minimum speed necessary to record and read out a given frequency signal with a specified accuracy and size of air-gaps in the heads can be obtained by assuming that the only effect of the gaps is to average the signal. The averaging interval is taken as the length of time it takes a point on the magnetic-storage media to travel a distance equal to the air-gap width. Since two air-gaps are involved, the signal is averaged twice. The averaging time interval during recording T_w is

(4) $$T_w = \frac{x_w}{v}$$

where

x_w = write-head air-gap width

v = speed of magnetic-storage media

and the averaging time interval during reading T_r is

(5) $$T_r = \frac{x_r}{v}$$

where

x_r = read-head air-gap width

[1] S. J. Begun, "A Survey of Magnetic Recording", Electrical Engineering, December 1954, pp 1115-1118.

The output signal will be proportional to the double average of the input signal. For a sinusoidal input signal

(6) $$V_{out} = \frac{K}{T_r} \int_t^{t+T_r} \frac{1}{T_w} \int_t^{t+T_w} A \sin 2\pi ft \, dt \, dt$$

where

V_{out} = output signal

A = amplitude of input signal

f = frequency of input signal

K = constant of proportionality

Evaluating the integrals gives

(7) $$V_{out} = \frac{KA}{T_r T_w 4\pi^2 f^2} \Big[\sin 2\pi f(t+T_r) - \sin 2\pi ft - \sin 2\pi f(t+T_r+T_w) + \sin 2\pi f(t+T_w) \Big]$$

Equation (7) can be reduced to

(8) $$V_{out} = \frac{KA \sin \pi fT_r \sin \pi fT_w}{T_r T_w \pi^2 f^2} \sin 2\pi f\left(t + \frac{T_r+T_w}{2}\right)$$

For $T_r \ll 1$ and $T_w \ll 1$, (8) reduces to

(9) $$V_{out} = KA \sin 2\pi ft$$

as expected.

No distortion of the signal results if the amplitude is constant and the phase shift is linearly proportional to the frequency. Equation (8) gives the amplitude as

(10) $$V_{out}^{amp} = \frac{KA \sin \pi fT_r \sin \pi fT_w}{T_r T_w \pi^2 f^2}$$

and the phase shift as

Declassified in Part - Sanitized Copy Approved for Release @ 50-Yr 2014/01/31 : CIA-RDP81-01043R002900240002-8

(11) $\quad \underline{/V_{out}} - \underline{/V_{in}} = \pi f(T_r + T_w)$

Equations (10) and (11) show that the amplitude decreases with higher frequencies and longer averaging intervals but the phase shift is linearly proportional to frequency, indicating that no phase distortion occurs. Both T_r and T_w should be made as small as possible for minimum amplitude distortion. Since the write-head and read-head air-gaps usually have the same practical minimum size, T_r and T_w can be taken equal. The time averaging interval can then be designated as T_a for either gap, where

(12) $\quad T_a = \dfrac{x_g}{v}$

where

x_g = head air-gap width

This reduces (10) and (11) to

(13) $\quad V_{out}^{amp} = \dfrac{KA \sin^2 \pi f T_a}{\pi^2 f^2 T_a{}^2}$

and

(14) $\quad \underline{/V_{out}} - \underline{/V_{in}} = 2\pi f T_a$

Figure 84 shows plotted curves of the amplitude and phase shift of the output signal, calculated from (13) and (14).

For any allowable amplitude distortion, a maximum value of fT_a can be found. Since the highest frequency to be recorded and read-out is known, the maximum value of T_a that is allowable is known. Equation (12) determines the minimum speed v necessary to achieve the desired amplitude response with the air-gap width x_g.

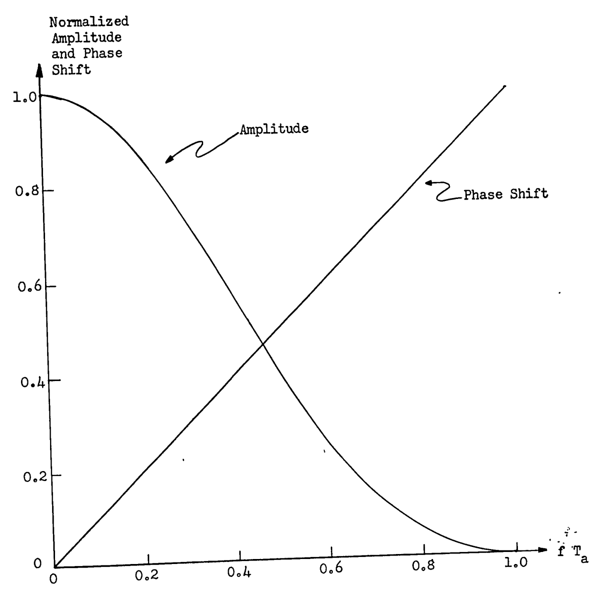

Normalized Amplitude and Phase Shift of Double Time Averaged Sinusoidal Signal

Figure 84

Declassified in Part - Sanitized Copy Approved for Release @ 50-Yr 2014/01/31 : CIA-RDP81-01043R002900240002-8

As an example, suppose a video signal is to be recorded and read out with only a 3 db drop at 5 MC. The normalized amplitude of a signal 3 db down is 0.707, which gives a maximum fT_a of 0.31, and thus a maximum T_a of 0.062×10^{-6} second. With air-gap widths of 0.00025 inch each (Brush BK -1090), the minimum speed necessary would be 4,040 inches per second or 336 feet per second. To produce this surface speed, a one foot diameter drum would have to rotate at 6,400 revolutions per minute. There are in current use data recording systems which use speeds up to 4,700 revolutions per minute on eleven inch diameter drums. (Bendix Aviation Corporation Computer).

The short-time stability necessary in the magnetic-storage media speed depends upon the highest frequency to be efficiently integrated. The outputs of the read-heads are added together to get the integrated output signal. For optimum integration of TRI echoes, all the read-head outputs should be in phase with each other. Speed variations during the modulation cycle will cause effective phase differences between the read-head outputs.

An upper limit to the allowable speed variation during one modulation cycle is obtained by assuming that the maximum allowable phase spread of the outputs of the read-heads is 120 degrees at the highest frequency of interest. This is based on the fact that the sum of two equal amplitude and frequency sinusoidal signals has an amplitude greater than the components only if the phase

difference between the components is less than 120 degrees. Thus, the signals on the magnetic-storage media must not be more than one-third wavelength out of phase as they pass under the read-heads. This means that a speed deviation v_d, acting over one modulation cycle, should not produce a distance error greater than one-third wavelength of the highest frequency of interest. That is

$$v_d T_M \leq \frac{\lambda}{3} = \frac{v}{3f} \tag{15}$$

where

T_M = length of modulation cycle

Equation (15) can be arranged to give the maximum allowable fractional speed deviation during one modulation cycle as

$$\frac{v_d}{v} \leq \frac{1}{3fT_M} \tag{16}$$

which can be expressed as

$$\frac{v_d}{v} = \leq \frac{f_M}{3f} \tag{17}$$

where

f_M = maximum unambiguous repetition rate

For example, consider a radar with f_M equal to 450 pulses per second (200 miles maximum range) and the highest frequency of interest to be 5 MC. Then the maximum allowable speed deviation over one modulation cycle is 3×10^{-3} percent.

Write-Head and Read-Head Positioning

It can be seen from Figures 81 and 83 and previous discussion that the time intervals between transmitter

Declassified in Part - Sanitized Copy Approved for Release @ 50-Yr 2014/01/31 : CIA-RDP81-01043R002900240002-8

pulses depend upon the magnetic-storage media speed and the read-head spacings along the trigger-track. To accomplish the function of discrimination, the spacings should be all different by at least the length of a transmitter pulse. The differences can be random providing no two are alike.

The total distance from the write-head to the last read-head determines the length of the modulation cycle. This is

(18) $$T_M = \frac{\sum_i x_i}{v}$$

where

x_i = distance between heads

The length of the modulation cycle is chosen approximately equal to the round trip time of an echo from a target located at the maximum range of the radar, that is

(19) $$T_M \simeq \frac{2R_M}{c}$$

where

R_M = maximum range of the radar

c = speed of light

Equations (18) and (19) give

(20) $$\sum_i x_i \simeq \frac{2vR_M}{c}$$

The unambiguous repetition rate f_M of the radar is

(21) $$f_M = \frac{1}{T_M}$$

and the number of intervals in the modulation cycle is

defined as

(22) $$n = \frac{f_s}{f_m} = f_s T_M$$

where

f_s = actual repetition rate of the radar

The average spacing of the read-heads is

(23) $$\overline{x}_i = \frac{\sum_i x_i}{n} = \frac{v}{f_s}$$

The read-head spacing along the echo-track is just the reverse of the spacing of the read-heads along the trigger-track in the Series-Read System. The write-head spacing along the echo-tracks is the same as the read-head spacing along the trigger-track in the Series-Write System.

Consider the example of the previous section, with a maximum range of 200 miles, a repetition rate of 5,000 pulses per second, and a pulse duration of 1 microsecond. The average spacing between the heads, from (23), is 0.81 inch. From (19) the modulation cycle length is approximately 2.15 milliseconds. Equation (22) gives a value of 10.75 for n, which is rounded off to 11, giving the exact value of 2.20 milliseconds for T_M. The total distance from the first write-head to the last read-head is, from (18), 8.88 inches. Each head-spacing must differ from every other spacing by at least one pulse width, which is 0.00404 inch for the one microsecond pulses.

The spacing accuracy of the write-heads and read-heads along the tracks must be sufficiently good so that the signal integration of the highest frequency of interest is not adversely affected. The situation is similar to the stability requirement in the speed, and using the same criteria gives

(24) $$x_d \leq \frac{\lambda}{3} = \frac{v}{3f}$$

where

x_d = maximum allowable deviation in head position

For the previous example, where the highest frequency of interest is 5 MC, x_d must be less than 0.27×10^{-3} inch.

Figures-of-Merit

The figures-of-merit for the Magnetic-Storage Ambiguity Filter, when operated linearly and under ideal optimum conditions, are easily determined.

For a TRI echo, the output of the filter is n times the output obtained from one read-head, because of the addition of n in-phase signals. The output of the filter, due to a FRI echo, is just the output due to one read-head, since the FRI echoes do not appear under the read-heads simultaneously. For a given target, the TRI and FRI echoes have the same magnitude at the input to the filter, and hence the ambiguity-suppression figure-of-merit is

(25) $$F_{AS} = \left.\frac{V_{TRI}}{V_{FRI}}\right|_{out} = n$$

where

V_{TRI} = voltage due to TRI echo

V_{FRI} = voltage due to FRI echo

n = number of intervals in PIM modulation cycle

The random noise output of the filter is the sum of the uncorrelated random noise outputs of n channels. The random noise voltage from the filter (due to the input random noise only) is thus $\sqrt{n}$ times the random noise voltage from one read-head. Since the TRI echo voltage increases proportionally to n, and the random noise voltage increases proportionally to $\sqrt{n}$, the signal-to-noise ratio increases proportionally to $\sqrt{n}$. The noise-suppression figure-of-merit is thus

(26) $$F_{NS} = \frac{S_N^V\ out}{S_N^V\ in} = \sqrt{n}$$

where

S_N^V = voltage signal-to-noise ratio

If the Magnetic-Storage Ambiguity Filter is operating linearly but not under ideal optimum conditions the figures-of-merit will be less than the values given by (25) and (26). Detailed investigation is necessary to determine how much the system imperfections reduce F_{AS} and to see how much the inherent noise in the system reduces F_{NS}.

If the Magnetic-Storage Ambiguity Filter is operated non-linearly, the figures-of-merit may be quite different from those for linear operation. Further detailed study is necessary to determine these differences, but it appears possible to increase the figures-of-merit above the values obtained for linear operation by judicious selection of the non-linearities employed. Non-linear operation will change the noise characteristics which may serve to improve F_{NS}.

If a property of the TRI echoes other than their voltage amplitude is used as a measure of their presence (base-line break, for example), a greater than n to one difference between the TRI echo output and the FRI echo output may be produced, thus improving F_{AS}.

Conclusion

The Magnetic-Storage Ambiguity Filter has several advantages. The system itself is simple in concept, can be applied to existing radars, provides the functions of discrimination and suppression of FRI echoes in one step, and presents the entire range in one continuous display. The disadvantage of the system is the high speed required in order to record and read-out video signals. This is primarily a mechanical problem. If this difficulty can be resolved, the Magnetic-Storage Ambiguity Filter System is expected to be practical.

VI. CONCLUSIONS

1. The analysis of a physical model, more general than found in the literature, shows that the phosphor brightness build-up and decay variation can be accurately expressed as the sum of several exponential functions. The number of exponentials necessary, their relative amplitudes, and their time constants are determined by the number of different types of luminescent-centers in the phosphor and their excitation and decay probability time densities. Theoretical-experimental agreement within 10 percent was obtained using double exponential functions for P1, P2, and P11 phosphors.

2. Equipment for combining subrange displays in the Optical-Electronic Ambiguity Filter has been constructed and the combination of the first three subranges into an integrated display has been experimentally demonstrated. More subranges may be combined by duplication of equipment. Complexity of this combining system together with greater promise in other directions indicate that further development of this combining system is not warranted.

3. The theoretically determined optimum operating parameters for the Storage-Tube Ambiguity Filter in the absence of random noise are given in Figures 70 thru 72. Under optimum operating conditions the ambiguity suppression figure-of-merit is infinitely large in the absence of noise. A direct experimental

verification of this was not obtained due to equipment limitations.

4. The Storage-Tube Ambiguity Filter, operating under noisy non-optimum conditions, had an experimentally determined ambiguity suppression figure-of-merit (F_{AS}) of 50 and a noise suppression figure-of-merit (F_{NS}) of 15. Substantial improvement is expected as optimum operating conditions are approached. This is to be contrasted with an ideal linear integration which, under the same conditions, would have $F_{AS} = 14$ and $F_{NS} = \sqrt{14}$.

5. The Magnetic-Storage Ambiguity Filters presented have the highly desirable feature of directly presenting the entire range in a simple display rather than in subrange displays as in the other PIM ambiguity filters.

VII. OVERALL CONCLUSIONS

Methods for accomplishing both the discrimination and the suppression of FRI echoes which also utilize the high PRF to improve the signal-to-noise ratio have been devised. The two most promising methods of imparting the information to the target echoes necessary for discrimination are the PIM System and the Mixed PRF System. The FRI echo suppression and signal-to-noise ratio improvement can be accomplished by an Optical-Electronic, Storage-Tube, or Magnetic-Storage Ambiguity Filter in the PIM System and by a Comb-Type Ambiguity Filter in the Mixed PRF System.

A. The PIM System has the advantages of

a) allowing the utilization of the high PRF for signal-to-noise ratio improvement,

b) applicability to existing radars,

c) simplicity of equipment involved.

The disadvantage of having the range resolved into several subranges when the Optical-Electronic or Storage-Tube Ambiguity Filters are used is not objectionable if it is desirable to view a single expanded subrange, and does not occur when the Magnetic-Storage Ambiguity Filter is used.

1. First order theoretical investigation of the Optical-Electronic Ambiguity Filter shows that the ambiguity suppression figure-of-merit (F_{AS}) increases monotonically as n increases and the noise suppression figure-of-merit

Declassified in Part - Sanitized Copy Approved for Release @ 50-Yr 2014/01/31 : CIA-RDP81-01043R002900240002-8

(F_{NS}) has a maximum value of 135. Experimental values of F_{AS} = 80 and F_{NS} = 100 were obtained under conditions for which an ideal linear integrator would have F_{AS} = 12 and $F_{NS} = \sqrt{12}$. The amount of equipment required to implement this system, particularly when subranges are combined into a single display, is such that the other ambiguity filters appear more practical.

2. First order theoretical investigation of the Storage-Tube Ambiguity Filter shows that F_{AS} increases monotonically as n increases and can be made infinitely large for a finite n under optimum operating conditions in the absence of random noise. The theoretical analysis of the operation under noisy conditions remains to be done. Experimental values of F_{AS} = 50 and F_{NS} = 15 were obtained under conditions for which an ideal linear integrator would have F_{AS} = 14 and $F_{NS} = \sqrt{14}$.

3. The Magnetic-Storage Ambiguity Filter, for use in the PIM System, appears to overcome the principal disadvantage of the Optical-Electronic and Storage-Tube Ambiguity Filters in that it presents the entire radar range in a single continuous display. Theoretical and experimental investigation of this ambiguity filter remains to be done.

B. The Mixed PRF System has the same advantages as the PIM System and in addition presents the full range in a single display.

1. First order theoretical investigation of the ideal linear Comb-Type Ambiguity Filter, for use in the Mixed PRF System, shows that F_{AS} = n and $F_{NS} = \sqrt{n}$.

Declassified in Part - Sanitized Copy Approved for Release @ 50-Yr 2014/01/31 : CIA-RDP81-01043R002900240002-8

VIII. RECOMMENDATIONS

1. Theoretical and experimental determination of the optimum operating parameters and figures-of-merit for the Storage-Tube Ambiguity Filter in the presence of random noise.
2. Theoretical, and if warranted, experimental determination of the optimum operating parameters and figures-of-merit for the Magnetic-Storage Ambiguity Filter in the presence of random noise and utilizing system non-linearities.
3. Theoretical, and if warranted, experimental determination of the optimum operating parameters and figures-of-merit for the Mixed PRF System employing a Comb-Type Ambiguity Filter.
4. Experimental demonstration of the operating characteristics of the PIM System on an actual radar set:
   - A. without any auxiliary FRI echo and noise suppression equipment other than the ordinary display scope
   - B. with the Storage-Tube Ambiguity Filter to suppress FRI echoes and random noise
   - C. with the Optical-Electronic Ambiguity Filter to suppress FRI echoes and random noise.

STAT

Page Denied

Declassified in Part - Sanitized Copy Approved for Release @ 50-Yr 2014/01/31 : CIA-RDP81-01043R002900240002-8